TÉCNICO LISBOA

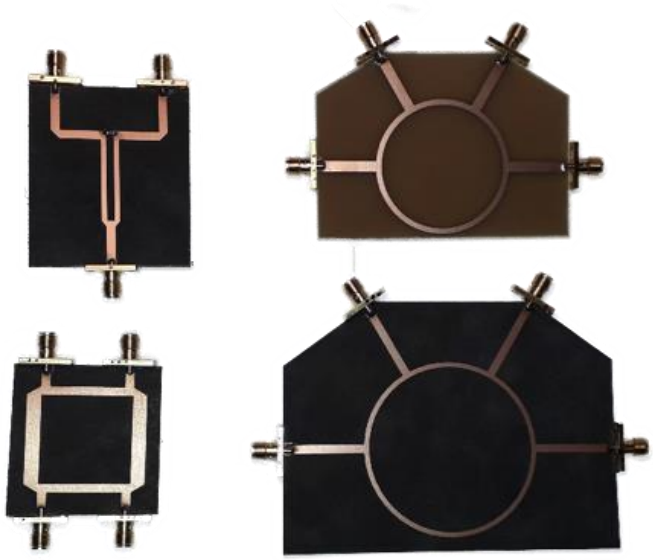

Design, Manufacture and Testing of Microstrip Directional Couplers

Salvador Vasques Seabra Águas

Thesis to obtain the Master of Science degree in

Electrical and Computer Engineering

Supervisor: Prof. Doutor António Luís Campos da Silva Topa

Examination Committee

Chairperson: Prof. José Eduardo Charters Ribeiro da Cunha Sanguino
Supervisor: Prof. António Luís Campos da Silva Topa
Member of Committee: Prof. João Manuel Torres Caldinhas Simões Vaz

June 2019

Declaration

I declare that this document is an original work of my authorship and that it fulfils all the requirements of the Code of Conduct and Good Practices of the Universidade de Lisboa.

Acknowledgments

This master thesis represents my last step to become an Electrical and Computer Engineer, representing one of the most important achievements in my academic career. All of these would not have been possible without the contribution of several individuals.

Firstly, I would like to thank Professor António Topa, who accepted to guide me through this final journey and whose expertise helped me when I needed the most. Not only his valuable advice was crucial, but also for being always available to lead me into the right path, being a true friend.

Secondly, I would like to thank Mr. Carlos Brito for teaching me and providing all his technical proficiency in the construction of the four directional couplers, always with patience and encouragement. Many thanks go to Mr. António Almeida for his knowledge and guidance in measuring the circuits.

I am also grateful to Professor Custódio Peixeiro, Professor Carlos Fernandes, Professor João Vaz, and to Mr. João Felício for their cooperation, interest and support on finding the materials required for the prototypes.

To all my friends, especially to my girlfriend Inês, that, directly or indirectly, contributed to this achievement, being my second family.

Finally, I would like to thank my parents. Even from a big distance you have always been by my side, supporting and motivating me. You have made all of this possible, and I cannot thank you enough for all the sacrifices made, especially during this last years. You are a true example.

This thesis was developed under the Instituto de Telecomunicações developed activity.

Resumo

Os acopladores direcionais são dispositivos essenciais nos campos da Radio Frequência e das Microondas, frequentemente utilizados para dividir e combinar sinais elétricos. Os últimos avanços nestas áreas resultaram num interesse acrescido em análises precisas e em design eficiente destes circuitos, para acompanhar a evolução futura destes campos de conhecimento.

Esta dissertação consiste no estudo, projeto e construção de três acopladores direcionais através da tecnologia de linhas impressas em microstrip: o Híbrido de Quadratura, o Rat-Race e o Divisor de Wilkinson. Consideram-se três substratos diferentes: o RT DUROID 5880, o FR-4 e o EPSILAM-10. Os três dispositivos são analisados de forma a perceber o impacto que o seu desenho e o substrato em que foram implementados, têm no seu funcionamento.

Na análise destes circuitos foi utilizado o software CST para a simulação, que permitiu uma análise mais detalhada dos seus parâmetros S, assim como uma melhor compreensão dos fluxos de potência e elétricos dos mesmos, para a frequência que foram dimensionados.

Os circuitos projetados foram construídos, e após a sua medição obteve-se uma excelente concordância com os resultados de simulação, o que permite concluir que a metodologia utilizada nesta dissertação é indicada para o projeto deste tipo de dispositivos.

Palavras-chave: Circuitos Impressos, Microstrip, Acoplador Direcional, Divisor de Wilkinson, Rat-Race, Híbrido de Quadratura.

Abstract

Directional couplers are one of the most required devices in the Radio Frequency and microwave fields, frequently utilized to divide and combine electric signals. The last advances in these areas have resulted in an increased interest in efficient, precise analysis and design of these circuits in order to keep up with future developments in these fields.

This dissertation consists in the analysis, design and manufacture of three different directional couplers, using the microstrip printed lines technology: The Quadrature Hybrid, the Rat-Race and the Wilkinson Power Divider. Three different substrates are considered: the RT DUROID 5880, the FR-4 and the EPSILAM-10. The analysis of these three devices enables to understand what is the impact of the design and of the substrate in which they were applied, in their overall performance.

The simulation results were obtained with the CST software that allowed a deeper analysis of the S-parameters, as well as a better understanding of the electric and power flows of these devices at the dimensioned frequency.

After being manufactured the projected circuits were measured, obtaining and excellent agreement with the simulation results, which allows to conclude that the methodology applied in this dissertation is appropriated to this type of circuit projection.

Keywords: Printed Circuits, Microstrip, Directional Couplers, Wilkinson Power Divider, Rat-Race, Quadrature Hybrid.

Contents

Chapter 1 - Introduction 1
1.1 Motivation 1
1.2 Objectives 1
1.3 Document Structure 2
1.4 Main Contributions 3
Chapter 2 – Microstrip Line Components 5
2.1 Microstrip Line 5
2.1.1 Microstrip parameters 5
2.1.2 Effective Dielectric Constant 7
2.2 Coupled Lines 10
2.3 Directional Couplers 13
2.3.2 Rat-race 13
2.3.3 Quadrature Hybrid 19
2.3.4 Wilkinson Power Divider 22
Chapter 3 – Computer Simulation 27
3.1 Numerical Simulator 27
3.2 Circuit Design 27
3.2.1 Substrate Materials 27
3.2.2 Circuit Layout 29
3.3 Simulation Results 31
3.3.1 Quadrature Hybrid 31
3.3.2 Rat-Race 37
3.3.3 Wilkinson Power Divider 42
Chapter 4 – Circuit Manufacturing and Testing 49
4.1 Circuit Printing 49
4.2 Circuit Testing and Results 51
4.2.1 Quadrature Hybrid 51
4.2.2 Rat-Race 55
4.2.3 Wilkinson Power Divider 62
Chapter 5 - Conclusion 67
5.1 Review of the Performed Work and Main Findings 67
5.1.1 Summary 67
5.1.2 Main Findings 67
5.2 Limitations and Future Work 69
Bibliography 71

List of Figures

Figure 1.1 Outline of the main objectives of the dissertation. 2
Figure 2.1 Microstrip Circuit Example. 6
Figure 2.2 Different types of microstrip layouts. 6
Figure 2.3 Example of 2 coupled lines. 10
Figure 2.4 Even and odd mode on 2 coupled lines. 11
Figure 2.5 Characteristic impedances on even and odd mode for two coupled lines with w/h variation [13]. 11
Figure 2.6 Dispersion effect on the characteristic impedance on even and odd modes [13]. 12
Figure 2.7 Dispersion effect on the effective dielectric constants on even and odd mode [13]. 12
Figure 2.8 Rat-Race Layout. 14
Figure 2.9 Rat-Race S-parameters and phase analysis. 14
Figure 2.10 Rat-race even mode analysis at port (1) excitation. 16
Figure 2.11 Rat-race odd mode analysis at port (1) excitation. 16
Figure 2.12 Rat-race even mode analysis at port (4) excitation. 17
Figure 2.13 Rat-race odd mode analysis at port (4) excitation. 17
Figure 2.14 Rat-race S-parameters. 18
Figure 2.15 Quadrature Hybrid layout. 19
Figure 2.16 Quadrature Hybrid Circuit. 19
Figure 2.17 Even-odd analysis. 20
Figure 2.18 Quadrature Coupler even analysis. 20
Figure 2.19 Quadrature Coupler odd analysis. 21
Figure 2.20 Wilkinson Power Divider Layout [9]. 22
Figure 2.21 Wilkinson Power Divider S-parameters. 23
Figure 2.22 WPD odd mode symmetric scheme [27]. 23
Figure 2.23 WPD odd mode circuit [27]. 24
Figure 2.24 WPD odd mode equivalent circuit [27]. 24
Figure 2.25 Even mode symmetric scheme [27]. 25
Figure 2.26 Even mode circuit [27]. 25
Figure 2.27 Even mode equivalent circuit [27]. 25
Figure 3.1 Quadrature Hybrid Computer Layout. 30
Figure 3.2 Wilkinson Power Divider Computer Layout. 30
Figure 3.3 Rat-Race Computer Layout. 31
Figure 3.4 RT DUROID 5880 Quadrature Hybrid S-parameters. 31
Figure 3.5 RT DUROID 5880 Quadrature Hybrid Return Loss. 32
Figure 3.6 RT DUROID 5880 Quadrature Hybrid Ports 2 and 3 Phase Comparison. 32
Figure 3.7 RT DUROID 5880 Quadrature Hybrid Insertion Loss. 33
Figure 3.8 RT DUROID 5880 Quadrature Hybrid E-field Simulation. 33
Figure 3.9 RT DUROID 5880 Quadrature Hybrid Power Field Simulation. 33
Figure 3.10 FR-4 Quadrature Hybrid S-parameters. 34
Figure 3.11 FR-4 Quadrature Hybrid Return Loss. 34
Figure 3.12 FR-4 Quadrature Hybrid Insertion Loss. 35
Figure 3.13 FR-4 Quadrature Hybrid Ports 2 and 3 Phase Comparison. 35
Figure 3.14 FR-4 Quadrature Hybrid E-Field Simulation. 36
Figure 3.15 FR-4 Quadrature Hybrid Power Field Simulation. 36
Figure 3.16 EPSILAM-10 Quadrature Hybrid S-parameters. 37
Figure 3.17 EPSILAM-10 Quadrature Hybrid Return Loss. 37

Figure 3.18 RT DUROID 5880 Rat-Race S-parameters. 38
Figure 3.19 RT DUROID 5880 Rat-Race Return Loss. 38
Figure 3.20 RT DUROID 5880 Rat-Race Insertion Loss. 38
Figure 3.21 RT DUROID 5880 Rat-Race ports 2 and 3 phase comparison degree. 39
Figure 3.22 RT DUROID 5880 Rat-Race ports 2 and 3 comparison dB. 39
Figure 3.23 RT DUROID 5880 Rat-Race E-Field Simulation. 39
Figure 3.24 RT DUROID 5880 Rat-Race Power Field Simulation. 40
Figure 3.25 FR-4 Rat-Race S-parameters. 40
Figure 3.26 FR-4 Rat-Race Return Loss. 41
Figure 3.27 FR-4 Rat-Race Ports 2 and 3 Phase Comparison. 41
Figure 3.28 FR-4 Rat-Race Insertion Loss. 41
Figure 3.29 FR-4 Rat-Race E-Field Simulation. 42
Figure 3.30 FR-4 Rat-Race Power Field Simulation. 42
Figure 3.31 Wilkinson Power Divider First Layout. 43
Figure 3.32 RT DUROID 5880 Wilkinson Power Divider S-parameters. 43
Figure 3.33 RT DUROID 5880 Wilkinson Power Divider Return Loss. 43
Figure 3.34 RT DUROID 5880 Wilkinson Power Divider Insertion Loss. 44
Figure 3.35 RT DUROID 5880 Wilkinson Power Divider Ports 2 and 3 Phase Comparison. 44
Figure 3.36 RT DUROID 5880 Wilkinson Power Divider E-Field Simulation. 44
Figure 3.37 RT DUROID 5880 Wilkinson Power Divider Power Field Simulation. 45
Figure 3.38 FR-4 Wilkinson Power Divider S-parameters. 45
Figure 3.39 FR-4 Wilkinson Power Divider Return Loss. 46
Figure 3.40 FR-4 Wilkinson Power Divider Insertion Loss. 46
Figure 3.41 FR-4 Wilkinson Power Divider Ports 2 and Phase Comparison. 46
Figure 3.42 FR-4 Wilkinson Power Divider E-Field Simulation. 47
Figure 3.43 FR-4 Wilkinson Power Divider Power Field Simulation. 47
Figure 4.1 Circuit Layouts Exported. 49
Figure 4.2 Circuits Exposure to Ultraviolet Light. 50
Figure 4.3 Rat-Race Circuit Cutting. 51
Figure 4.4 RT DUROID 5880 Quadrature Hybrid Prototype. 51
Figure 4.5 RT DUROID 5880 Quadrature Hybrid VNA Connections. 52
Figure 4.6 RT DUROID 5880 Quadrature Hybrid VNA Analysis. 52
Figure 4.7 RT-DUROID 5880 Quadrature Hybrid S-parameters. 53
Figure 4.8 RT-DUROID 5880 Quadrature Hybrid Return Loss. 53
Figure 4.9 RT-DUROID 5880 Quadrature Hybrid Insertion Loss. 54
Figure 4.10 RT-DUROID 5880 Quadrature Hybrid Ports 2 and 3 Phase Comparison. 55
Figure 4.11 RT DUROID 5880 Rat-Race Prototype. 55
Figure 4.12 RT DUROID 5880 Rat-Race VNA Analysis. 56
Figure 4.13 RT DUROID 5880 Rat-Race S-parameters. 56
Figure 4.14 RT DUROID 5880 Rat-Race Return Loss. 57
Figure 4.15 RT DUROID 5880 Rat-Race Insertion Loss. 58
Figure 4.16 RT DUROID 5880 Rat-Race Ports 2 and 3 Phase Comparison. 58
Figure 4.17 FR-4 Rat-Race Prototype. 59
Figure 4.18 FR-4 Rat-Race VNA Connections and Analysis. 59
Figure 4.19 FR-4 Rat-Race S-parameters. 60
Figure 4.20 FR-4 Rat-Race Return Loss. 60
Figure 4.21 FR-4 Rat-Race Insertion Loss. 61
Figure 4.22 FR-4 Rat-Race Ports 2 and 3 Phase Comparison. 62

Figure 4.23 RT-DUROID 5880 Wilkinson Power Divider prototype. 62
Figure 4.24 RT-DUROID 5880 Wilkinson Power Divider VNA Analysis. 63
Figure 4.25 RT DUROID 5880 Wilkinson Power Divider S-parameters. 63
Figure 4.26 RT DUROID 5880 Wilkinson Power Divider Return Loss. 64
Figure 4.27 RT DUROID 5880 Wilkinson Power Divider Insertion Loss. 65
Figure 4.28 RT DUROID 5880 Wilkinson Power Divider Ports 2 and 3 Phase Comparison. 65
Figure 5.1 Outline of the main work done in this dissertation. 68

List of Acronyms

3D	Tridimensional
ADS	Advanced Design System
CAD	Computer Aided Design
CS	Cable Studio
CST	Computer Simulation Technology
DS	Design Studio
DXF	Drawing Exchange File
HF	High Frequency
ITT	International Telephone & Telegraph
MPS	MPHYSICS Studio
MWS	Microwave Studio
PCB	Printed Circuit Board
PS	Particle Studio
PTFE	Polytetrafluoroethylene
RF	Radio Frequency
TEM	Transverse Electro Magnetic
VNA	Vector Network Analyser

List of Tables

Table 1 Dielectric vs Microstrip analysis. 7
Table 2 - RT DUROID 5880 Line Impedance Parameters. 28
Table 3 - FR-4 Line Impedance Parameters. 29
Table 4 - EPSILAM-10 Line Impedance Parameters. 29
Table 5 RT-DUROID 5880 Quadrature Hybrid Return Loss Values. 54
Table 6 RT DUROID 5880 Rat-Race Return Loss Values. 57
Table 7 FR-4 Rat-Race Return Loss Values. 61
Table 8 RT DUROID 5880 Wilkinson Power Divider Return Loss Values. 64

Chapter 1

Introduction

1.1 Motivation

The potential to distribute and combine signals is a primary function in several microwave systems, and especially functional if it can be achieved over a wide frequency range and with phase shifted signals [1]. Moreover, passive microwave components such as directional couplers and power dividers, have played an important role in recent years and have been extensively utilized in microwave applications. The objective of such devices is to divide (or couple) a signal into *n* others, depending on the application and requirements. The most typical implementation of this type of circuits is to divide an input signal to feed low power amplifiers, and later recombine them.

There are numerous types of directional couplers to facilitate effective signal splitting and recombination, therefore the motivation of the present work was to analyse three of them, which are quite different but very commonly used in the Radio Frequency (RF) and microwave designer's toolbox, and perform some simulations, modelling, fabrication and experimentation with them.

1.2 Objectives

The main purpose of this work was to design, simulate, manufacture and analyse three different directional couplers - the Quadrature Hybrid, the Rat-Race and the Wilkinson Power Divider, in three very different substrates, the RT DUROID 5880, the FR-4 and the EPSILAM-10, with the aim of studying the possible differences between the circuits, specifically how the signal is split and what the resultant output signals look like in terms of amplitude and phase (Fig. 1.1).

The present research also seeks to describe the Microstrip Line technology and the Coupled Lines technique used to print the directional couplers, as well as the characterization of the main features of the three directional couplers and the even-odd mode circuit analysis, in order to understand their performance characteristics and derived scattering matrices.

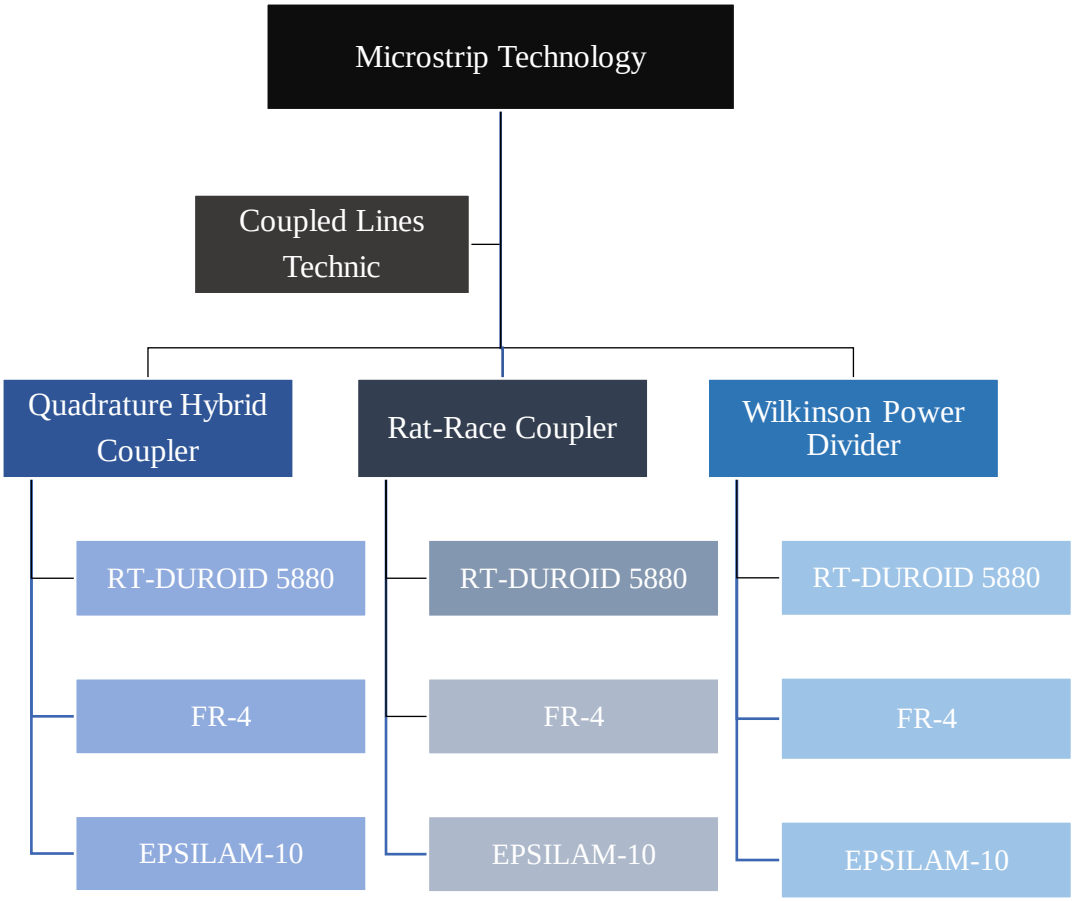

Figure 1.1 Outline of the main objectives of the dissertation.

1.3 Document Structure

This document is organized in five chapters, each one composed by different sections. The first chapter briefly describes the present research, the main motivation, the research aim and objectives as well as some main contributions.

Chapter 2 discusses the literature review and theoretical background regarding directional couplers and power dividers. It also describes the three different components studied - Microstrip lines, Coupled Lines and Directional Couplers, with which one representing a key aspect of the Printed Circuit Board (PCB).

Chapter 3 summarizes the design and calculation of each circuit. It also presents the various hypothesis and simulations done with the CST® software and the main data and results obtained.

Chapter 4 illustrates the circuit printing method and the different stages of the process. It goes on analysing each device by using a VNA machine. These results are compared with the theoretical analysis as well as with the simulation results presented on Chapter 3.

Chapter 5 discusses the main conclusions and presents the final considerations. This chapter also discusses the nature of the contribution of this research and identifies opportunities for further research.

1.4 Main Contributions

The present work indicates that the three directional couplers applied here – the Quadrature Hybrid, the Rat-Race and the Wilkinson Power Divider directional couplers - can be built using simple microstrip manufacture techniques and coupled lines techniques.

Moreover, the analysis, design and manufacture of the three different directional couplers allowed to understand the overall impact of the design and of the substrate in which they were applied, in their final performance. The CST software enabled an accurate analysis of the S-parameters along with a good comprehension of the electric and power flows of the devices at the dimensioned frequency.

The results acquired with the physical devices were very similar to the simulation results, demonstrating an excellent agreement between the results and therefore validating that the methodology applied in this dissertation is appropriated to this type of circuit projection.

Chapter 2

Microstrip Line Components

The microstrip line is almost certainly the most popular among the variety of guided wave structures employed in the transmission of microwave signals. The simplicity of its geometry, along with the small size and the facility with which it can be integrated, turned it the natural choice to be used in the present research. Moreover, the coupled transmission lines allowed an effective correspondence of real loads in different frequency ranges which allowed a consensus between the measured and predicted performance of the coupled line.

The option for three different directional couplers - Rat-race, Quadrature Hybrid Coupler and Wilkinson Power Divider – was made because they can be easily fabricated, and they are among the most widely utilized couplers in radio frequency circuit design for power combing and power divisions.

2.1 Microstrip Line

The microstrip line is a planar transmission line, similar to stripline and coplanar waveguide, developed by the ITT Federal Telecommunications Laboratories, generally used to transmit microwave signals [2] . This system is based on a conducting strip divided from the ground plan by a dielectric, and it can originate different types of components, like couplers[1]. One of the major advantages of this type of line is that is cheaper, more compact and lighter when compared with other traditional waveguide methods, and this is assured by the fact that it can be produced with impressed circuit board technology.

2.1.1 Microstrip parameters

As stated above, this circuit is composed by a small dimension conducting line, with width w and thickness t, impressed on a dielectric substrate with height h and relative dielectric constant ε_r, based on the ground plan, with physical length L as illustrated in figure 2.1 [3].

[1] See section 2.3 for a description

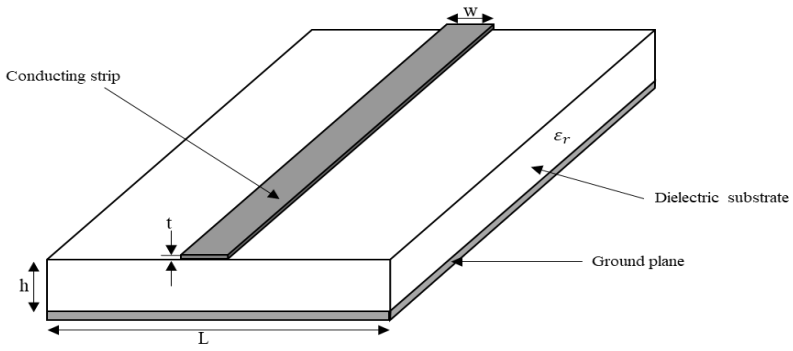

Figure 2.1 Microstrip Circuit Example.

The main condition for this circuit to work is that $L \gg w$ must be fulfilled.

A microstrip line is also characterised by a:

- Frequency range from 300 MHz to dozens of GHz;
- Possibility to build compact circuits on a single substrate
- Easiness to access components
- Conductors with low losses
- Capability of supporting multiple frequency bands

But it has some disadvantages such as:

- Cross polarization radiation
- Dielectric superficial waves exciting
- Dielectric losses offering low efficiency
- Low attenuation

In order to deal with part of the mentioned disadvantages, other variations of the microstrip line were developed (fig. 2.2):

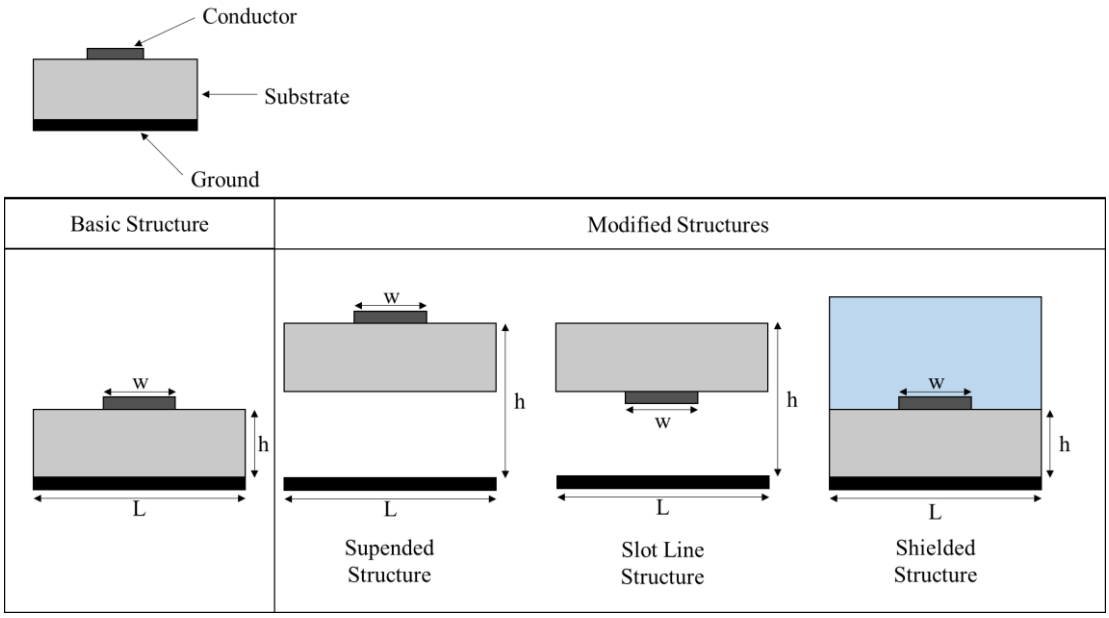

Figure 2.2 Different types of microstrip layouts.

- Suspended Structure – this structure is used to diminish dielectric losses, by using an air line with near 1 relative dielectric constant. Given an ε_r from this range, these structures are the most similar of propagating on TEM mode.
- Slot Line Structure – this structure is used because of the facility to connect new components to the line in shunt, and also due to the fact that high impedances are easy to achieve in a slot line [4].
- Shielded Structure – this structure is used to reduce the radiation. In this implementation, the shield must have big dimensions when compared to the microstrip, to avoid walls resonances and attenuations.

As a result of the major disadvantages presented above, it is not possible to achieve a TEM propagation mode on this kind of line but, nevertheless, we are able to use a propagation mode valid until the direct current. This propagation mode, named Quasi-TEM (Transverse ElectroMagnetic) [5], emerges with the effective dielectric constant.

2.1.2 Effective Dielectric Constant

The effective dielectric constant, ε_{ef} is the key factor that allows the approximation of the microstrip to an air line, by replacing the both dielectrics existing on a microstrip and obtaining the longitudinal propagation constant *k*.

$$1 < \varepsilon_{ef} < \varepsilon_r \tag{2.1}$$

Table 1 presents a comparison between the dielectric line versus the microstrip line, taking into consideration the characteristic impedance, Z_c, the wavelength, λ, and the attenuation due to the conductors, α. $Z_{c0}, \lambda_0,$ and α_0 concerns the respective equivalent air line values [6].

Table 1 Dielectric vs Microstrip analysis.

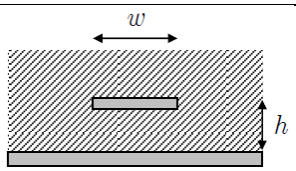	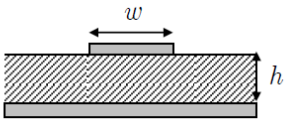	
Dielectric	Microstrip	Correlation
$Z_c = \frac{Z_{c_0}}{\sqrt{\varepsilon_r}}$	$Z_c = \frac{Z_{c_0}}{\sqrt{\varepsilon_{ef}}}$	$\frac{Z_c}{Z_{c_0}} = \frac{1}{\sqrt{\varepsilon_r}}$

$\lambda = \frac{\lambda_0}{\sqrt{\varepsilon_r}}$	$\lambda = \frac{\lambda_0}{\sqrt{\varepsilon_{ef}}}$	$\frac{\lambda}{\lambda_0} = \frac{k_0}{k} = \frac{1}{\sqrt{\varepsilon_r}}$
$\alpha = \alpha_0\sqrt{\varepsilon_r}$	$\alpha = \alpha_0\sqrt{\varepsilon_{ef}}$	$\frac{\alpha}{\alpha_0} = \sqrt{\varepsilon_r}$

2.1.2.1 Low Frequency Approximation

Regarding the microstrip line, the capacity *C*, is given by $C = \varepsilon_{ef} C_0$, so to obtain the effective dielectric constant that the line capacity requires. The low frequency approximation is utilized for this process [7], obtaining:

$$\varepsilon_{ef} = \frac{\varepsilon_r + 1}{2} + \frac{\varepsilon_r - 1}{2}(1 + 12\frac{h}{w})^{\frac{1}{2}} + F(\varepsilon_r, h) - 0.217\,(\varepsilon_r - 1)\frac{t}{\sqrt{wh}} \tag{2.2}$$

Where

$$F(\varepsilon_r, h) = \begin{cases} 0.02(\varepsilon_r - 1)(1 - \frac{w}{h})^2 & \frac{w}{h} < 1 \\ 0 & \frac{w}{h} \geq 1 \end{cases} \tag{2.3}$$

2.1.2.2 Dispersive Model

Another model has been developed, that takes into consideration the frequency effect [8]. The next set of equations describe this model:

$$\varepsilon_{ef} = \varepsilon_r - \frac{\varepsilon_r + \varepsilon_{ef0}}{1 + \left(\frac{f}{f_a}\right)^m} \tag{2.4}$$

Where

$$f_a = \frac{f_b}{0.75 + (0.75 - 0.332{\varepsilon_r}^{-1.73})\frac{w}{h}} \tag{2.5}$$

With

$$f_b = \frac{47.476}{h\sqrt{\varepsilon_r - \varepsilon_{ef0}}} tan^{-1}\left[\varepsilon_r\sqrt{\frac{\varepsilon_{ef0} - 1}{\varepsilon_r - \varepsilon_{ef0}}}\right] \tag{2.6}$$

$$m = m_0 m_c \tag{2.7}$$

If the result of (2.7) is bigger than 2.32, then $m = 2.32$ must be considered, but if it is lower than 2.32, m_0 and m_c should be according to the following formulas:

$$m_0 = 1 + \frac{1}{1+\sqrt{\frac{w}{h}}} + 0.32\left(1+\sqrt{\frac{w}{h}}\right)^{-3} \tag{2.8}$$

and

$$m_c = \begin{cases} 1 + \frac{1.4}{1+\frac{w}{h}}\left(0.15 - 0.235^{-0.45\frac{f}{f_a}}\right) & \frac{w}{h} \leq 0.7 \\ 1 & \frac{w}{h} \leq 0.7 \end{cases} \tag{2.9}$$

The frequency is expressed in GHz and the *h* value in mm. With these formulas, it is possible to calculate the effective dielectric constant for a *w/h* between 0.1-10 and an ε_r between 1-128, with a 0.6% precision.

Since it is not possible to precisely account the frequency effect, this method will not be applied in the present work.

2.1.2.3 Dimensioning Equations

Most of the calculations presented at the beginning of section 2.1.2, were based on the *w/h* relation, nevertheless it is also necessary to calculate the reverse relation of the Z_c and ε_r values, as shown in the following formulas [9].

$$\begin{cases} \frac{w}{h} = \frac{8e^A}{2e^A - 2} & \frac{w}{h} < 2 \\ \frac{w}{h} = \frac{2}{\pi}\left[B - 1 - ln(2B+1) + \frac{\varepsilon_r - 1}{2\varepsilon_r}B_1\right] & \frac{w}{h} > 2 \end{cases} \tag{2.10}$$

With

$$A = \frac{Z_c}{60}\sqrt{\frac{\varepsilon_r + 1}{2}} + \frac{\varepsilon_r - 1}{\varepsilon_r + 1}\left(0.23 + \frac{0.11}{\varepsilon_r}\right) \tag{2.11}$$

$$B = \frac{377\pi}{2Z_c\sqrt{\varepsilon_r}} \tag{2.12}$$

$$B_1 = ln(B-1) + 0.39 - \frac{0.61}{\varepsilon_r} \tag{2.13}$$

2.2 Coupled Lines

Coupled transmission lines are two unshielded transmission lines in close proximity to each other, where energy can be coupled from one line to the other due to the interaction of the electromagnetic fields [10]. The application of these lines in the design of couplers have been widely investigated and described in the literature, and in general, the best microstrip case scenario happens with parallel strips impressed on the same dielectric substrate [11] (Fig. 2.3).

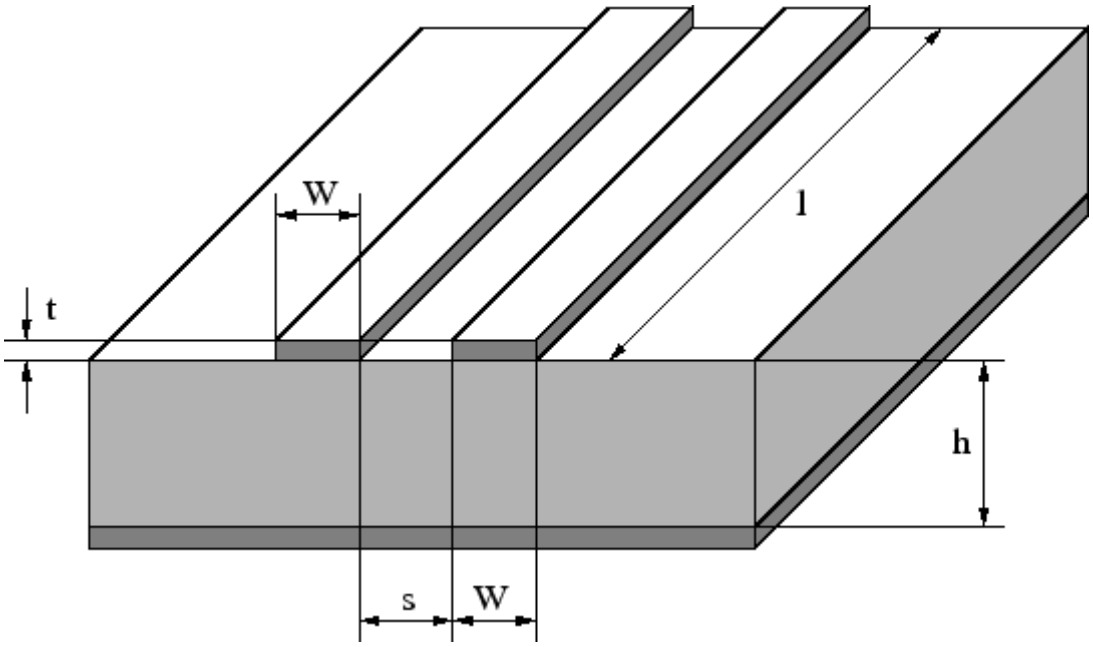

Figure 2.3 Example of 2 coupled lines.

Like with effective dielectric constant, coupled lines also propagate on the quasi-TEM mode. This characteristic makes the consequent analysis simpler and, since the circuits are symmetric, the superposition method can be applied. Therefore, the circuits can be divided into two different types of coupled microstrip lines: (a) Even mode and (b) Odd mode.

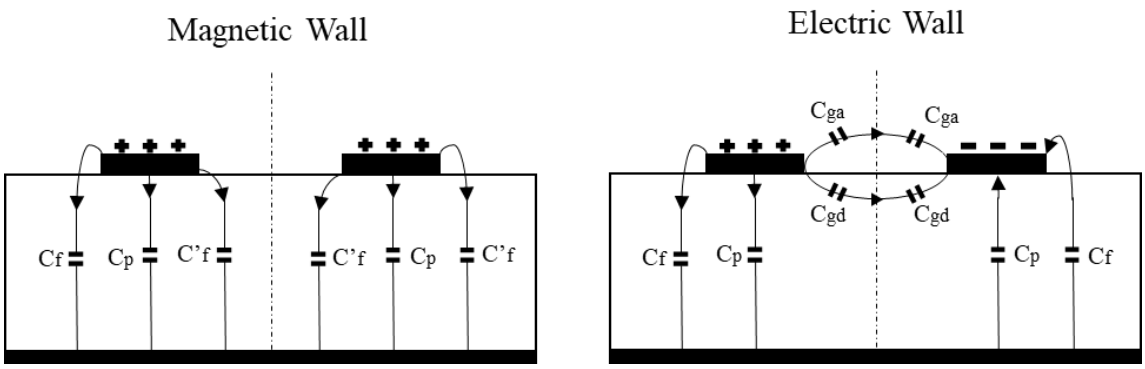

Figure 2.4 Even and odd mode on 2 coupled lines.

Figure 2.4 illustrates that the electric propagation constant on the even mode is higher than on the odd mode, which implies a lower phase velocity [12].

The analysis of the even mode shows that a capacity, C_e, only exists between the line and the ground plan. Nevertheless, this is not verified in the odd mode, becoming necessary to add another capacity between the lines, as shown in the following equation:

$$\begin{cases} C_e = C_1 \\ C_o = C_1 + 2C_2 \end{cases} \Rightarrow C_e < C_o \tag{2.14}$$

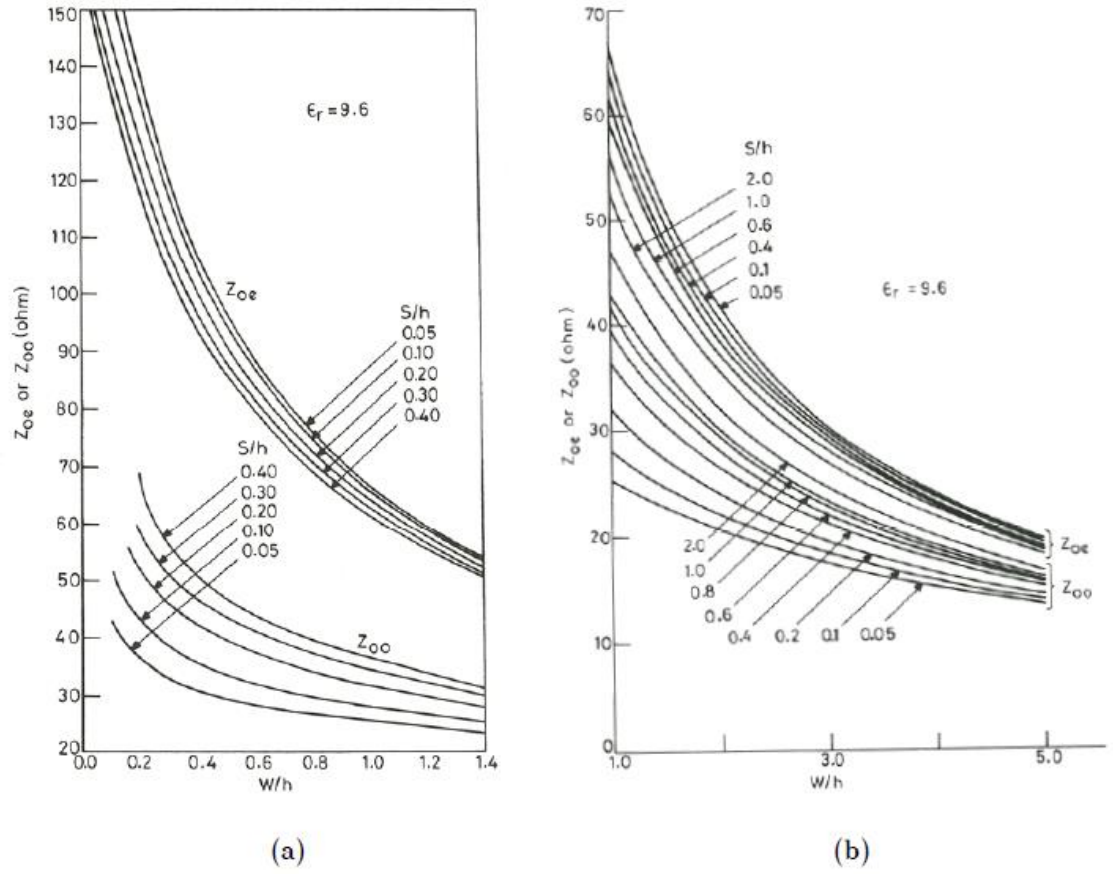

Figure 2.5 Characteristic impedances on even and odd mode for two coupled lines with w/h variation [13].

As shown in figure 2.5, for a given ε_r, the characteristic impedance variation with a given *s/h* value is opposite between the two modes, but when *s/h*→ ∞, the odd and even values are the same.

As can be seen in figure 2.6, the impedance for the even mode is always larger than the impedance of the odd mode. The reason for this can be found in figure 2.4, where it is possible to see that for the odd mode there is a large number of electric field lines in the air region. For the same reason, the effective dielectric constant of the even is larger than the odd mode (Fig. 2.7).

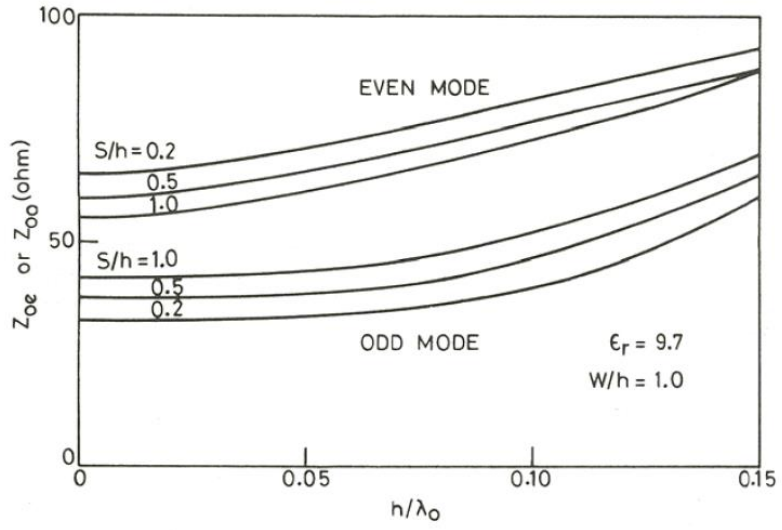

Figure 2.6 Dispersion effect on the characteristic impedance on even and odd modes [13].

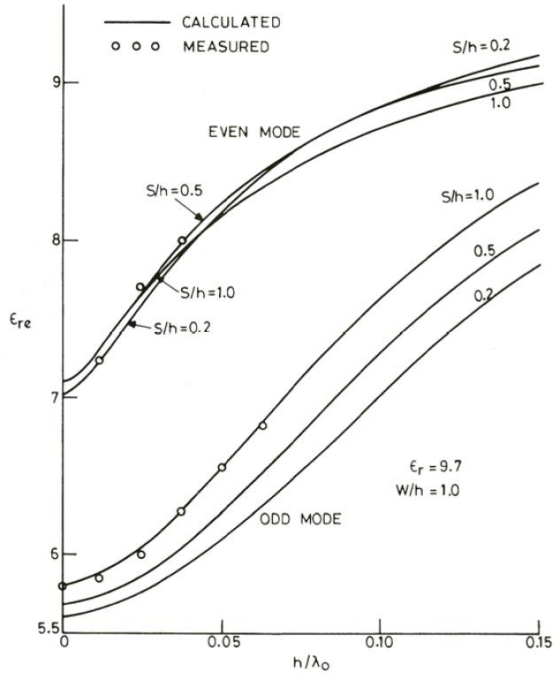

Figure 2.7 Dispersion effect on the effective dielectric constants on even and odd mode [13].

2.3 Directional Couplers

A directional coupler is a four-port passive device, built from two coupled transmission lines. In theory all ports are matched and one of them is isolated. They can be built using different techniques, like waveguide, microstrip, stripline and coax. These types of circuits are based on the microwave properties, and normally work within a multiple of quarter-wavelength device [14].

Directional couplers are built based on the two lines energy and the field interactions between them, connecting each other's signals. In general, they are used in the radio technology field, but they have many other multiple applications, for instance they are also utilized to put together several circuit elements, most commonly in microwaves frequencies, as for example, in feedback and combining feeds to and from antennas.

This research will develop this subject through three different directional couplers that can be easily fabricated using microstrip printed circuits. Also they are all widely utilized couplers in radio frequency circuit design for power combing and power divisions.

- Rat-Race;
- Quadrature Hybrid Coupler;
- Wilkinson Power Divider.

2.3.2 Rat-race

The rat-race coupler, which structure is exemplified in figure 2.8, has two major advantages: a simple design and offers a very good isolation between the ports. This type of microstrip is a four port component, with a wavelength between ports, but it is also symmetric and lossless, being this the main reason why is widely used as a power divider or combiner [15].

The ring hybrid has four ports with the terminal impedance Z_0, whereas the space between ports 2 and 4 is $3\lambda_g/4$, and the space between all other adjacent ports is $\lambda_g / 4$ [16].

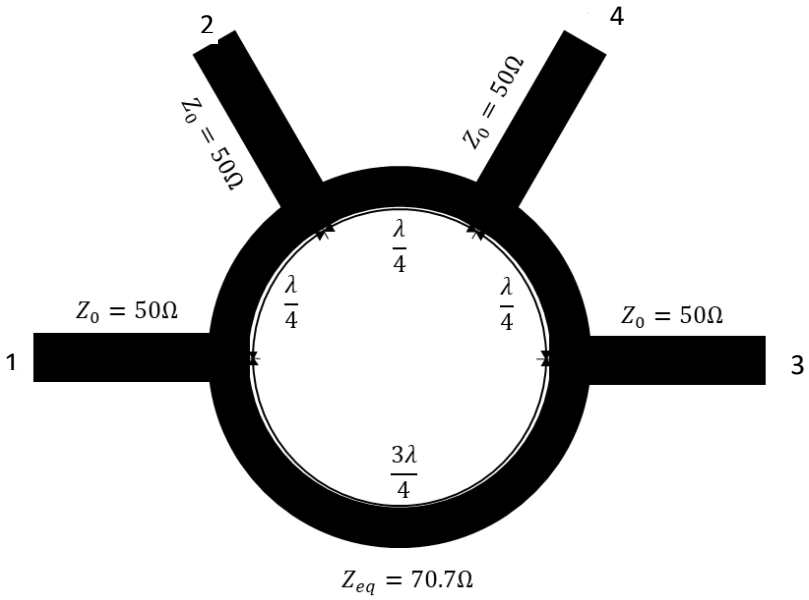

Figure 2.8 Rat-Race Layout.

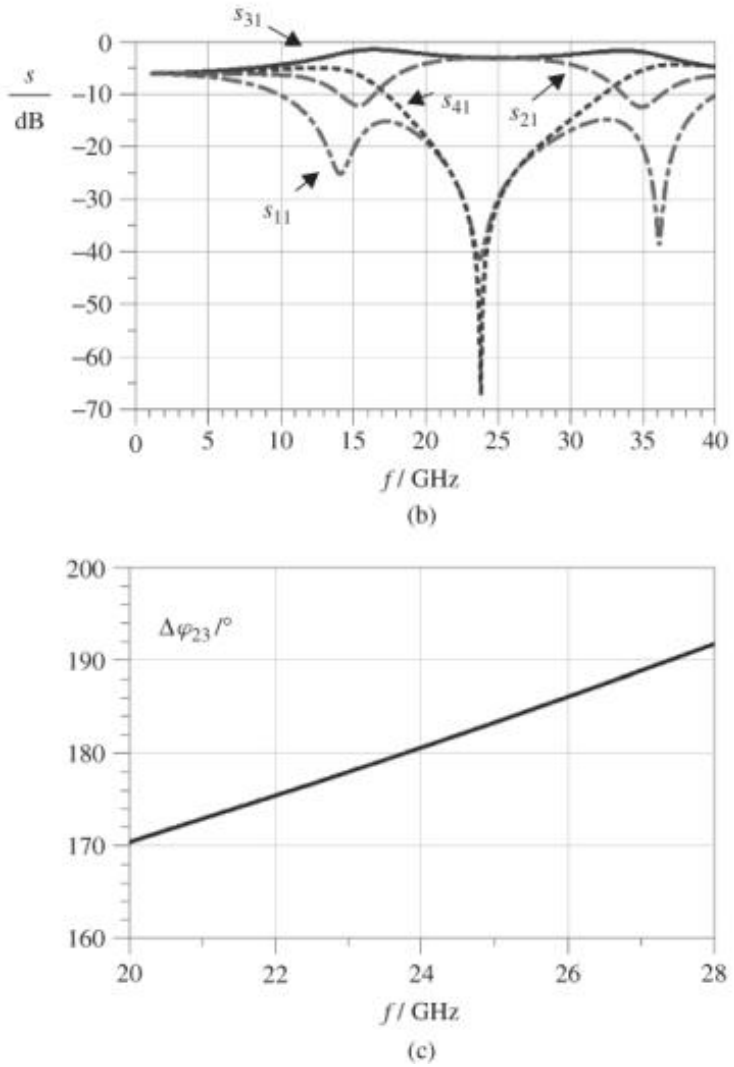

Figure 2.9 Rat-Race S-parameters and phase analysis.

The rat-race symmetry, about the centre line, is establish on the above figure 2.9 and demonstrated by the $S_{Rat-race}$ matrix exhibited bellow [17].

$$S_{Rat-race} = \frac{1}{\sqrt{2}} \begin{pmatrix} 0 & -i & i & 0 \\ -i & 0 & 0 & -i \\ i & 0 & 0 & -i \\ 0 & -i & -i & 0 \end{pmatrix} \quad (2.15)$$

Given the fact that (1) and (4) or (2) and (3) are connected by two paths that differ $\frac{\lambda}{2}$, is easily observable that $s_{14} = s_{23} = 0$.

The comparison between the $S_{Rat-race}$ matrix and the magic-T S-matrix[2], has revealed identical features, namely an 180º phase relation between ports.

The application of a coupler like this can bring a lot of benefits, such as a [18]:

- Good return loss at its ports;
- Good isolation between ports;
- Good amplitude/phase balance in whole microstrip band frequency.

However, it can have some drawbacks, such as:

- Short bandwidth;
- By having a $\frac{3\lambda}{4}$ length between ports, it will occupy a big area.

2.3.2.1 Even-odd mode analysis

The analysis of a rat-race hybrid coupler can be carried out using the even and odd-mode approach [19]. Figures 2.10 and 2.11 represents respectively a rat-race even and odd mode analysis excitation at the port 1 hybrid ring.

[2] A magic tee (or magic T or hybrid tee) is a hybrid or 3 dB coupler used in microwave systems. It was first published by W. A. Tyrell of Bell Labs in a 1947 IRE paper, even tough Robert L. Kyhl and Bob Dicke independently created magic tees around the same time. It is an alternative to the rat-race coupler but its three-dimensional structure makes it less readily constructed in planar technologies such as microstrip or stripline.

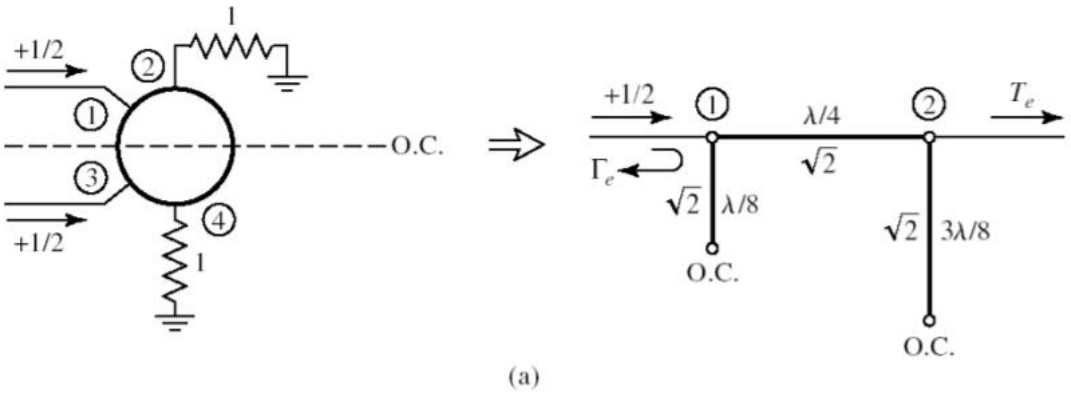

Figure 2.10 Rat-race even mode analysis at port (1) excitation.

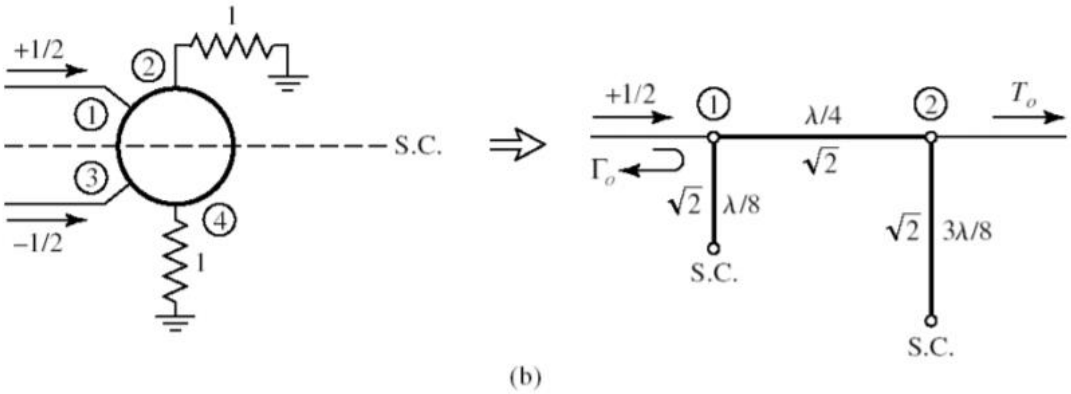

Figure 2.11 Rat-race odd mode analysis at port (1) excitation.

The information gathered from the figures 2.10 and 2.11 enables to calculate the amplitudes of the scattered waves:

$$B_1 = \frac{1}{2}\Gamma_e + \frac{1}{2}\Gamma_o, \tag{2.16}$$

$$B_2 = \frac{1}{2}\mathrm{T}_e + \frac{1}{2}\mathrm{T}_o, \tag{2.17}$$

$$B_3 = \frac{1}{2}\Gamma_e - \frac{1}{2}\Gamma_o, \tag{2.18}$$

$$B_4 = \frac{1}{2}\mathrm{T}_e - \frac{1}{2}\mathrm{T}_o, \tag{2.19}$$

Where $\Gamma_e = \mathrm{T}_e = \mathrm{T}_o = \frac{-j}{\sqrt{2}}$ and $\Gamma_o = \frac{j}{\sqrt{2}}$, getting:

$$B_1 = 0, \tag{2.20}$$

$$B_2 = \frac{-j}{\sqrt{2}}, \tag{2.21}$$

$$B_3 = \frac{-j}{\sqrt{2}}, \tag{2.22}$$

$$B_4 = 0, \tag{2.23}$$

This result proves that port (4) is isolated, and the power is equally divided in phase between ports (2) and (3), i.e. the input signal applied to port 1 is evenly split between ports 2 and 3 at the dimensioned frequency.

Likewise, if port (4) is now excited and port (1) isolated, it is expected that the power arrives with an 180º phase difference to ports (2) and (3).

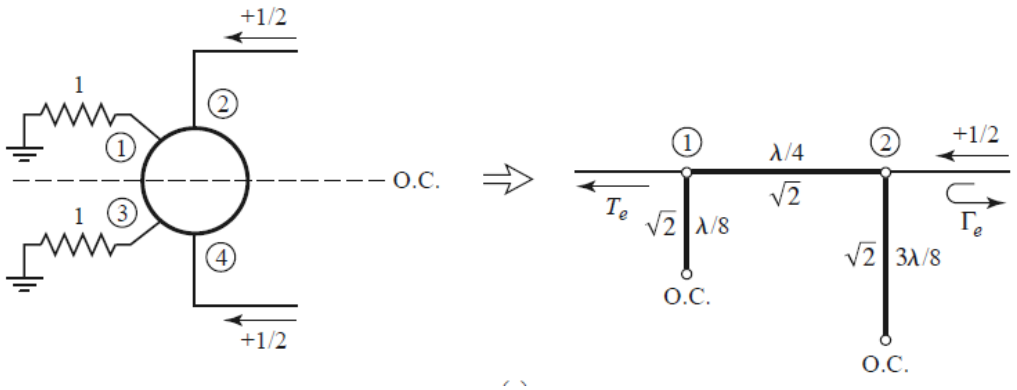

Figure 2.12 Rat-race even mode analysis at port (4) excitation.

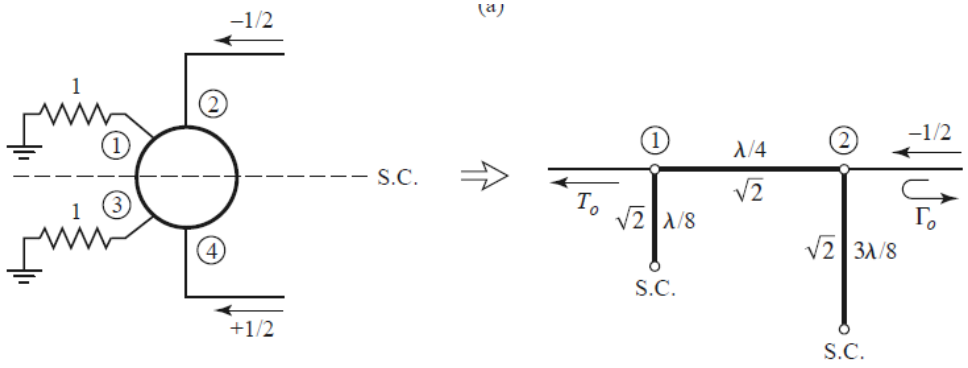

Figure 2.13 Rat-race odd mode analysis at port (4) excitation.

The data from the above pictures enables to calculate the amplitudes of the scattered waves:

$$B_1 = \frac{1}{2}\mathrm{T}_e - \frac{1}{2}\mathrm{T}_o, \tag{2.24}$$

$$B_2 = \frac{1}{2}\Gamma_e - \frac{1}{2}\Gamma_o, \tag{2.25}$$

$$B_3 = \frac{1}{2}\mathrm{T}_e + \frac{1}{2}\mathrm{T}_o, \tag{2.26}$$

$$B_4 = \frac{1}{2}\Gamma_e + \frac{1}{2}\Gamma_o, \tag{2.27}$$

Where $\Gamma_o = \mathrm{T}_e = \mathrm{T}_o = \frac{-j}{\sqrt{2}}$ and $\Gamma_e = \frac{j}{\sqrt{2}}$, getting:

$$B_1 = 0, \tag{2.28}$$

$$B_2 = \frac{j}{\sqrt{2}}, \tag{2.29}$$

$$B_3 = \frac{-j}{\sqrt{2}}, \tag{2.30}$$

$$B_4 = 0, \tag{2.31}$$

This result proves that port (4) is now matched whereas port (1) is isolated and, as expected, the power was equally divided between the ports (2) and (3) with a 180º phase between them.

The comparison between the previous figures and the $S_{Rat-race}$ relations, highlights that the exciting wave arrives at port (4) at a 180º out of phase, and expectedly arrives in phase at ports (2) and (3).

Finally, it was found that the ring hybrid is a narrow-band device because of the transmission line lengths (Fig. 2.14)

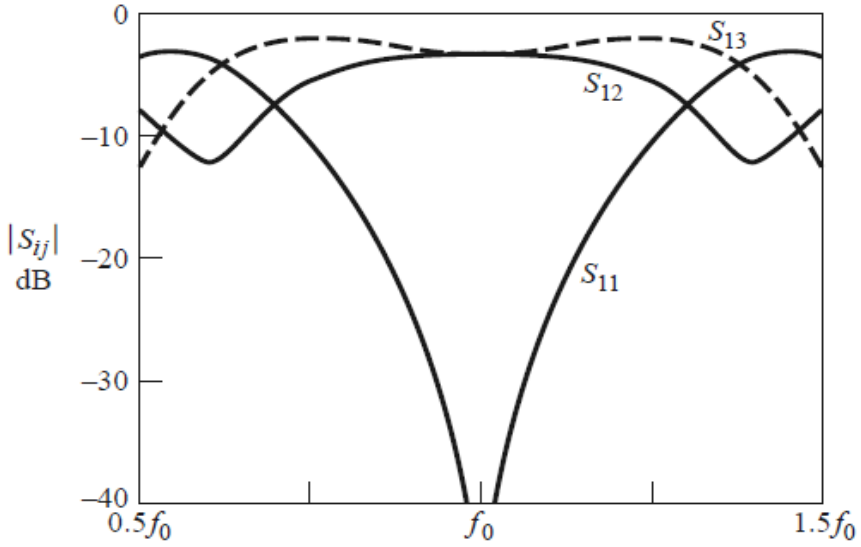

Figure 2.14 Rat-race S-parameters.

2.3.3 Quadrature Hybrid

Like the rat-race, the quadrature hybrid is a 4 ports directional hybrid coupler. The main difference from the previous one, is that this one has a 90º phase difference in the two output ports instead of 180º. In general, this hybrid coupler is used as power divider and to impedance match pairs of devices [20] (Fig. 2.15).

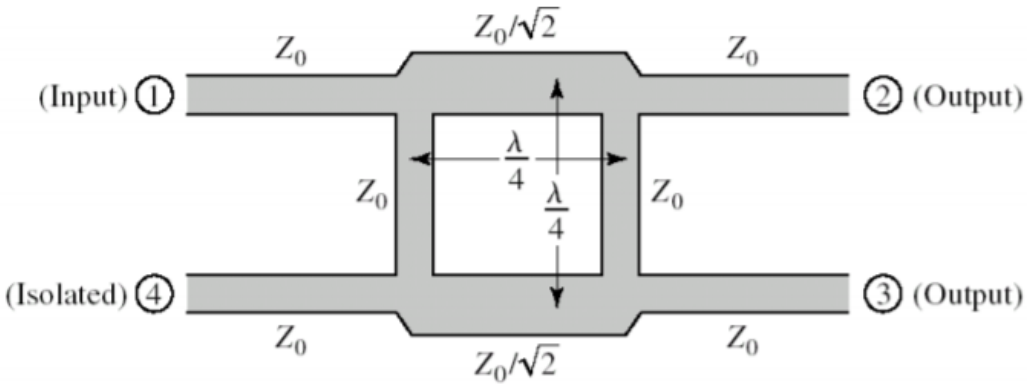

Figure 2.15 Quadrature Hybrid layout.

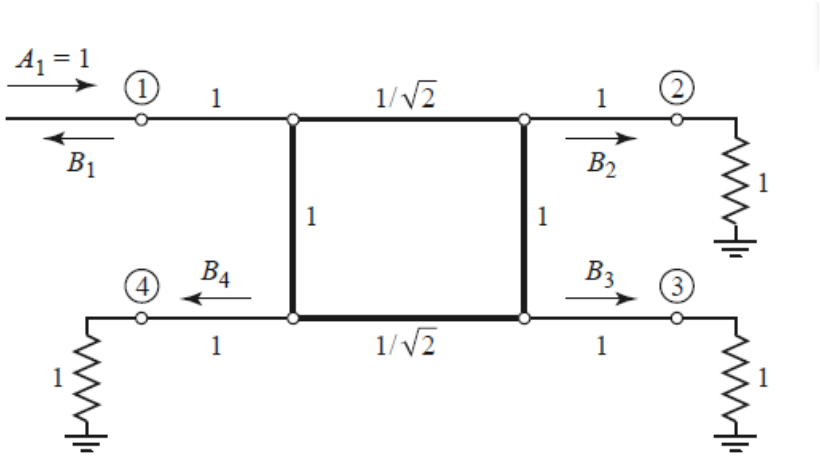

Figure 2.16 Quadrature Hybrid Circuit.

The main advantage of this system is that any port can work as an input or an output port [21]. This is demonstrated in the following scattering matrix.

$$S_{Quadrature} = \frac{1}{\sqrt{2}}\begin{pmatrix} 0 & -i & -1 & 0 \\ -i & 0 & 0 & -1 \\ -1 & 0 & 0 & -i \\ 0 & -1 & -i & 0 \end{pmatrix} \tag{2.32}$$

Examining the geometry of the coupler and the way it operates, a signal applied to port (1), will be evenly split between into two components with a 90°phase difference at ports (2) and (3) and

port (4) will be isolated, acting as power divider. This power signal (p) at port (1) can be described as:

$$\begin{cases} p_1 = p \\ p_2 = p_3 = p_4 = 0 \end{cases}, \tag{2.33}$$

2.3.3.1 Even-odd mode analysis

In the same way as with the Rat-race coupler, an even-odd mode analyses was applied to the quadrature hybrid coupler (Fig. 2.17).

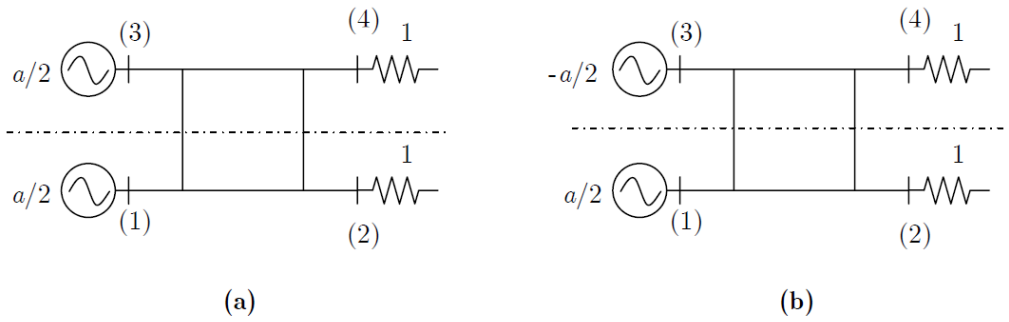

Figure 2.17 Even-odd analysis.

With an entering power described as:

- Even mode (a): $\begin{cases} p_1^e = p_3^e = \frac{p}{2} \\ p_2^e = p_4^e = 0 \end{cases}$
- Odd mode (b): $\begin{cases} p_1^o = -p_3^o = \frac{p}{2} \\ p_2^o = p_4^o = 0 \end{cases}$

This type of analysis resulted in a symmetric plan, and consequently in two simple circuits [22]: an open circuit in case of the even analysis (Fig. 2.18).

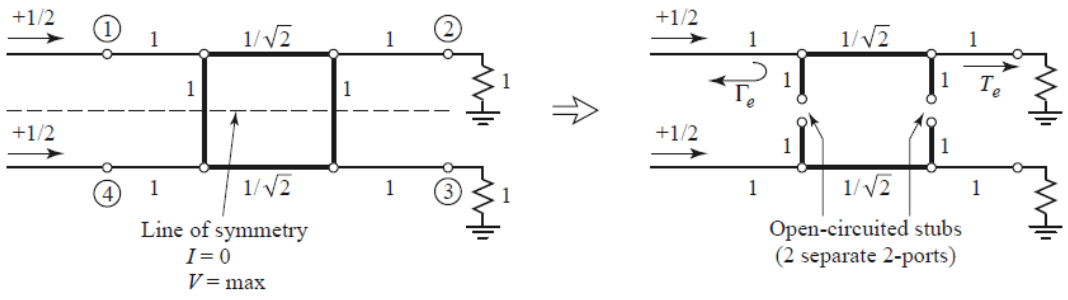

Figure 2.18 Quadrature Coupler even analysis.

And a short circuit in case of the odd analysis (fig 2.19).

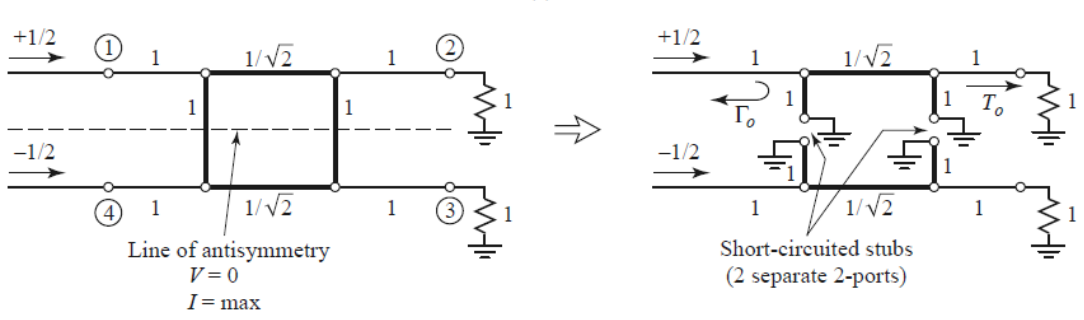

Figure 2.19 Quadrature Coupler odd analysis.

With an $\pm\frac{1}{2}$ incident wave for both ports, the amplitude of the incident wave at every single port is, similar to the rat-race, as expressed by:

$$B_1 = \frac{1}{2}\Gamma_e + \frac{1}{2}\Gamma_o, \tag{2.34}$$

$$B_2 = \frac{1}{2}\mathrm{T}_e + \frac{1}{2}\mathrm{T}_o, \tag{2.35}$$

$$B_3 = \frac{1}{2}\mathrm{T}_e - \frac{1}{2}\mathrm{T}_o, \tag{2.36}$$

$$B_4 = \frac{1}{2}\Gamma_e - \frac{1}{2}\Gamma_o, \tag{2.37}$$

Where:

$$\Gamma_e = \frac{\frac{(-1+j-j+1)}{\sqrt{2}}}{\frac{(-1+j+j-1)}{\sqrt{2}}} = 0, \tag{2.38}$$

$$\mathrm{T}_e = \frac{2}{\frac{(-1+j+j-1)}{\sqrt{2}}} = \frac{-1}{\sqrt{2}}(1+j), \tag{2.39}$$

$$\Gamma_o = 0, \tag{2.40}$$

$$\mathrm{T}_o = \frac{1}{\sqrt{2}}(1-j), \tag{2.41}$$

With these last equations, the amplitude of the incident wave can now be calculated, achieving the following results:

$$B_1 = 0, \tag{2.42}$$

$$B_2 = \frac{-j}{\sqrt{2}}, \tag{2.43}$$

$$B_3 = \frac{-1}{\sqrt{2}}, \tag{2.44}$$

$$B_4 = 0, \tag{2.45}$$

The results show that port (1) is matched, port (4) is isolated, and the incident power is equally divided between ports (2) and (3), with a 90º and 180º phase to port (1) respectively.

2.3.4 Wilkinson Power Divider

The Wilkinson power divider, developed around 1960 by Ernest Wilkinson, has a symmetric component like the previous couplers but it is a 3-port coupler. It splits an input signal into two equal phase output signals, or combines two equal-phase signals into one in the opposite direction. Nevertheless, the Wilkinson divider is not lossless, since reflected power is dissipated using a resistor [23]. It can be used both as power divider - achieving isolation between the output ports and at the same time maintaining a matched condition on all ports - as well as a power combiner - owing to the fact that it is made up of passive components and hence reciprocal [24]. The transmission line circuit of an equal-split (3 dB) Wilkinson divider is shown in Figure 2.20.

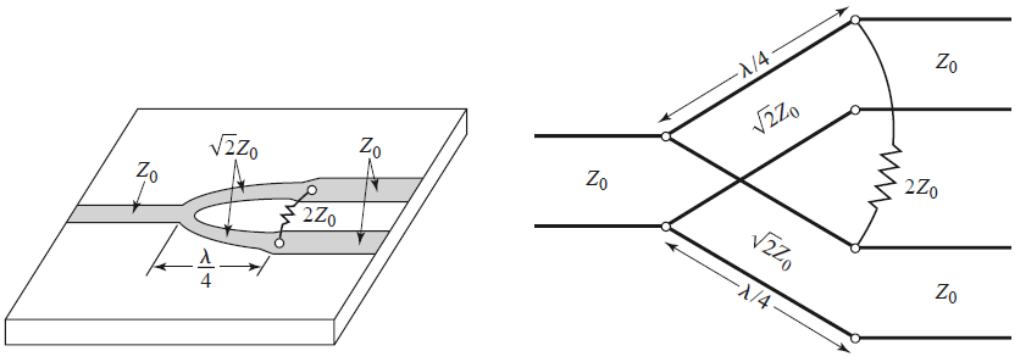

Figure 2.20 Wilkinson Power Divider Layout [9].

It is composed of two parallel transmissions, with a quarter wavelength, feeding the input, and the two outputs are terminated with twice the system impedance bridged between them [25].

As previous couplers, it also has some advantages such as [26]:

- Simplicity and low cost;
- By employing the perfect components, the Wilkinson coupler has no losses;
- Good isolation between output ports.

And some disadvantages like:

- Using quarter wave transmission lines (the coupler has limited bandwidth);
- Can be considered a big dimension component to some applications.

As stated above, when the outputs are matched they do not have losses [27], resulting in a perfect power splitter, as demonstrated in the $S_{Wilkinson}$ matrix and the S-parameters variation graph below (Fig. 2.21).

$$S_{Wilkinson} = \frac{1}{\sqrt{2}}\begin{pmatrix} 0 & -i & -i \\ -i & 0 & 0 \\ -i & 0 & 0 \end{pmatrix} \tag{2.46}$$

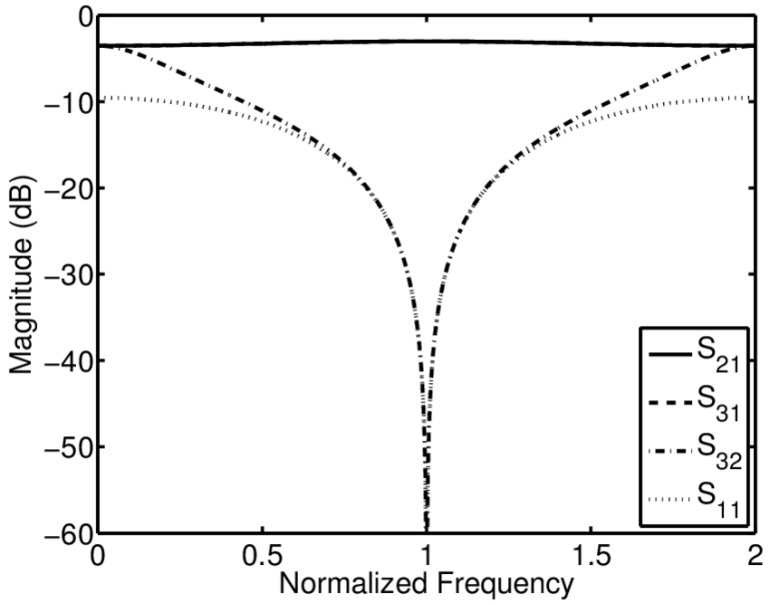

Figure 2.21 Wilkinson Power Divider S-parameters.

2.3.4.1 Even-odd mode analysis

Similarly, an even-odd mode analysis was performed using the symmetry of the circuit and the superposition principle.

- Odd mode analysis

It starts by turning off one positive source at each port, i.e. by applying a voltage source with impedance Z_0 at V_2^o with V_1^o and V_3^o terminated with Z_0 (Z_0 being the system impedance) (Fig. 2.22).

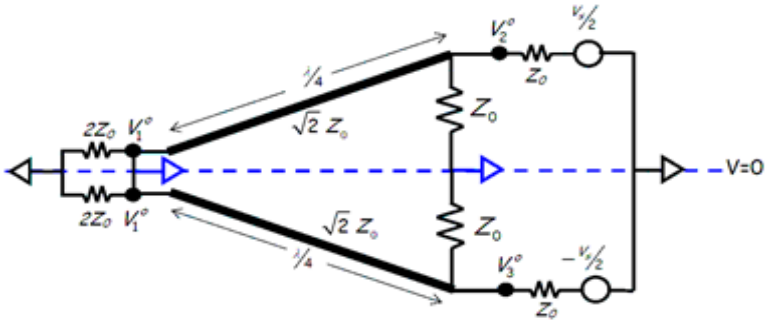

Figure 2.22 WPD odd mode symmetric scheme [27].

The analyses of each part of the circuit shows two half-circuits, with a positive port at the upper half and a negative at the lower half, as shown in Figure 2.23. Due to the odd symmetry of this circuit the symmetry line becomes a virtual short, and the upper and lower parts of the circuit can be treated separately.

Since this port is short circuited, we are able to verify that V_1^o is zero. Since the line is a quarter wavelength, the short is transformed to an open at V_2^o and V_3^o.

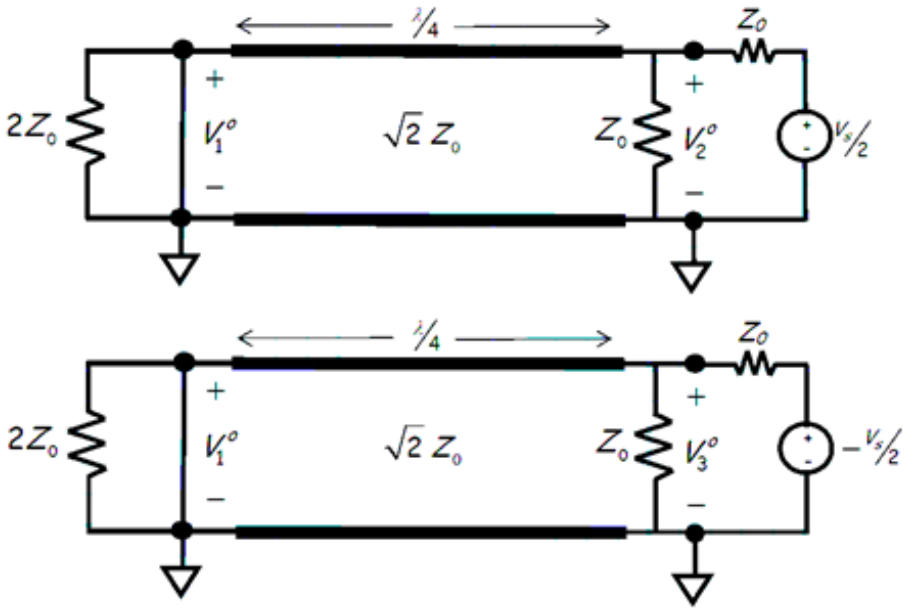

Figure 2.23 WPD odd mode circuit [27].

From simple voltage division (Fig. 2.24):

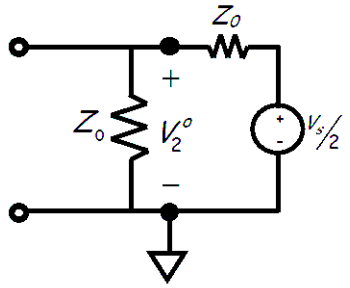

Figure 2.24 WPD odd mode equivalent circuit [27].

It is found that this two half-circuits are anti-symmetrical, so their power relation can be expressed by this equation:

$$V_2^o = -V_3^o = \frac{V_s}{4} \tag{2.47}$$

- Even mode analysis

The even mode analyses show that in the even mode symmetry, the symmetry line represents a virtual open (Fig. 2.25).

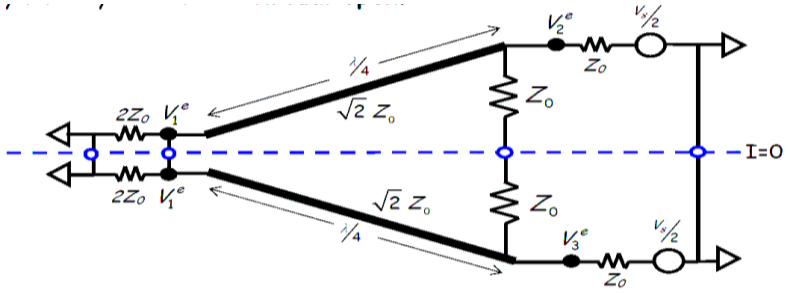

Figure 2.25 Even mode symmetric scheme [27].

The analysis of the two half-circuits (Fig. 2.26), shows that the $2*Z_0$ resistor at V_1^e transforms - using the quarter wavelength formula - to Z_0 at V_2^e and V_3^e

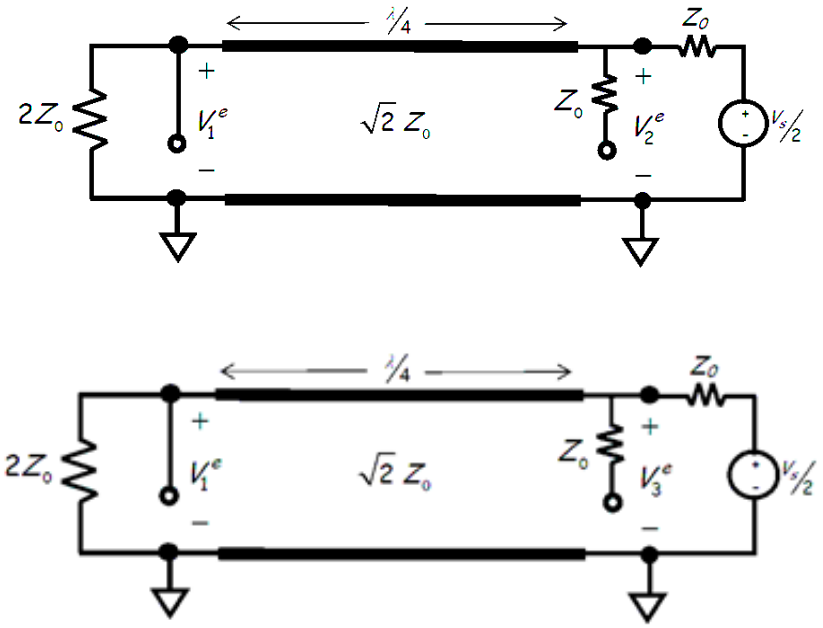

Figure 2.26 Even mode circuit [27].

That was simplified into an equivalent circuit as exemplified in the following scheme (Fig. 2.27),

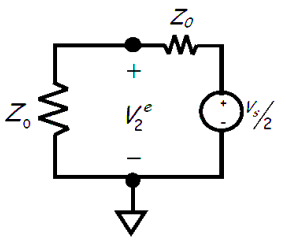

Figure 2.27 Even mode equivalent circuit [27].

The even mode power expressions can be reduced to:

$$V_2^e = V_3^e = \frac{V_s}{4} \tag{2.48}$$

$$V_1^e = -\frac{jV_s}{2\sqrt{2}} \tag{2.49}$$

In order to conclude the full circuit power calculation, the superposition principle was applied to the circuit symmetry. The sum of the incident and reflected voltages can be expressed by V_1=-$jV_s/(2\sqrt{2})$, V_2=V_s/4 and V_3=0. Because $V_{1\text{ and }}V_3$ are terminated in Z_0, the reflected voltages at these two ports must be zero, therefore V_1^+=0, V_1^-=-$jV_s/(2\sqrt{2})$, V_3^+=0 and V_3^-=0. Due to the fact that the source impedance at port 2 is matched to the line impedance, which is electrically small, we should have that V_2^+=V_s/2 and V_2^-=0. This gives the necessary voltages to find the following formulas:

$$V_1 = V_1^o + V_1^e = 0 - \frac{jV_s}{2\sqrt{2}} \tag{2.50}$$

$$V_2 = V_2^o + V_2^e = \frac{V_s}{4} + \frac{V_s}{4} = \frac{V_s}{2} \tag{2.51}$$

$$V_3 = V_3^o + V_3^e = -\frac{V_s}{4} + \frac{V_s}{4} = 0 \tag{2.52}$$

From symmetry we must have that $V_2^e = V_3^e = \frac{V_s}{4}$ and $V_2^o = -V_3^o = \frac{V_s}{4}$.

Chapter 3

Computer Simulation

3.1 Numerical Simulator

CST Studio Suite Design Environment is an acknowledged commercial electromagnetic simulation software that encompasses several independent functional studios - CST Microwave Studio (CST MWS), CST EM Studio (CST EMS), CST Particle Studio (CST PS), CST Cable Studio (CST CS), CST PCB Studio (CST PCBS), CST Boardcheck, CST MPHYSICS Studio (CST MPS) and CST Design Studio (CST DS). These modules are integrated in a user-friendly design environment that enables to choose the most appropriate method for the design and optimization of devices operating in a wide range of frequencies.

This dissertation uses the CST Microwave Studio as the simulation tool to document and replicate the theoretical model, because it allows optimization instead of experimentation and a virtual prototyping before the physical trial. The implementation of the CST MWS enables a fast and accurate 3D EM simulation of the high frequency (HF) found in the theoretical model and a quick insight into the EM behaviour of the high frequency designs.

The advantage of CST Microwave Studio is that contains the transient solver for efficient calculation of loss-free and lossy structures, it can calculate 3D eigenmodes and finally it contains an advanced ACIS based, parametric solid modelling front-end function with excellent structure visualization that are fundamental to the present work.

3.2 Circuit Design

3.2.1 Substrate Materials

In order to design the circuits three different substrate materials were selected due to their very different dielectric constant:

i. RT DUROID 5880 ($\varepsilon = 2.2$)
ii. FR-4 ($\varepsilon = 4.3$)
iii. EPSILAM-10 ($\varepsilon = 10.2$)

The first two substrates used for the design purpose were dimensioned to a 2 GHz frequency, since they both perform well at this value whereas the last substrate was dimensioned to 10 GHz, because it works better at this frequency.

The CAD equations developed on sub-section 2.1.2.3 allow to calculate the microstrip dimensions, and afterwards it will be possible to start designing them on CST.

3.2.1.1 RT DUROID 5880

The RT DUROID 5880 are PTFE composites reinforced with glass microfibers, which are randomly oriented for an exceptional dielectric constant uniformity It is a flexible material with a dielectric constant 2.2, dielectric thickness of 0.254 mm and its low dissipation factor extends to Ku-band and above. According to the manufacture "is designed for exacting microstrip circuit applications" because it "is easily cut, sheared and machined to shape. It has excellent dimensional stability and is resistant to all solvents and reagents, hot or cold, normally used in etching printed circuits or in plating edges and holes" [28].

The following equation allows to calculate the circuit wavelength for the RT DUROID 5880 substrate.

$$\lambda = \frac{c}{f} = \frac{3E8}{2E9} = 15\ cm$$

Analysing the three circuits, it is known that it would be required to calculate 3 different line impedance values, for a 50Ω, for a 35.36Ω and for a 70.71Ω lines. This operation was performed by using the CST Analytical Line Impedance Calculator, and the results are presented below (Table 2).

Table 2 - RT DUROID 5880 Line Impedance Parameters.

RT DUROID 5880					
50Ω		**35,36Ω**		**70,71Ω**	
h (mm)	0,787	**h (mm)**	0,787	**h (mm)**	0,787
w (mm)	2,445	**w (mm)**	3,968	**w (mm)**	1,403
ε_r	2,2	ε_r	2,2	ε_r	2,2
ε_{ef}	1,87	ε_{ef}	1,93	ε_{ef}	1,82
λ (m)	0,15	**λ (m)**	0,15	**λ (m)**	0,15
Guide λ (m)	0,11	**Guide λ (m)**	0,11	**Guide λ (m)**	0,11
Guide λ/4 (m)	0,027	**Guide λ/4 (m)**	0,027	**Guide λ/4 (m)**	0,028
In (mm)	27,42	**In (mm)**	26,99	**In (mm)**	27,80

3.2.1.2 FR-4

The FR-4 is a common material for printed circuit boards composed of woven fiberglass cloth with an epoxy resin binder that is flame resistant. The material contains significant mechanical

strength and keeps high mechanical values and electrical insulating qualities in both dry and humid conditions [29].

The following table 3 presents the wavelength data regarding the FR-4 substrate also done with CST Analytical Line Impedance Calculator.

Table 3 - FR-4 Line Impedance Parameters.

FR-4					
50Ω		**35,36Ω**		**70,71Ω**	
h (mm)	1,6	**h (mm)**	1,6	**h (mm)**	1,6
w (mm)	3,137	**w (mm)**	5,33	**w (mm)**	1,641
ε_r	4,3	ε_r	4,3	ε_r	4,3
ε_{ef}	3,27	ε_{ef}	3,42	ε_{ef}	3,11
λ (m)	0,15	**λ (m)**	0,15	**λ (m)**	0,15
Guide λ (m)	0,083	**Guide λ (m)**	0,081	**Guide λ (m)**	0,085
Guide λ/4 (m)	0,021	**Guide λ/4 (m)**	0,020	**Guide λ/4 (m)**	0,021
In (mm)	20,74	**In (mm)**	20,28	**In (mm)**	21,26

3.2.1.3 EPSILAM-10

The EPSILAM-10 is the trade name for the ceramic-filled resin. It was also conducted an analysis for the EPSILAM-10, with the same approach as before.

$$\lambda = \frac{c}{f} = \frac{3E8}{10E9} = 0{,}3\ cm$$

The CST Analytical Line Impedance Calculator was also utilized for this substrate and the results obtained are presented in table 4.

Table 4 - EPSILAM-10 Line Impedance Parameters.

Epsilam-10					
50Ω		**35,36Ω**		**70,71Ω**	
h (mm)	1,27	**h (mm)**	1,27	**h (mm)**	1,27
w (mm)	1,181	**w (mm)**	2,266	**w (mm)**	0,507
ε_r	10,2	ε_r	10,2	ε_r	10,2
ε_{ef}	6,83	ε_{ef}	7,25	ε_{ef}	6,49
λ (m)	0,030	**λ (m)**	0,030	**λ (m)**	0,030
Guide λ (m)	0,011	**Guide λ (m)**	0,011	**Guide λ (m)**	0,011
Guide λ/4 (m)	0,0027	**Guide λ/4 (m)**	0,0028	**Guide λ/4 (m)**	0,0029
In (mm)	2,87	**In (mm)**	2,78	**In (mm)**	2,94

3.2.2 Circuit Layout

The previous data along with the CST software enabled to accurately dimension and design the proposed circuits.

The *Quadrature Hybrid* is formed by two horizontal 50Ω lines, spaced by $\frac{\lambda}{4}$, and two vertical 35,36Ω, equally spaced by $\frac{\lambda}{4}$ (Fig. 3.1).

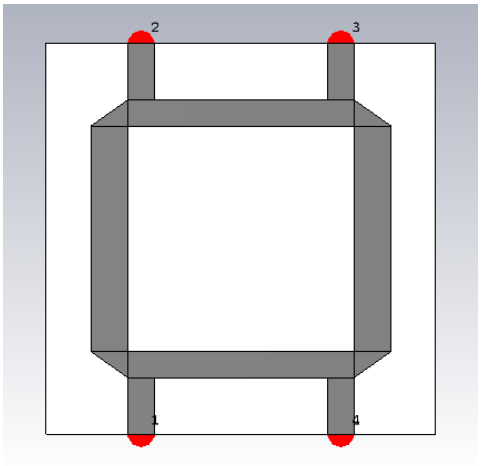

Figure 3.1 Quadrature Hybrid Computer Layout.

The *Wilkinson Power Divider*, comprises two horizontal 50Ω lines, and two vertical 70,71Ω, with a length of $\frac{\lambda}{4}$ (Fig. 3.2).

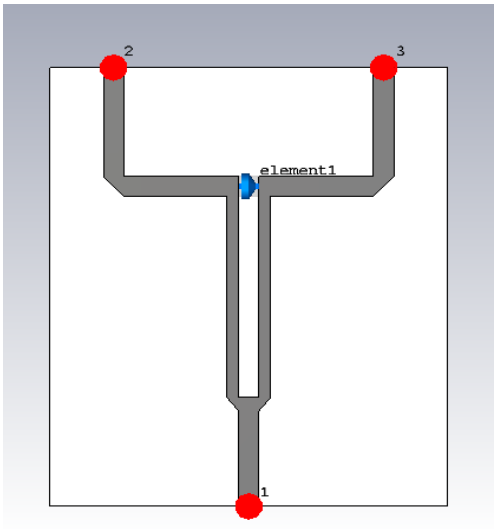

Figure 3.2 Wilkinson Power Divider Computer Layout.

The *Rat-Race*, composed by a 70.71Ω circular line, with four 50Ω lines (Fig. 3.3).

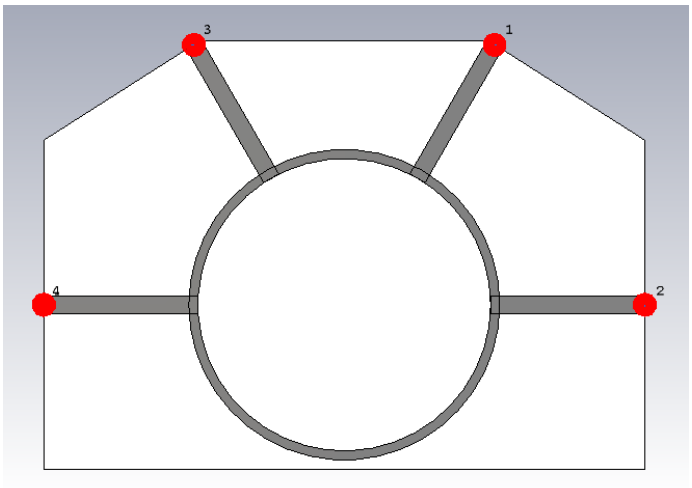

Figure 3.3 Rat-Race Computer Layout.

Since all the circuit layouts were similar for the different substrates with the exception of the respective dimensions, it was best accepted to present one image of each kind of circuit.

3.3 Simulation Results

After designing all the circuits, the CST *Frequency Domain Server* was used to simulate the circuits behaviour, obtaining the outcomes presented in this section.

Due to the circuits symmetry and reciprocity some of the results are overlapping other, for example S14 and S41.

3.3.1 Quadrature Hybrid

As stated before, each circuit was dimensioned and simulated for the three different substrates: RT DUROID 5880, FR-4 and EPSILAM-10, from the lowest to the highest dielectric constant.

3.3.1.1 RT DUROID 5880

The Rogers RT DUROID 5880 substrate applied in this work has a 31 mils thickness (0.787 *mm*), a 2.2 dielectric permittivity, with low losses and good homogeneity.

The simulations outcomes are clearly illustrated in figures 3.4 and 3.5.

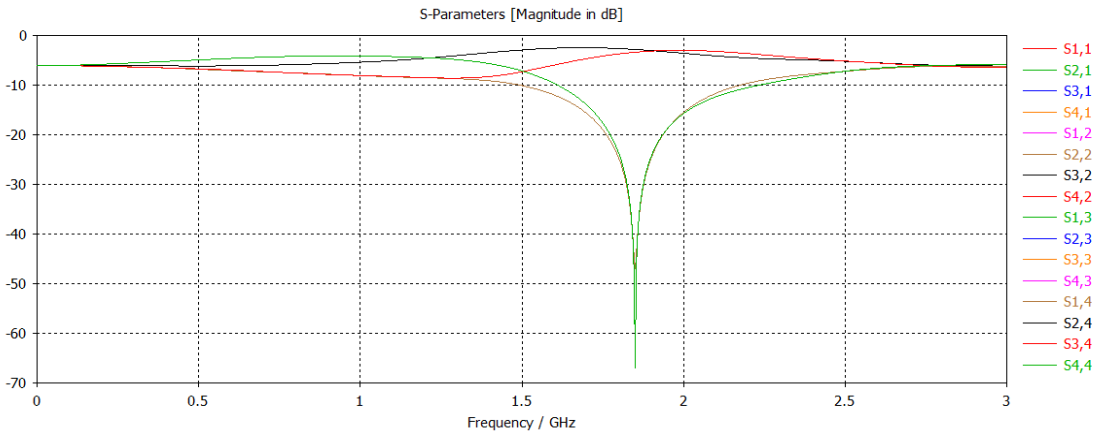

Figure 3.4 RT DUROID 5880 Quadrature Hybrid S-parameters.

These figures reveal that the circuit may not have been perfectly constructed, since it was expected to be dimensioned to 2GHz and not 1.85GHz. This difference might be a consequence of some material losses, since the chosen substrate is lossy.

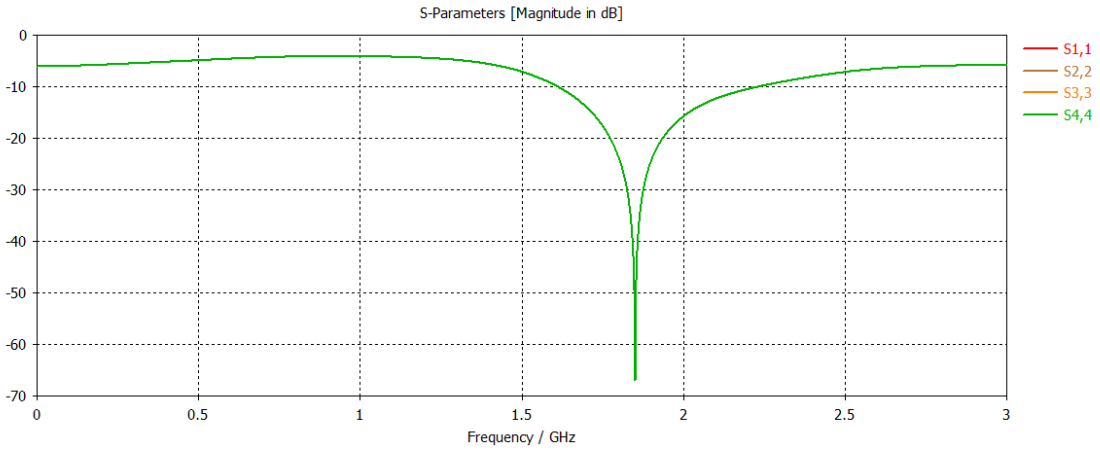

Figure 3.5 RT DUROID 5880 Quadrature Hybrid Return Loss.

Nevertheless, as expected, the phase difference between ports 2 and 3, demonstrated in figure 3.6, is almost perfect, i.e., with almost 90 degree, and maintained for nearly 0.6 GHz range. The insertion loss plot shown in figure 3.7, with the previous analysis, allows the conclusion that the microstrip was built correctly.

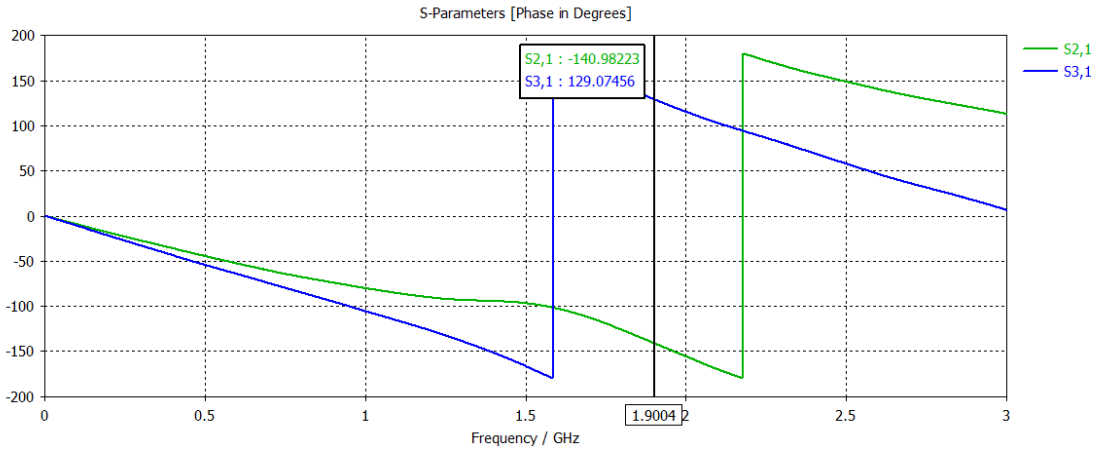

Figure 3.6 RT DUROID 5880 Quadrature Hybrid Ports 2 and 3 Phase Comparison.

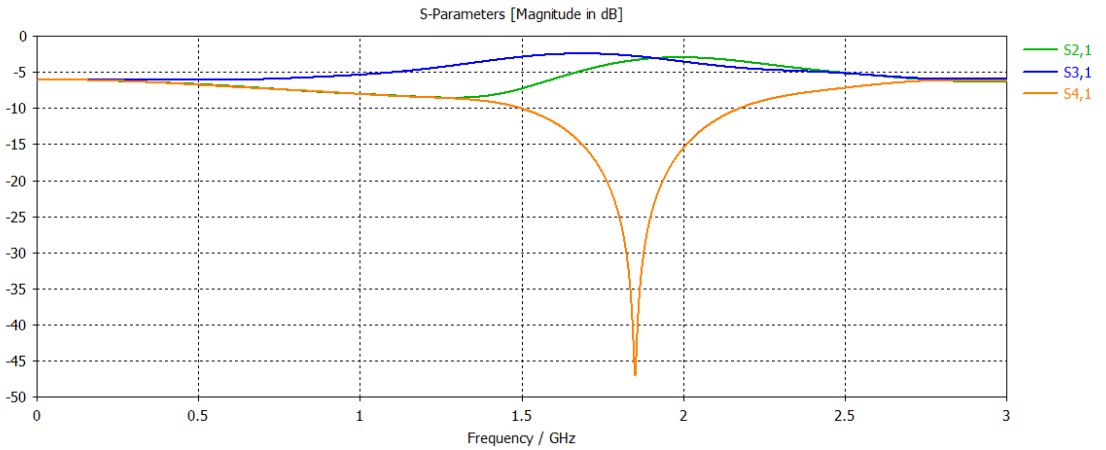

Figure 3.7 RT DUROID 5880 Quadrature Hybrid Insertion Loss..

Electric (e-field) and power field simulations have also been carried out to complement this study (Figs. 3.8 and 3.9).

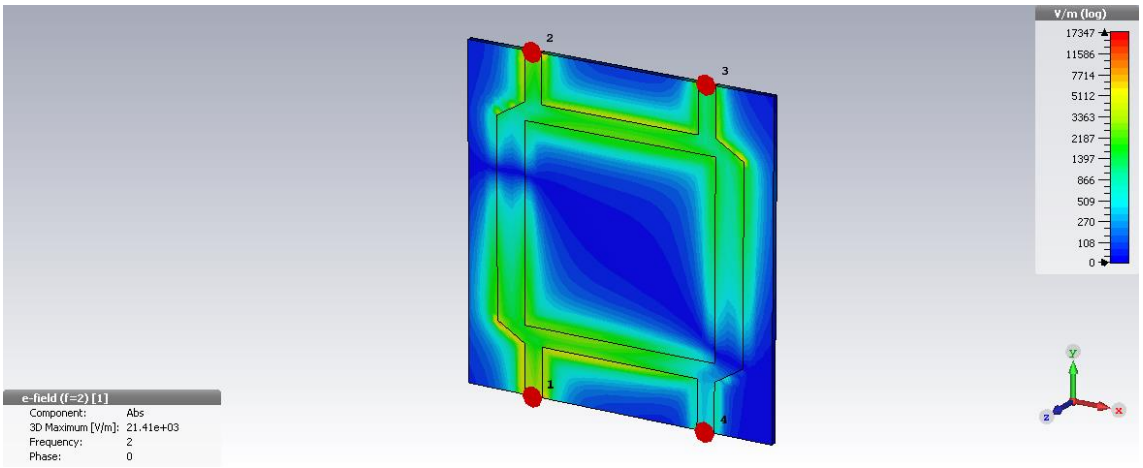

Figure 3.8 RT DUROID 5880 Quadrature Hybrid E-field Simulation.

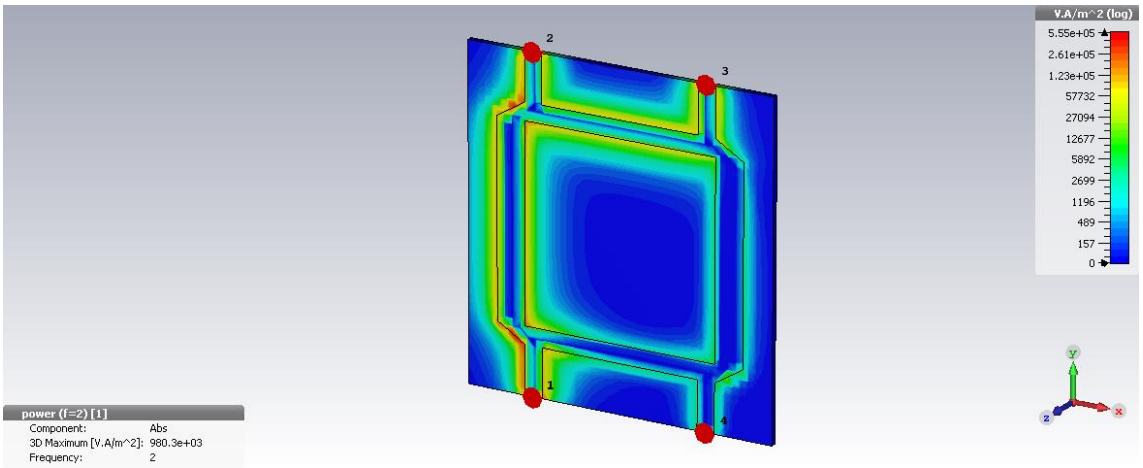

Figure 3.9 RT DUROID 5880 Quadrature Hybrid Power Field Simulation.

3.3.1.2 FR-4

The FR-4 substrate employed in this study had a 62 mils thickness (1.6 mm), with a 4.3 dielectric permittivity, that also presents low losses but not as homogeneous as the previous ones.

The results obtained with this substrate were pretty similar to the ones acquired with the RT DUROID 5880 (Fig. 3.10).

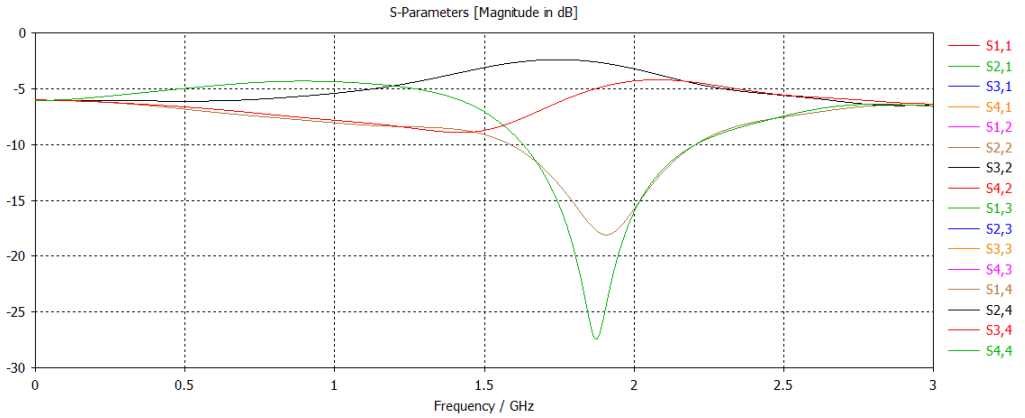

Figure 3.10 FR-4 Quadrature Hybrid S-parameters.

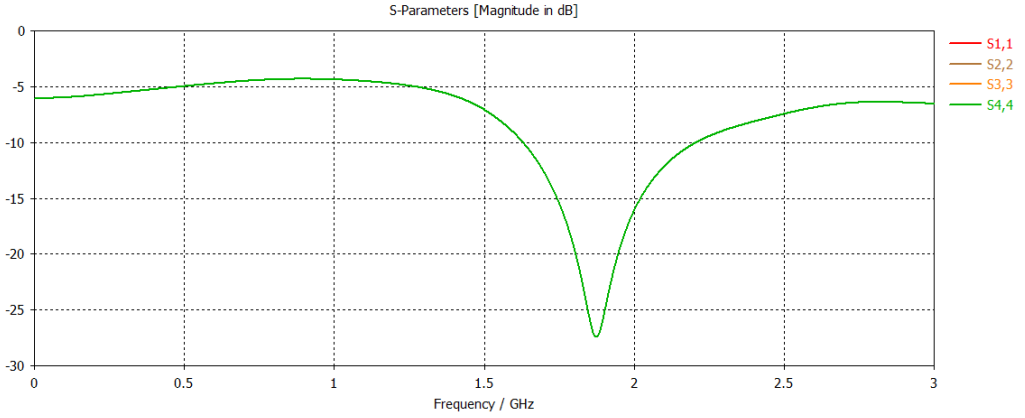

Figure 3.11 FR-4 Quadrature Hybrid Return Loss.

The analysis and comparison of the two substrates leads immediately to the conclusion that even though that both results are adequate, the RT DUROID 5880 achieves a better return loss - approx. -66 dB -, (Fig. 3.5), when compared with the FR-4 - approx. -27 dB -, (Fig. 3.11), providing,

therefore, a better isolation. Moreover, the comparison of the insertion loss, presented in figure 3.12, shows that the outcome of the RT DUROID 5880 is better.

Nevertheless, this substrate presents an approximately 90 degree phase between the second and third port (Fig. 3.13), consistent with the theoretical analysis.

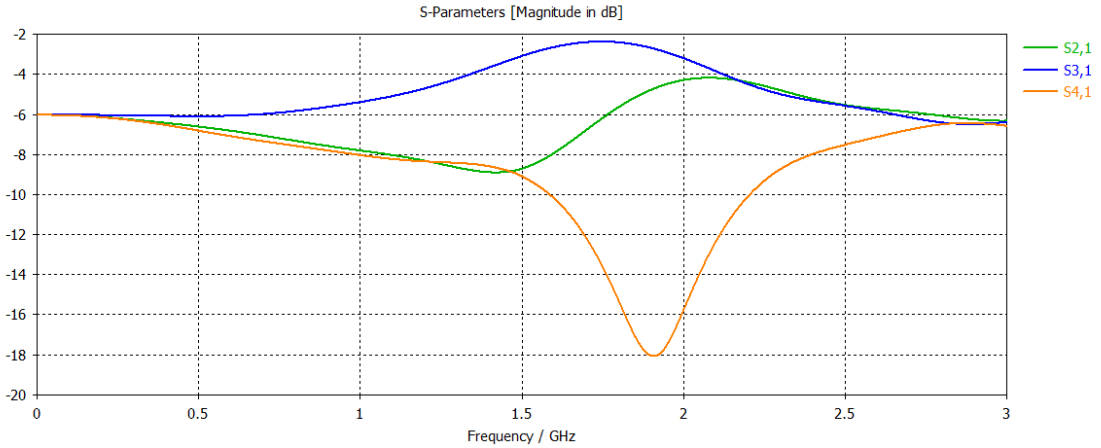

Figure 3.12 FR-4 Quadrature Hybrid Insertion Loss.

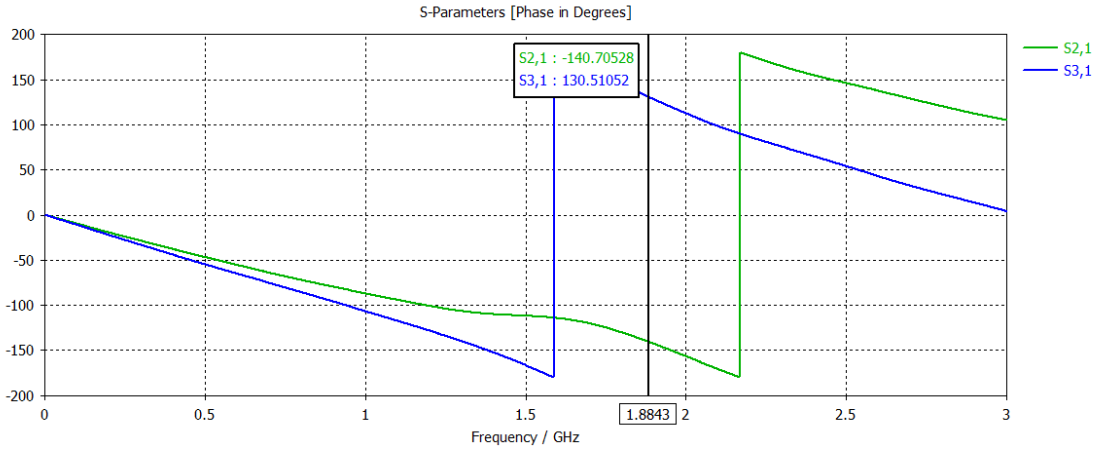

Figure 3.13 FR-4 Quadrature Hybrid Ports 2 and 3 Phase Comparison.

Despite the fact that RT DUROID 5880 does a very good job concerning the isolation of the Port 4, the analysis of the FR-4 shows that this last one performs better. The following pictures show the electric and power fields simulations of this aspect.

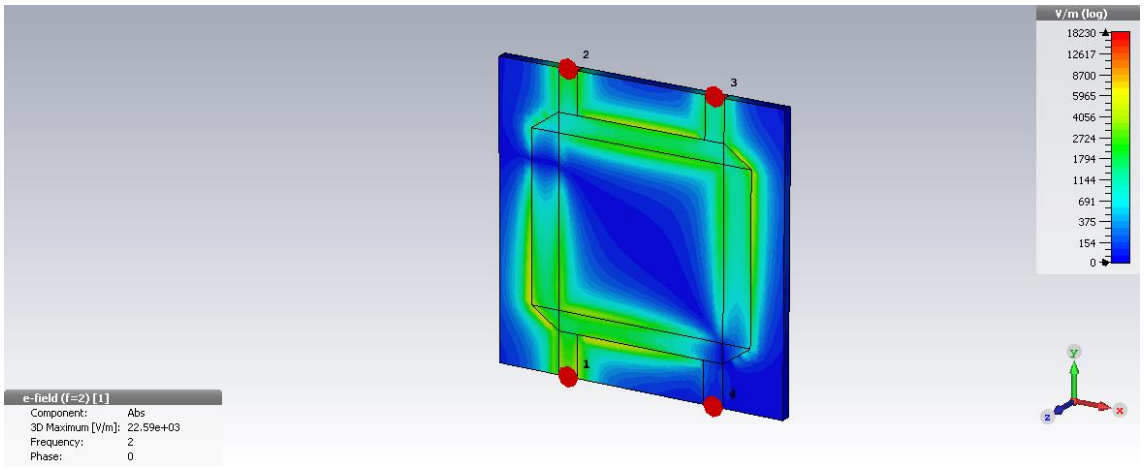

Figure 3.14 FR-4 Quadrature Hybrid E-Field Simulation.

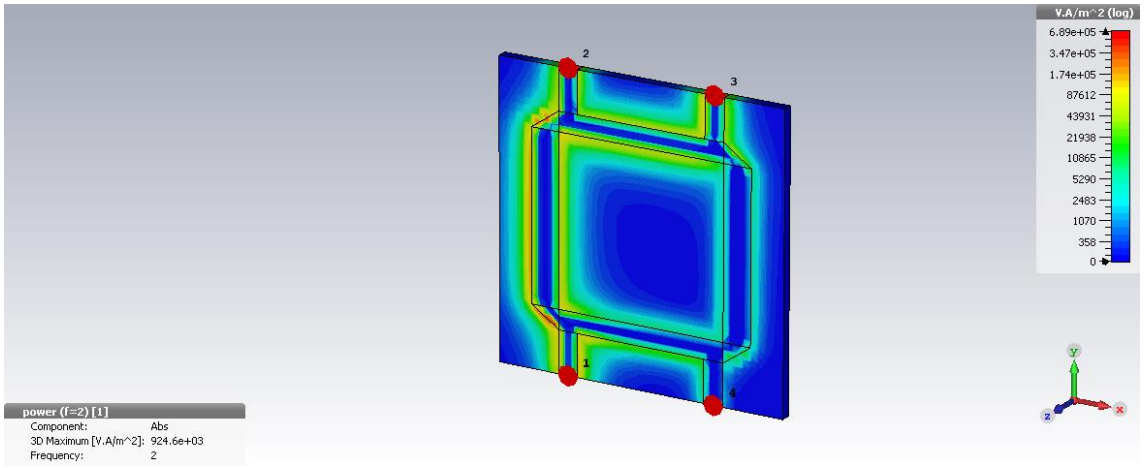

Figure 3.15 FR-4 Quadrature Hybrid Power Field Simulation.

3.3.1.3 EPSILAM-10

The EPSILAM-10 model was constructed according to the already mentioned calculated dimensions (Table 4). Although it seemed to be well dimensioned (Fig. 3.16), a deeper and accurately analysis revealed that this model did not work as expected (Fig. 3.17).

Based on the assumption Assuming that the model was done correctly - due to the fact that the other two were working as predicted -, it is presumed that the main reason for this circuit malfunction is the high amount of dielectric permittivity substrate for such a small circuit. For this reason, this substrate will not be considered forward in this study.

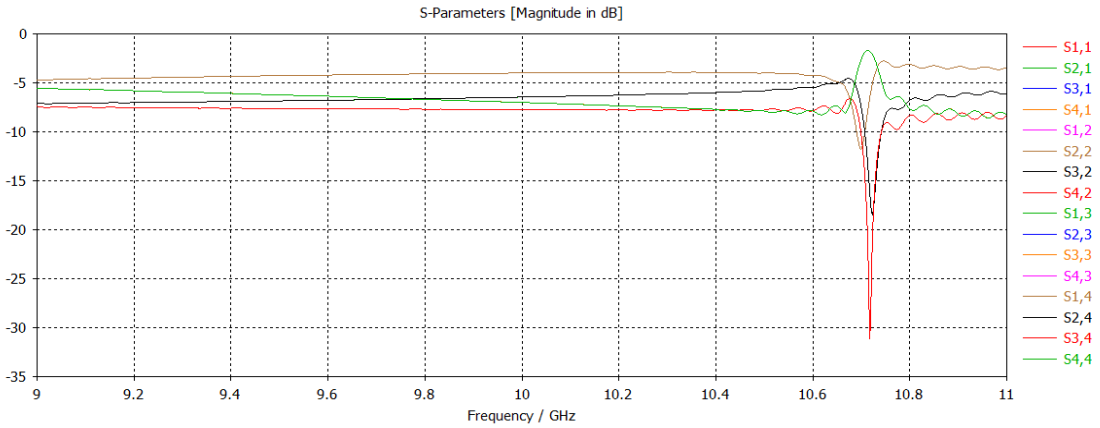

Figure 3.16 EPSILAM-10 Quadrature Hybrid S-parameters.

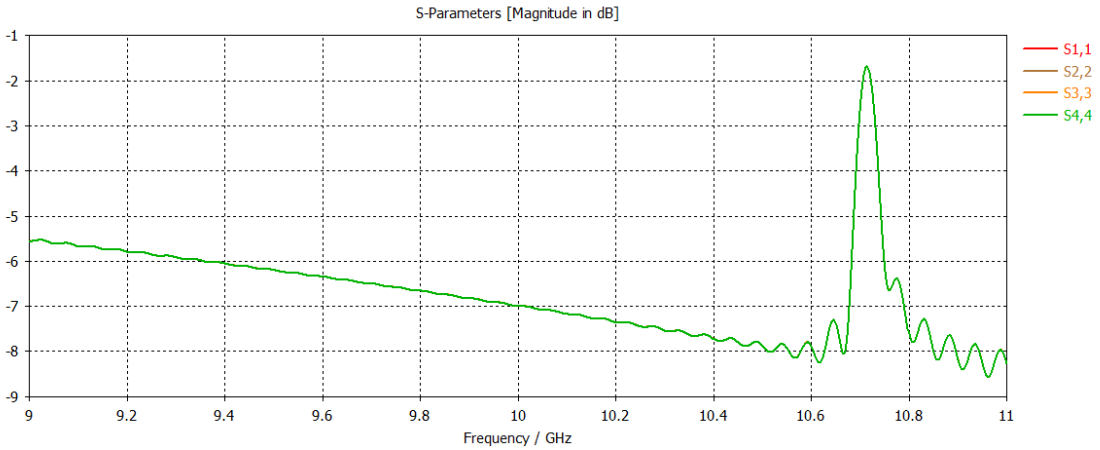

Figure 3.17 EPSILAM-10 Quadrature Hybrid Return Loss.

3.3.2 Rat-Race

As noted in the sub-section 3.3.1.3 and since the Rat-Race was not totally equal to the Quadrature Hybrid as it was expected, the development and simulation were only performed on the two working substrates, the RT DUROID 5880 and the FR-4. This was because it would not give relevant data regarding the main objectives of the present study

3.3.2.1 RT DUROID 5880

This simulation started with the lowest dielectric permittivity constant substrate, which allowed to achieve a very good result, i.e. the circuit main frequency performed very close of what it was expected, achieving the 2 GHz (Fig. 3.18).

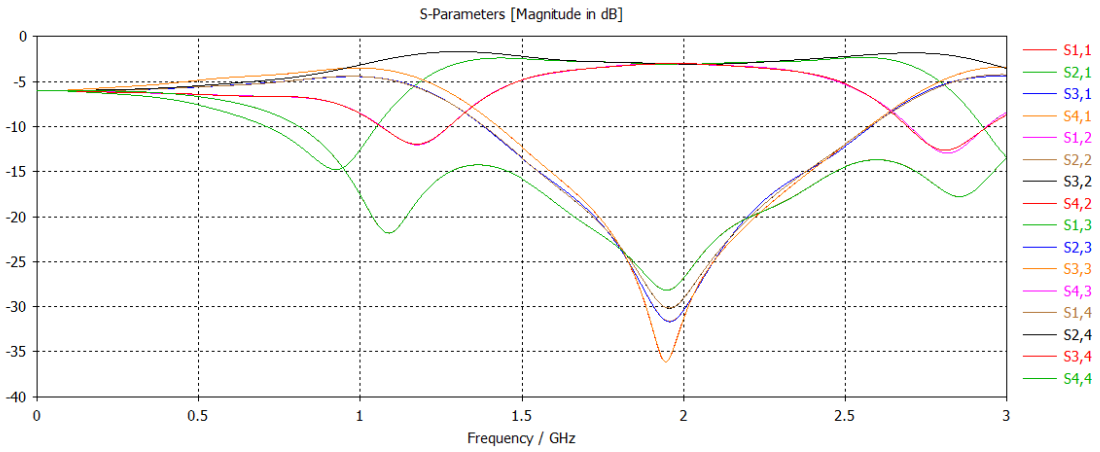

Figure 3.18 RT DUROID 5880 Rat-Race S-parameters.

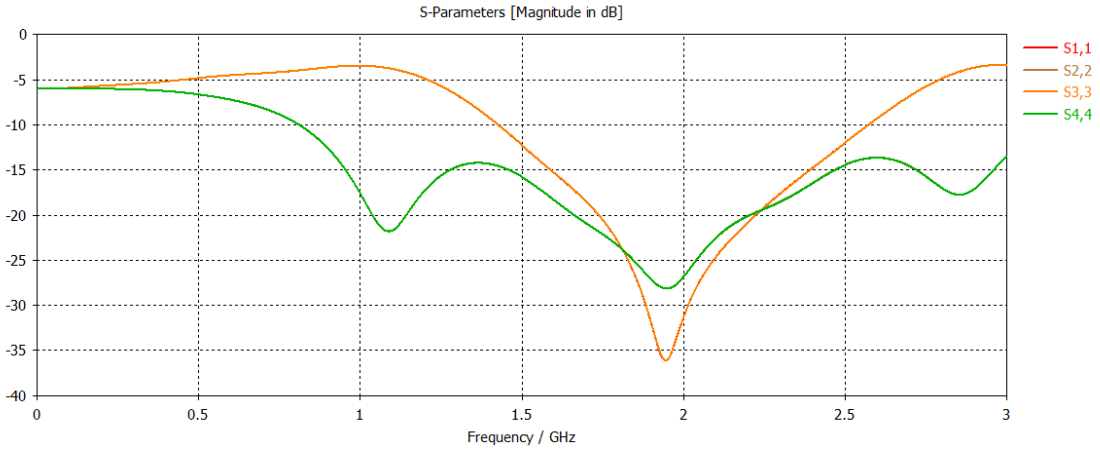

Figure 3.19 RT DUROID 5880 Rat-Race Return Loss.

The figure 3.20 shows that the insertion loss plot performed as expected and consistent with theoretical analysis, i.e., with the phase between port 2 and port 3 (Fig. 3.21), being very close to zero degrees and the port 1 achieving -3dB (Fig. 3.22).

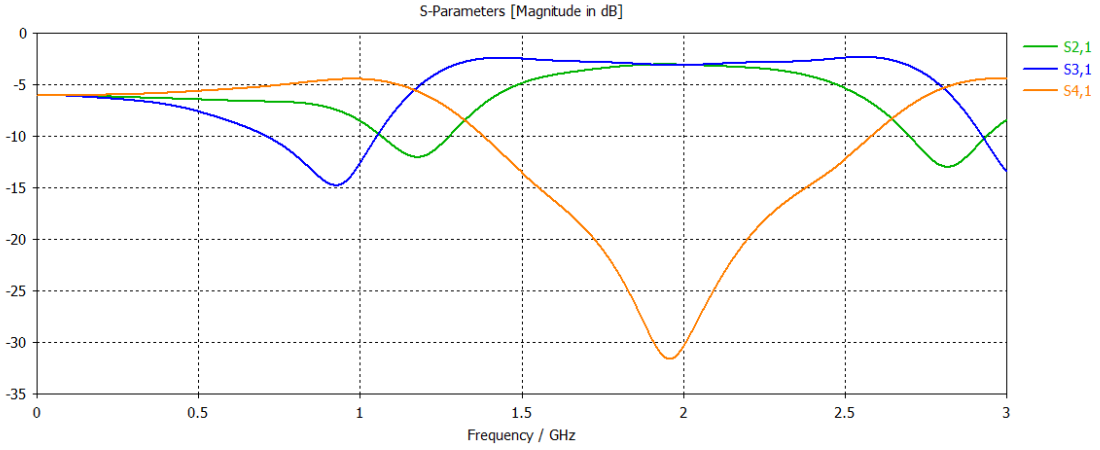

Figure 3.20 RT DUROID 5880 Rat-Race Insertion Loss.

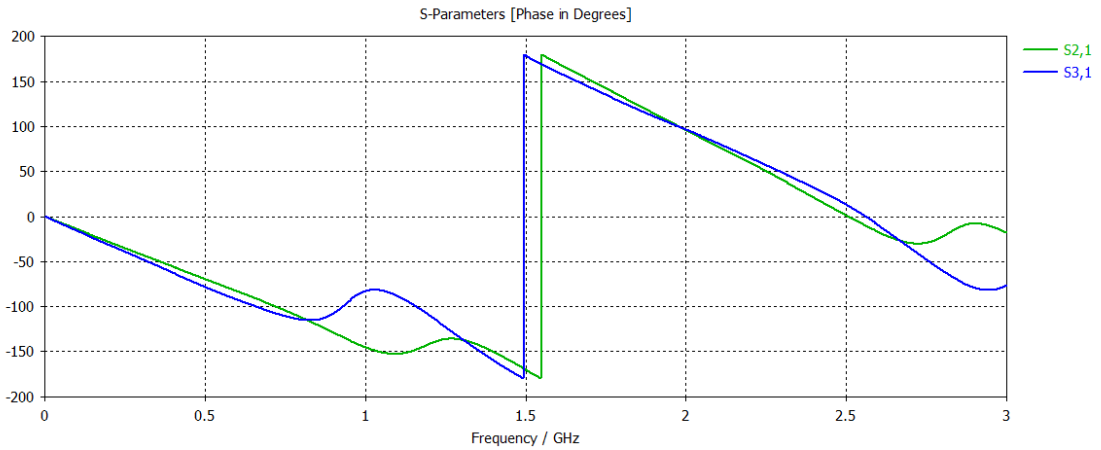

Figure 3.21 RT DUROID 5880 Rat-Race ports 2 and 3 phase comparison degree.

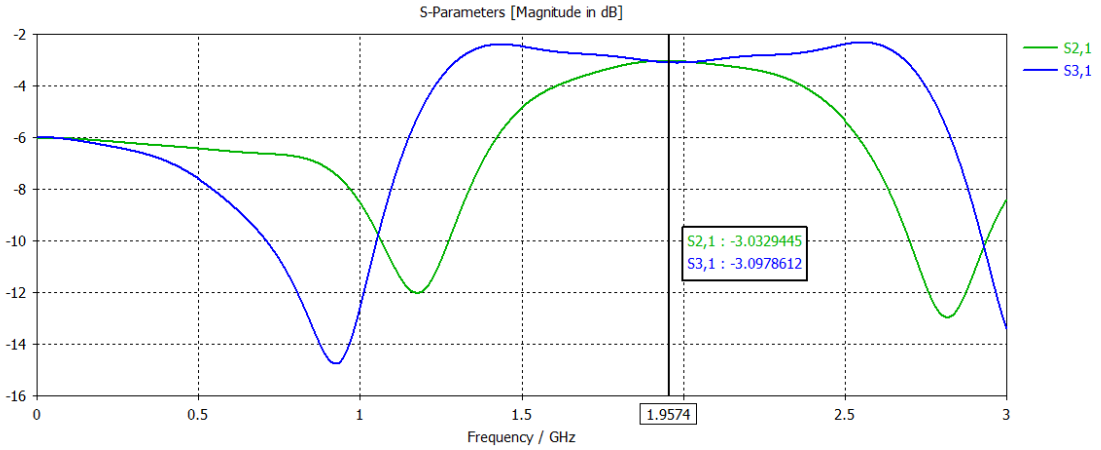

Figure 3.22 RT DUROID 5880 Rat-Race ports 2 and 3 comparison dB.

To conclude this aspect of the research, the electric, power and current view were plotted in order to validate the S-Matrix presented in the previous chapter, subsection 2.3.2 (figs. 3.23 and 3.24).

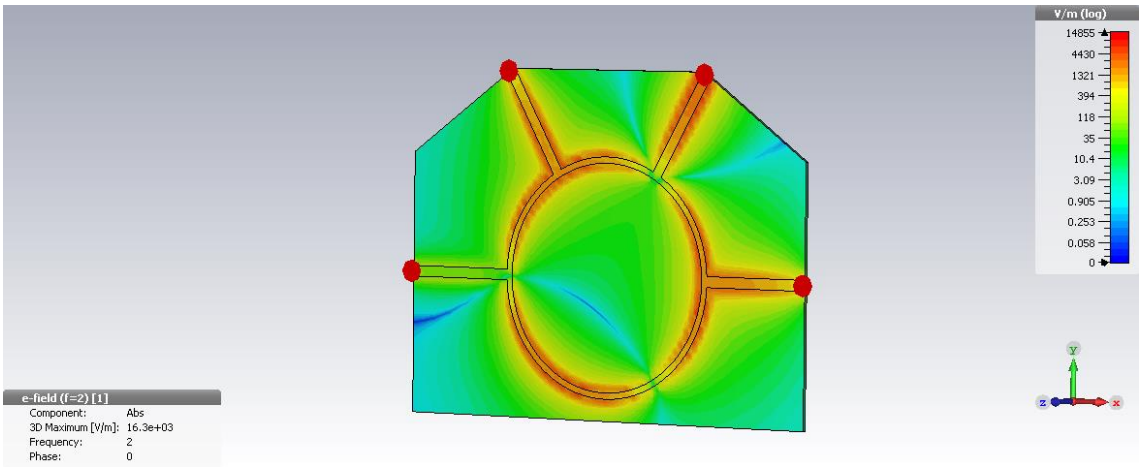

Figure 3.23 RT DUROID 5880 Rat-Race E-Field Simulation.

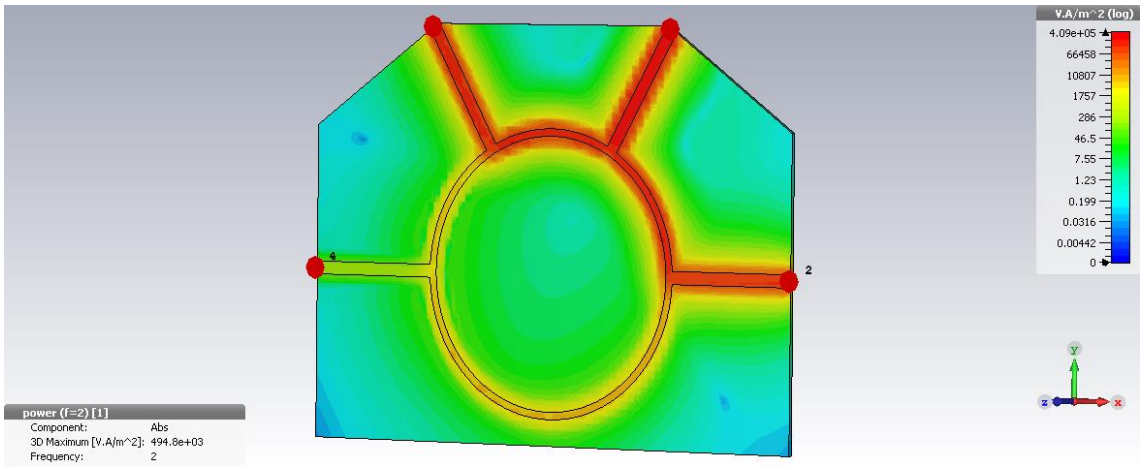

Figure 3.24 RT DUROID 5880 Rat-Race Power Field Simulation.

3.3.2.2 FR-4

The simulation performed with the FR-4 substrate presented results very similar to the ones achieved with the Quadrature Hybrid substrate. Both results, between the $\varepsilon_r = 2.2$ and the $\varepsilon_r = 4.3$ substrates, were closer to the values expected. The comparison between this substrate and the previous one regarding the return loss of the circuit, shows that ports 1 and 3 are less synchronized than before with ports 2 and 4 (figs. 3.25 and 3.26)

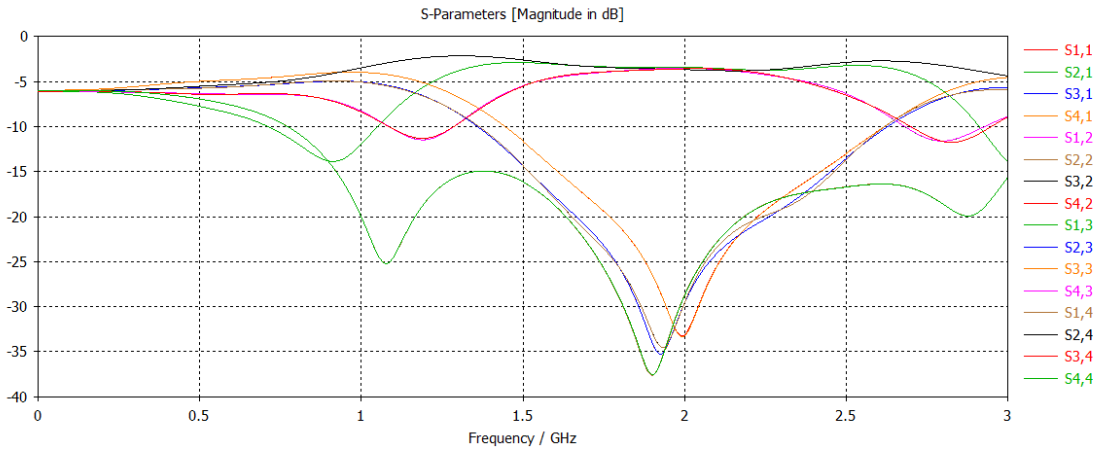

Figure 3.25 FR-4 Rat-Race S-parameters.

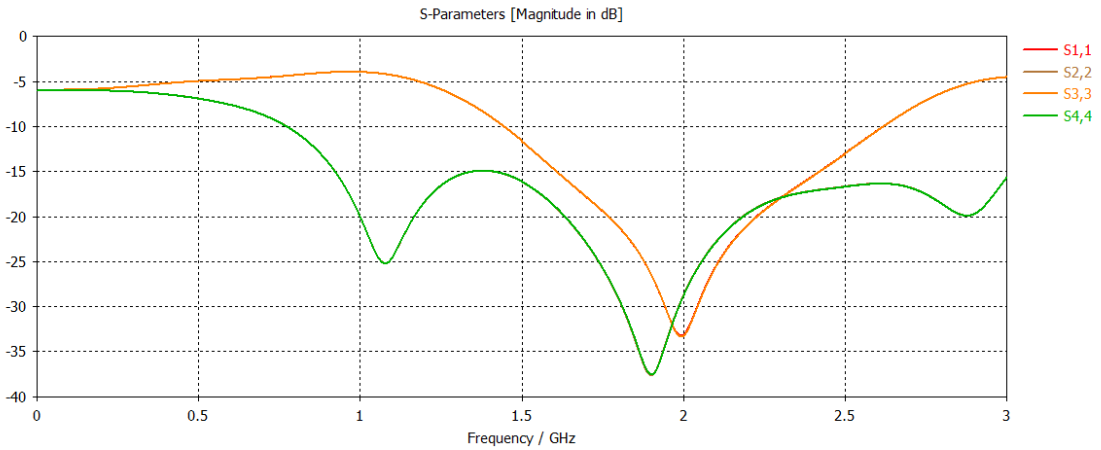

Figure 3.26 FR-4 Rat-Race Return Loss.

The transmission from the input of port 1 to the output of ports 2 and 3 show that they are close to phase, both in a -3 dB at central frequency (figs. 3.27 and 3.28).

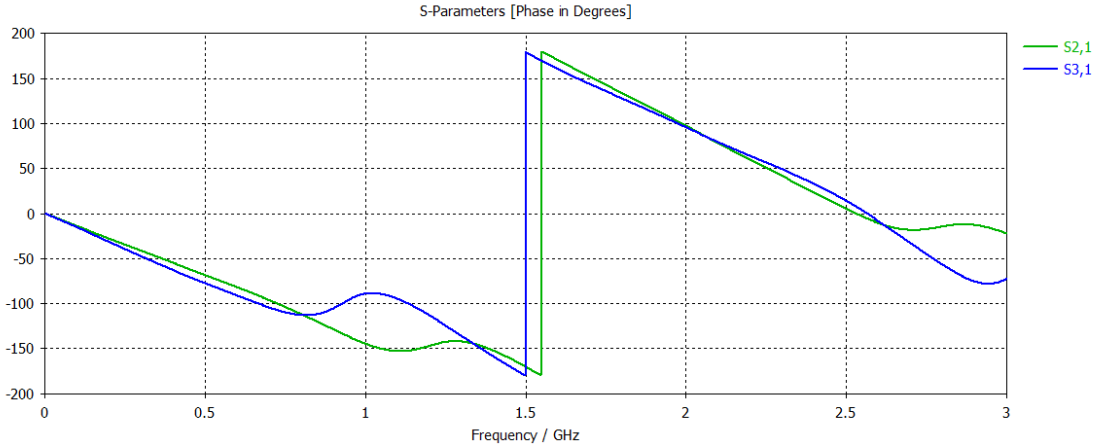

Figure 3.27 FR-4 Rat-Race Ports 2 and 3 Phase Comparison.

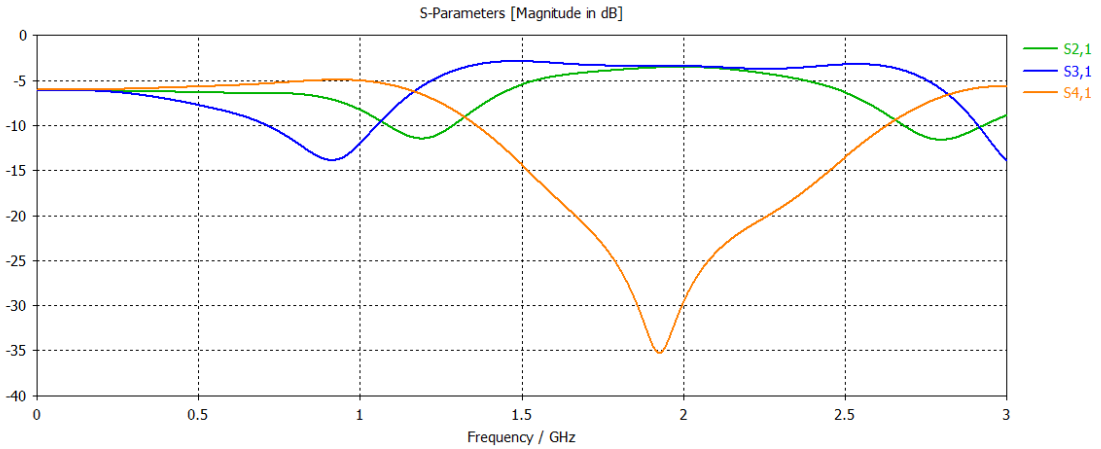

Figure 3.28 FR-4 Rat-Race Insertion Loss.

As in the previous sections, the following two figures enable to validate the preceding S-Matrix, demonstrating that when port 1 is used as the input port, the signal divides equally in-phase at ports 2 and 3, working as power divider, with port 4 as the isolation port (figs. 3.29 and 3.30).

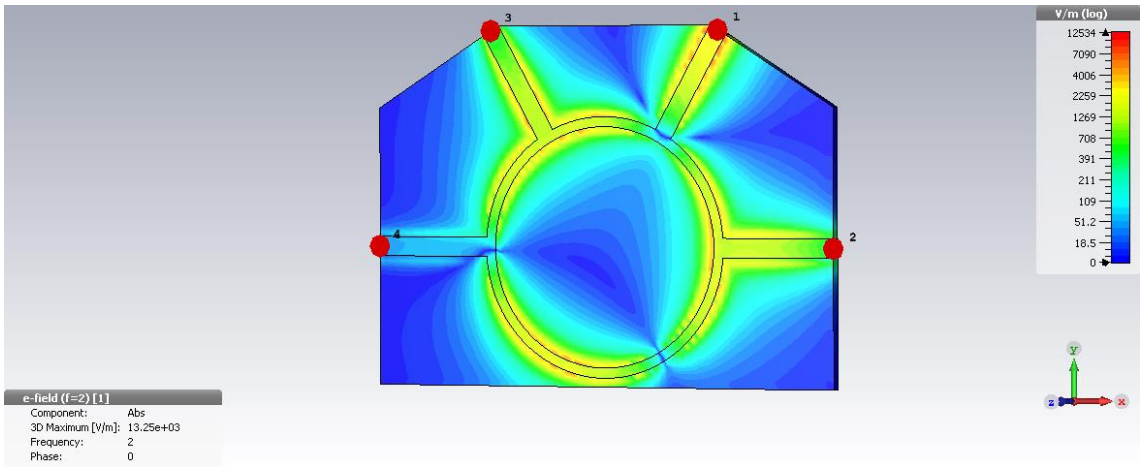

Figure 3.29 FR-4 Rat-Race E-Field Simulation.

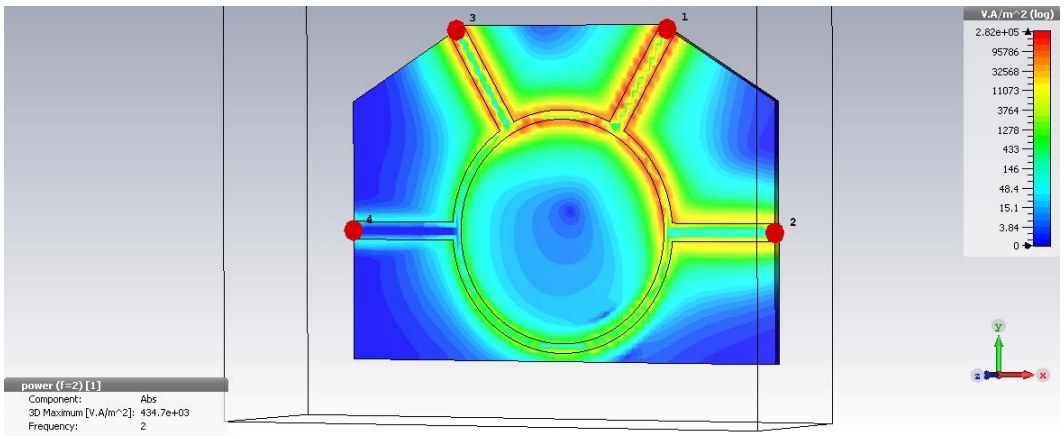

Figure 3.30 FR-4 Rat-Race Power Field Simulation.

3.3.3 Wilkinson Power Divider

The last simulations were done with the Wilkinson Power Divider. As with the last coupler, this one was only developed for the two lowest dielectric permittivity substrates – RT DUROID 5880 and FR-4. Two different models were designed and studied, nonetheless only the best solution is presented because the data obtained were not satisfactory for the scope of this work (Fig. 3.31).

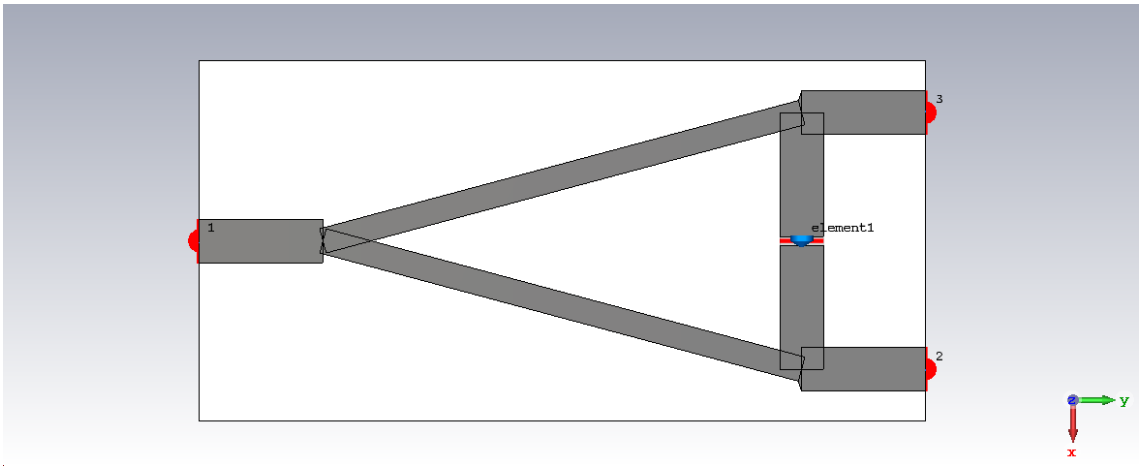

Figure 3.31 Wilkinson Power Divider First Layout.

3.3.3.1 RT DUROID 5880

The simulations done with the RT DUROID 5880 substrate show that even from the best model, the results were not perfect ones (Fig. 3.32). In this case, ports (2) and (3) have a large reflection coefficient (Fig. 3.33).

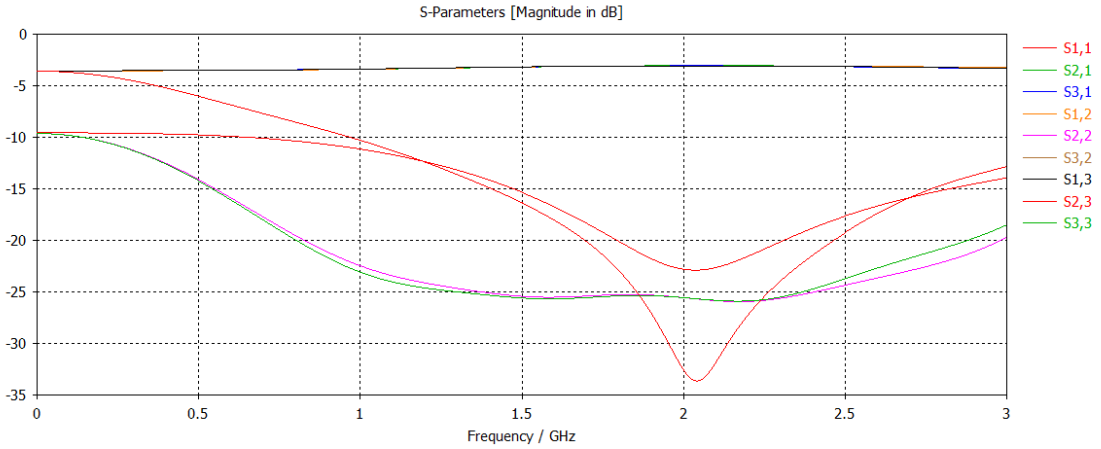

Figure 3.32 RT DUROID 5880 Wilkinson Power Divider S-parameters.

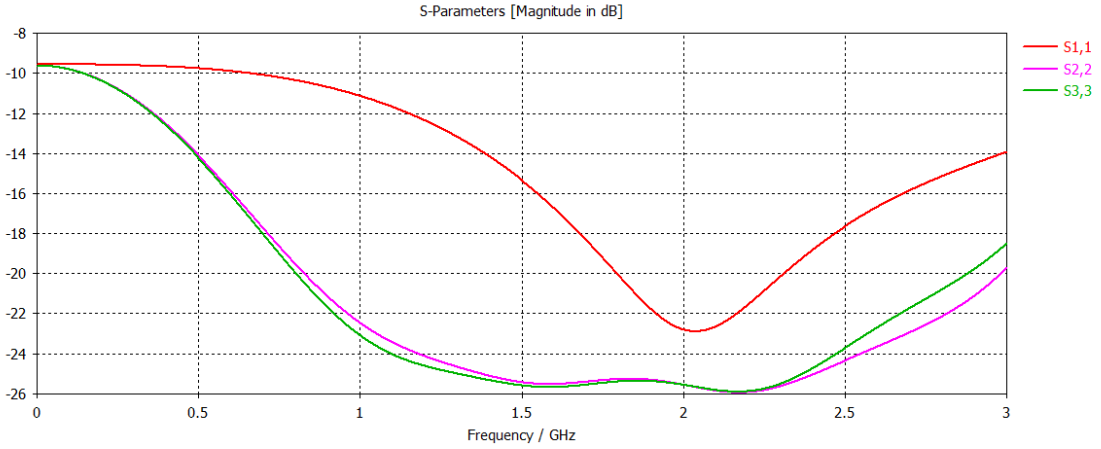

Figure 3.33 RT DUROID 5880 Wilkinson Power Divider Return Loss.

However, they have a very good insertion loss, near -3dB and are almost perfectly synchronized around the 0 degrees (figs. 3.34 and 3.35).

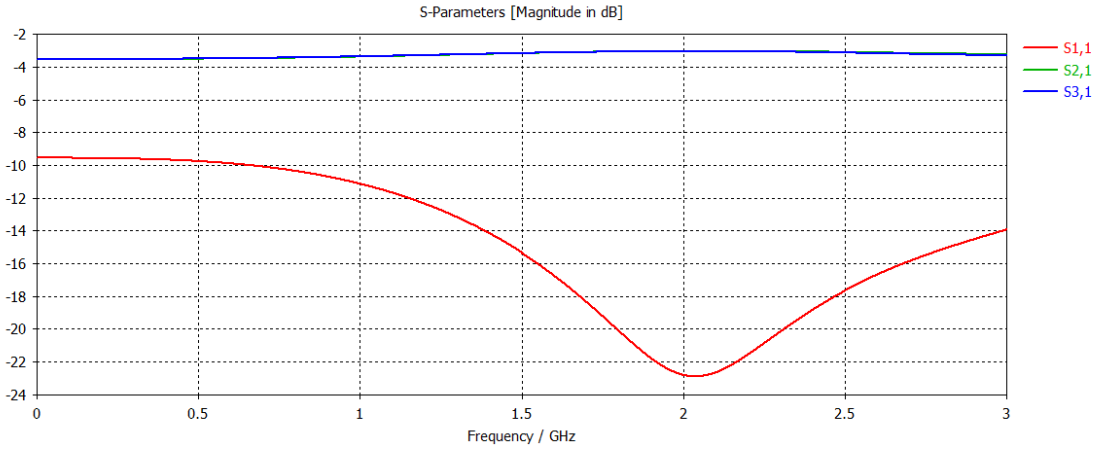

Figure 3.34 RT DUROID 5880 Wilkinson Power Divider Insertion Loss.

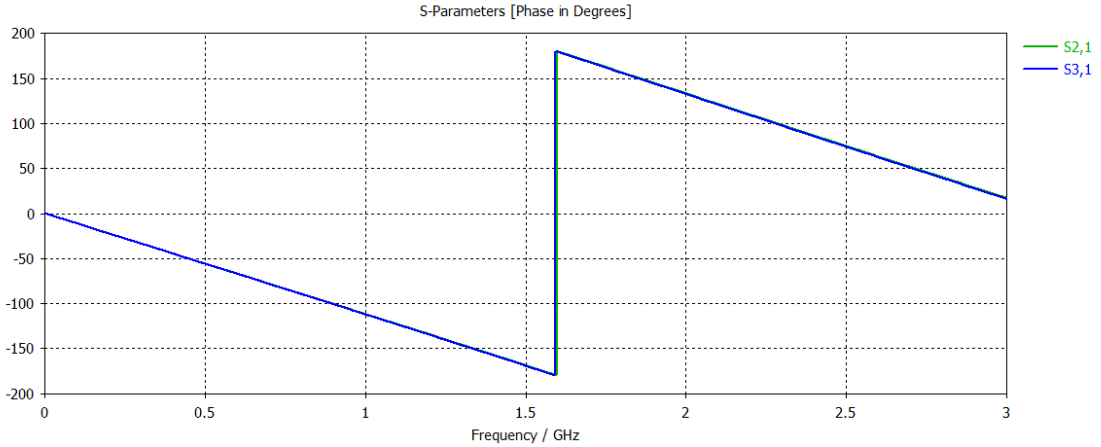

Figure 3.35 RT DUROID 5880 Wilkinson Power Divider Ports 2 and 3 Phase Comparison.

The following figures conclude this analysis by showing the great effectiveness of this power divider, working almost perfectly (figs. 3.36 and 3.37).

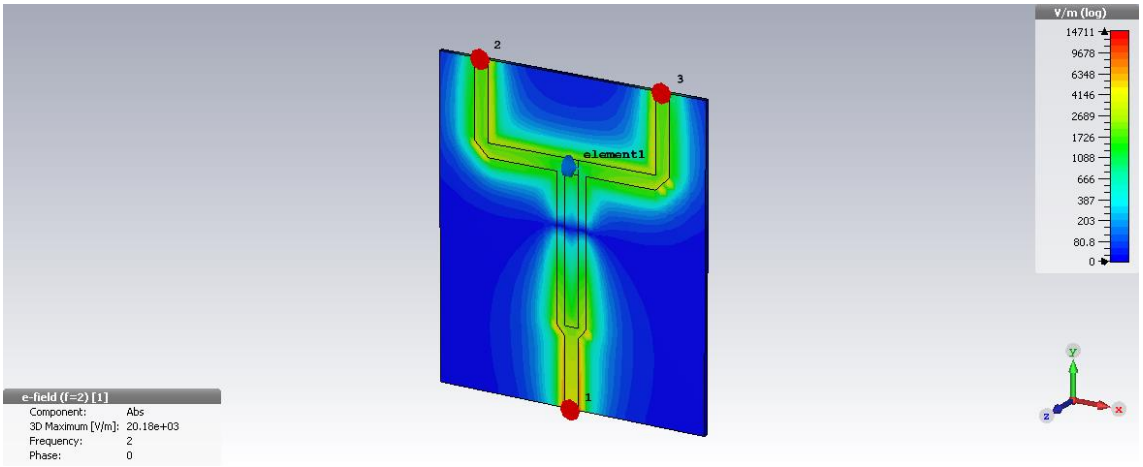

Figure 3.36 RT DUROID 5880 Wilkinson Power Divider E-Field Simulation.

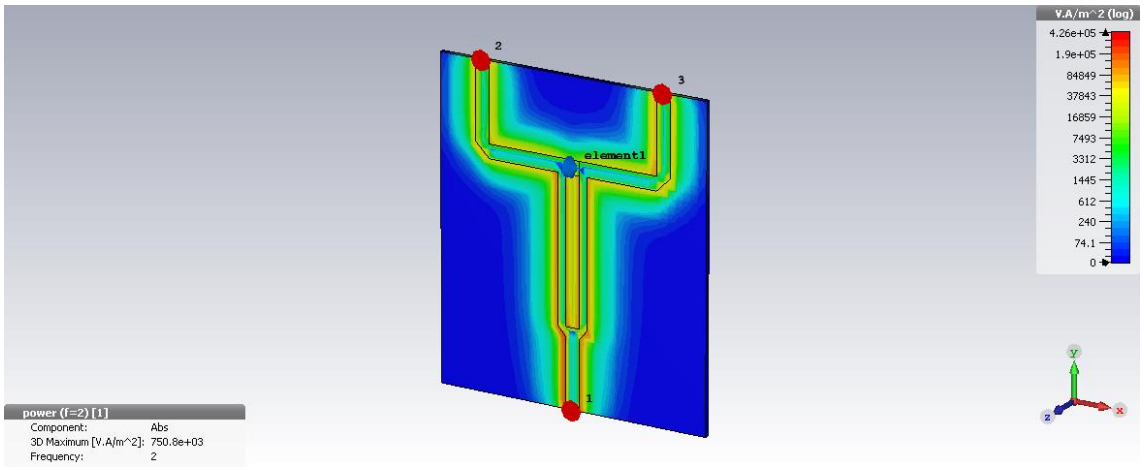

Figure 3.37 RT DUROID 5880 Wilkinson Power Divider Power Field Simulation.

3.3.3.2 FR-4

The comparison between the simulated and measured results done with the FR-4 substrate presented results similar to the previous substrate (figs. 3.38). It was expected to have a port 2 and 3 narrow bandwidth instead of the wide bandwidth shown in figure 3.39.

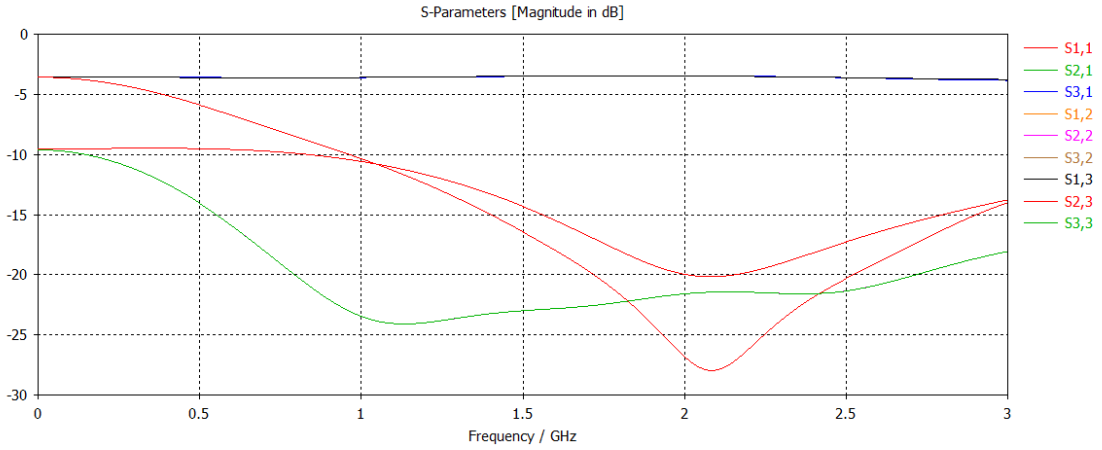

Figure 3.38 FR-4 Wilkinson Power Divider S-parameters.

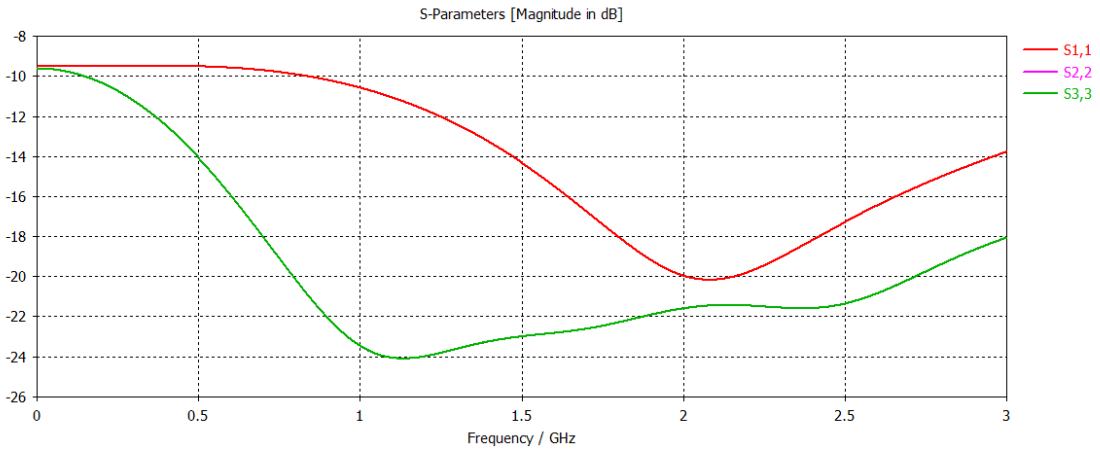

Figure 3.39 FR-4 Wilkinson Power Divider Return Loss.

Even though the ports 2 and 3 have a large bandwidth, the insertion loss performs better than the first one, presenting almost perfect synchrony with a 0 degree phase at -3dB, (figs. 3.40 and 3.41).

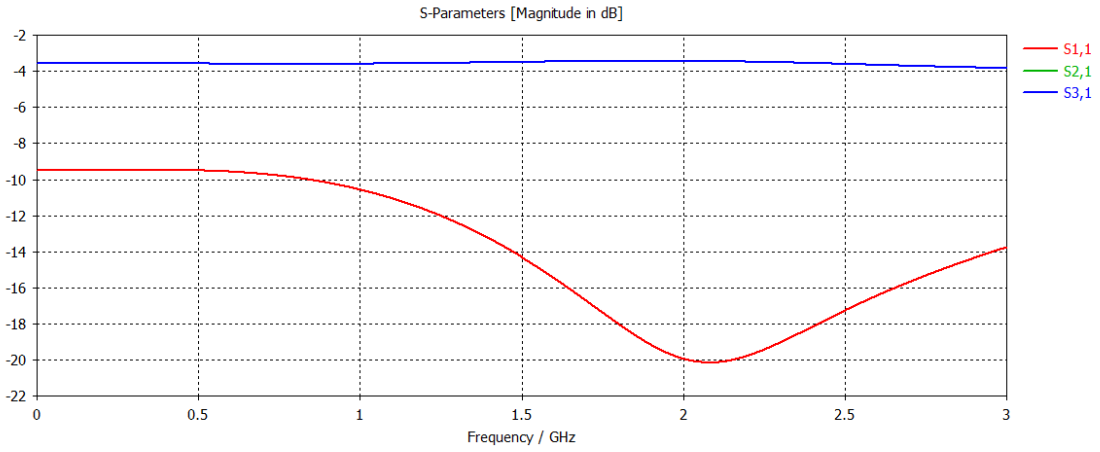

Figure 3.40 FR-4 Wilkinson Power Divider Insertion Loss.

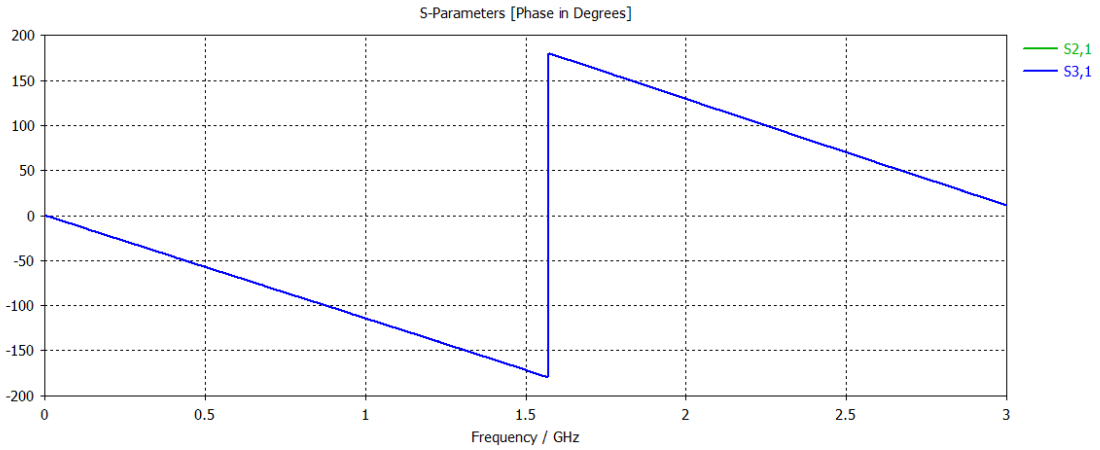

Figure 3.41 FR-4 Wilkinson Power Divider Ports 2 and Phase Comparison.

The following pictures shows that regardless the large bandwidth size of the ports 2 and 3, it works pretty well as power divider or as a coupler.

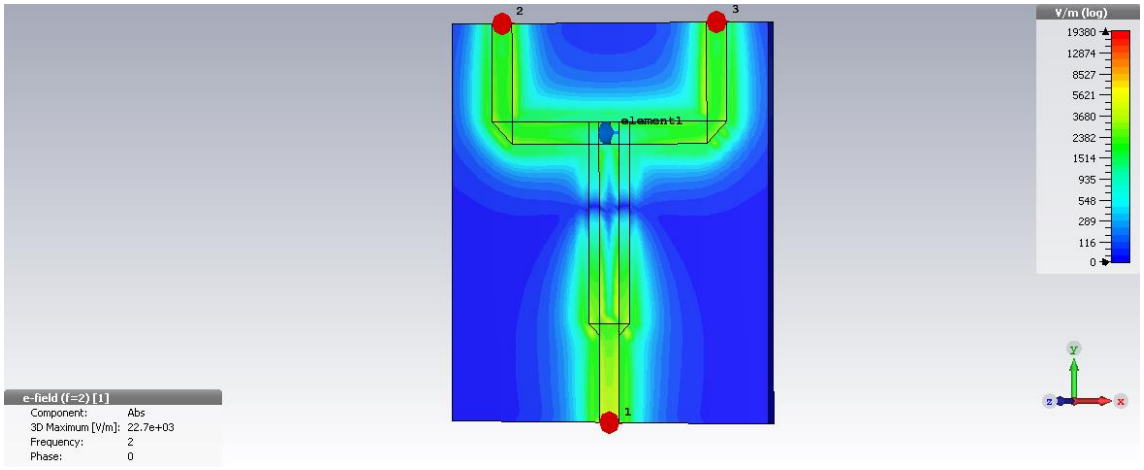

Figure 3.42 FR-4 Wilkinson Power Divider E-Field Simulation.

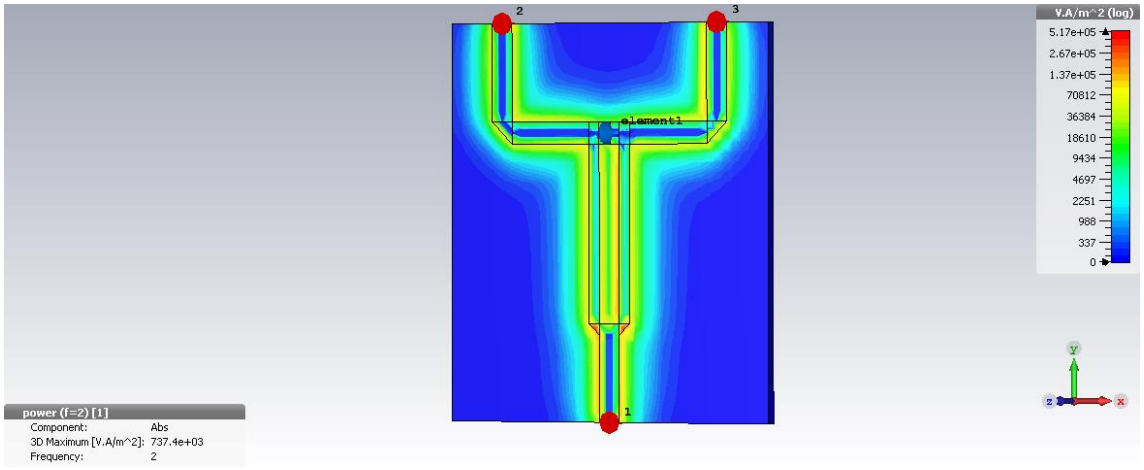

Figure 3.43 FR-4 Wilkinson Power Divider Power Field Simulation.

Chapter 4

Circuit Manufacturing and Testing

The manufacturing process consists of several steps. The first step was to export a DXF file from CST and, with the aid of the 2D CAD software ABViewer 14, import the DXF and export it to a PDF file (Fig. 4.1).

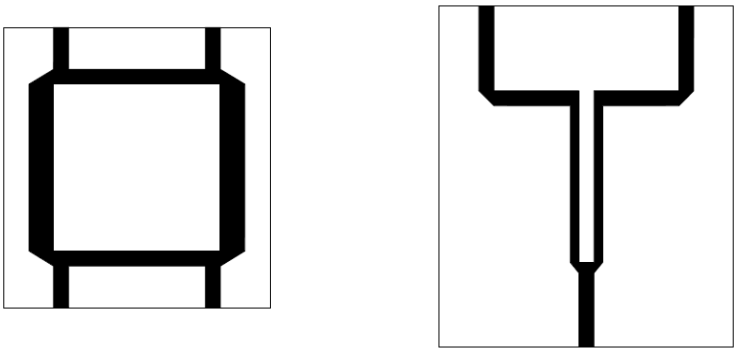

Figure 4.1 Circuit Layouts Exported.

This PDF file is later printed on a photo-sensitive acetate sheet, which allows to start the printed circuit process, described on the next subsection.

All the prototypes have been printed on the selected substrates on Laboratorio de Circuitos Impressos of Universidade de Lisboa – Instituto Superior Técnico.

4.1 Circuit Printing

The circuit printing process can be divided into several steps:

1. After cutting the desired substrate, it is necessary to apply a pre-treatment to the material by cleaning the surface with detergent to remove any dust or grease.
2. Then, a thin layer of varnish is applied on both faces of the material. The board is sprayed at a distance of 20 cm, and should not be exposed to daylight.
3. The board is now placed on a dark room and allowed to let dry at room temperature for 24 hours.

4. Next, the substrate is placed under the acetate sheet and exposed to an ultraviolet light. This light will burn the ultraviolet sensitive varnish in every part of the plate, with exception of the printed circuit marked on the sheet (Fig. 4.2).

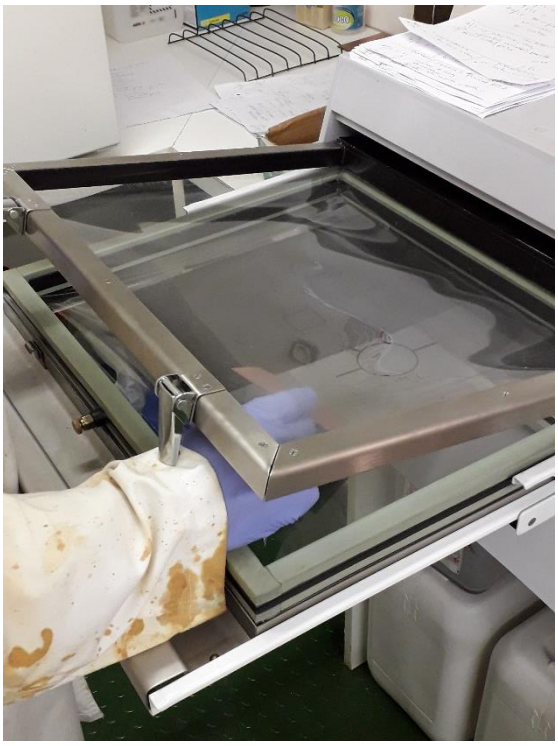

Figure 4.2 Circuits Exposure to Ultraviolet Light.

5. After the exposure, the board will be immersed into a developer liquid with a caustic soda and water solution. After a short period of time, the image of the conductor is now visible.
6. Since the varnish used is resistant to acid baths, the substrate placed on an iron chloride mixture that will remove every piece of cooper that isn't covered by varnish, revelling the circuit.
7. Later the circuit is washed and cut into the right dimensions as shown on the figure 4.3.
8. To conclude the process, the ports and the resistors are welded to the board with the final results presented on following subsection.

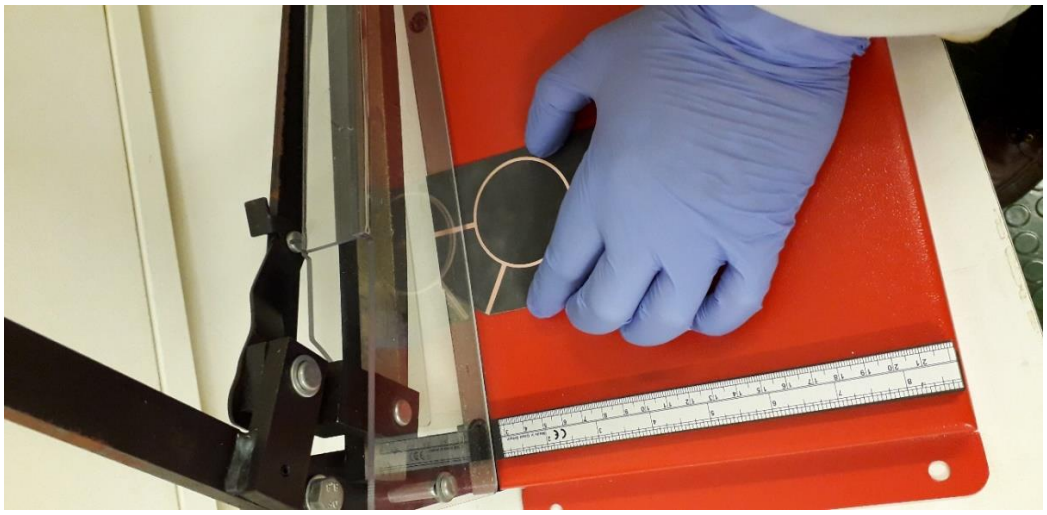

Figure 4.3 Rat-Race Circuit Cutting.

4.2 Circuit Testing and Results

As concluded on the previous chapter, of the three substrates that were designed, constructed and simulated, only two of them have achieved adequate results – the RT DUROID 5880 and the FR-4. Furthermore, and as specified before, the FR-4 is not a homogeneous substrate, so it is expected to have different results regarding the circuit testing. For these reasons it was decided to only test the FR-4 substrate on one circuit - the Rat-Race -, and test the RT-DUROID 5880 substrate on all circuits.

4.2.1 Quadrature Hybrid

Figure 4.4 shows the prototype of the quadrature hybrid impressed on the RT-DUROID 5880 substrate.

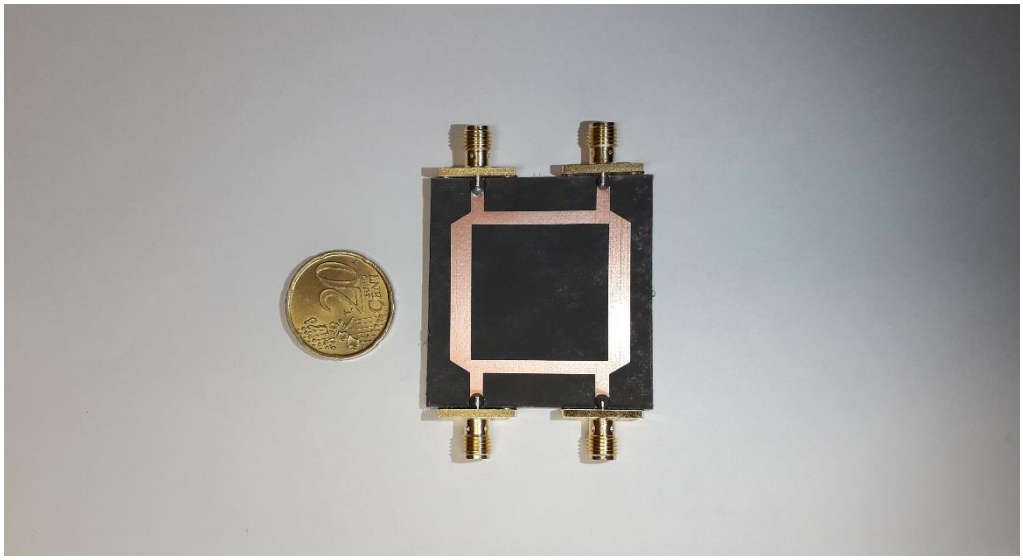

Figure 4.4 RT DUROID 5880 Quadrature Hybrid Prototype.

This circuit was fabricated and later measured with a Vector Network Analyzer (VNA), which was calibrated to measure the respective S-parameters (figs. 4.5 and 4.6).

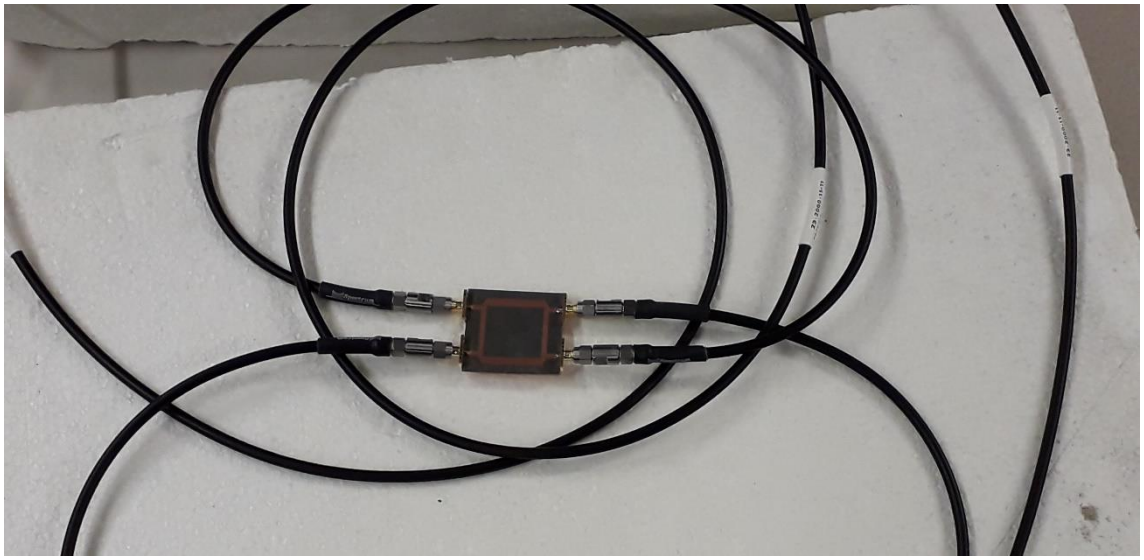

Figure 4.5 RT DUROID 5880 Quadrature Hybrid VNA Connections.

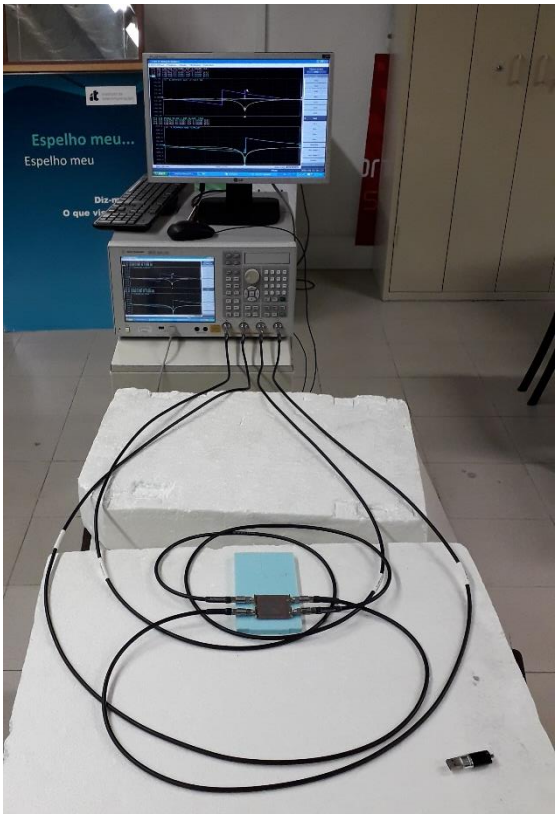

Figure 4.6 RT DUROID 5880 Quadrature Hybrid VNA Analysis.

Figure 4.7 shows the Quadrature Hybrid coupler S parameters with an operating frequency from 100 MHz to 3 GHZ. It could be concluded that the output presented is very similar to the simulated one, presented in figure.

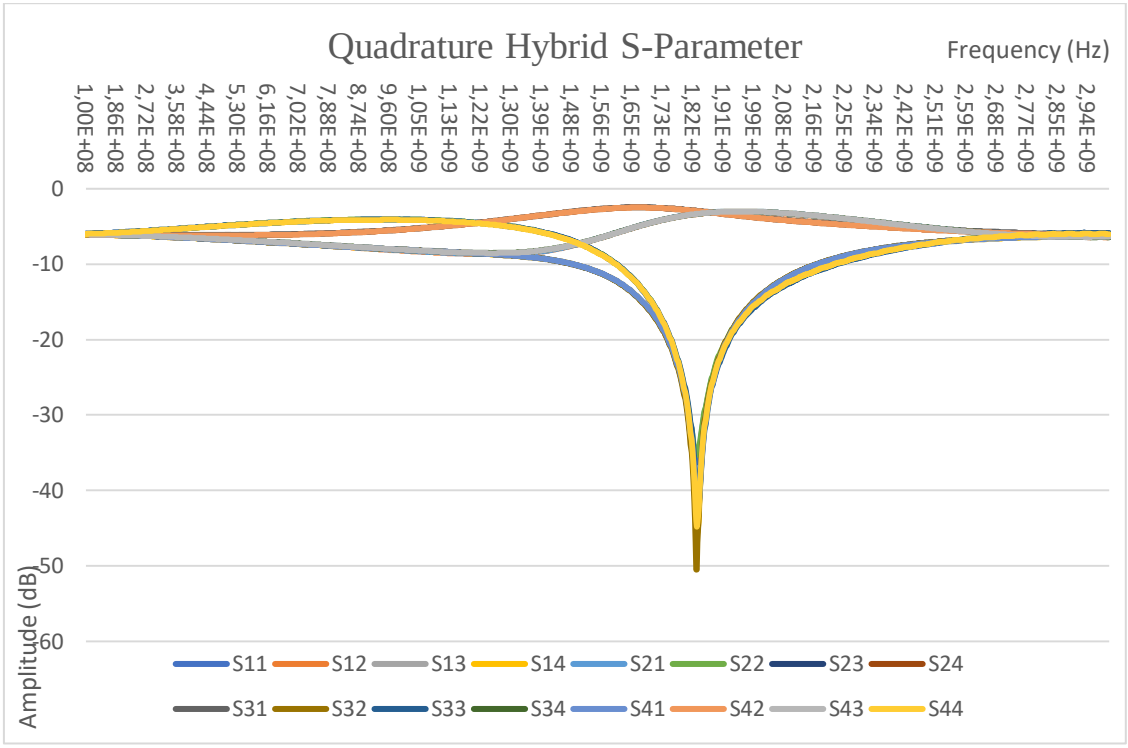

Figure 4.7 RT-DUROID 5880 Quadrature Hybrid S-parameters.

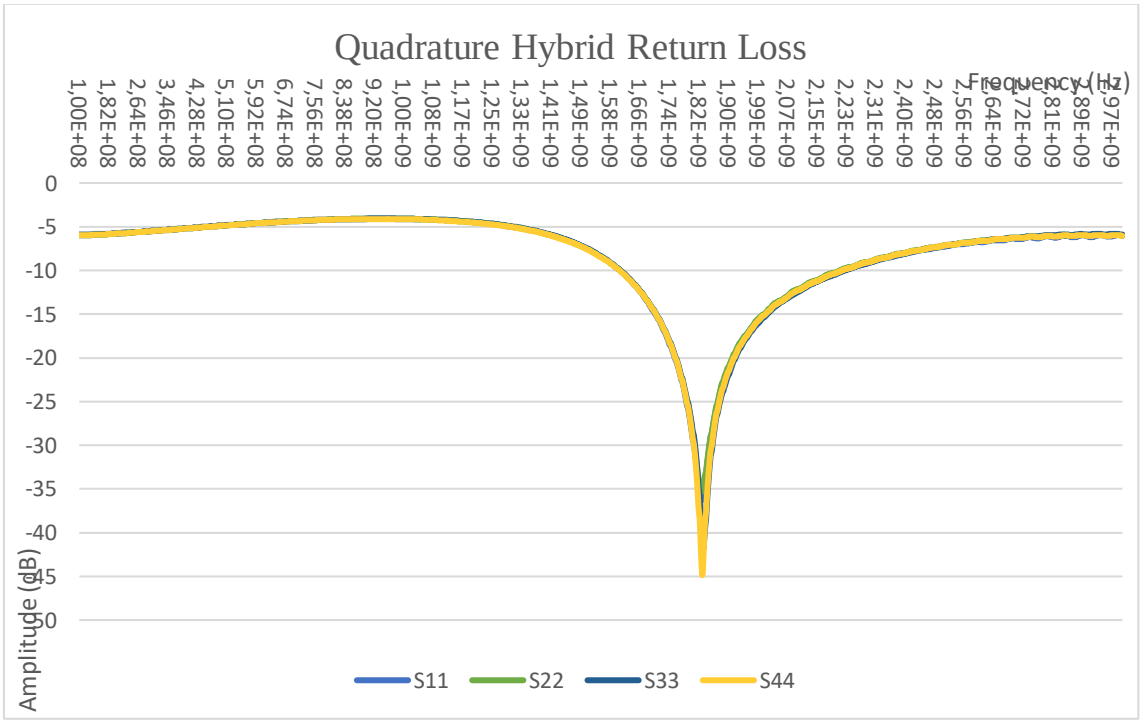

Figure 4.8 RT-DUROID 5880 Quadrature Hybrid Return Loss.

Figure 4.8 show the ports return losses, as happened in the simulation there is a small deviation of the centre frequency, but all ports achieve a lower than -35 dB at around 1,83 GHz (Table 5), revealing that the device is correctly isolated.

Table 5 RT-DUROID 5880 Quadrature Hybrid Return Loss Values.

Parameters	Centre Frequency (GHz)	Max Return Loss (dB)	Band > 15dB (GHz)
S11	1.830	-36.31	1.702 - 2.008
S22	1.830	-35.32	1.704 - 2.004
S33	1.834	-41.81	1.704 - 2.012
S44	1.832	-44.86	1.704 - 2.008

The figure 4.9 show the ports insertion losses. It is observed that there is an approximately -3dB equal power split between the 2 and 3 output ports, leaving port 4 isolated. The measured results are approximated the same as the theoretical and the simulated ones.

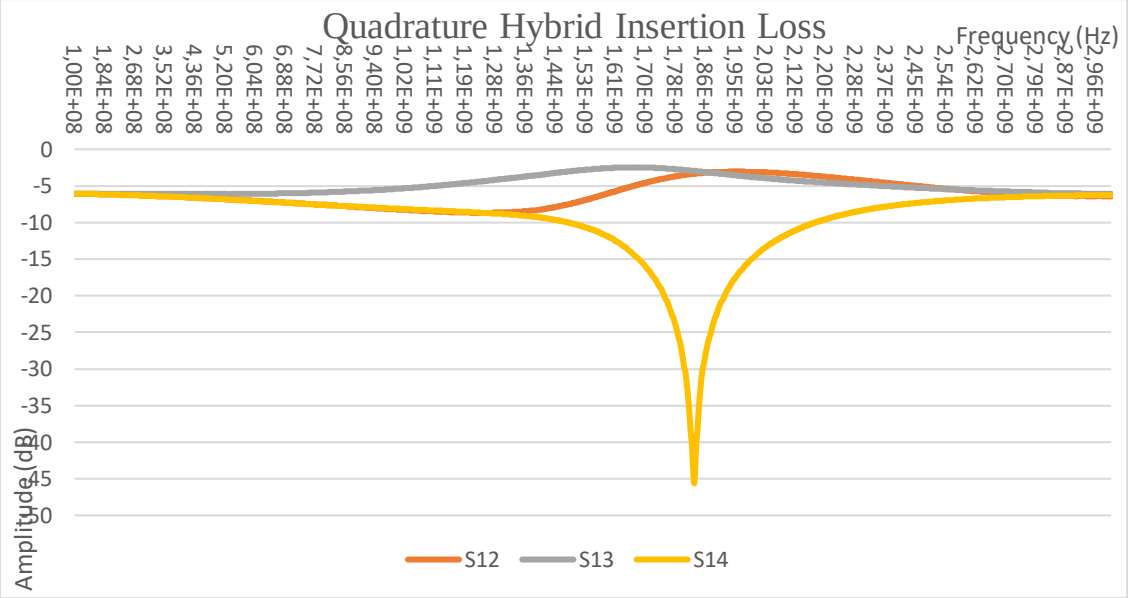

Figure 4.9 RT-DUROID 5880 Quadrature Hybrid Insertion Loss.

Figure 4.10 show the port 2 and 3 amplitude phase comparison. The simulated and measured phase results are alike, showing almost perfect quadrature between (2) and (3).

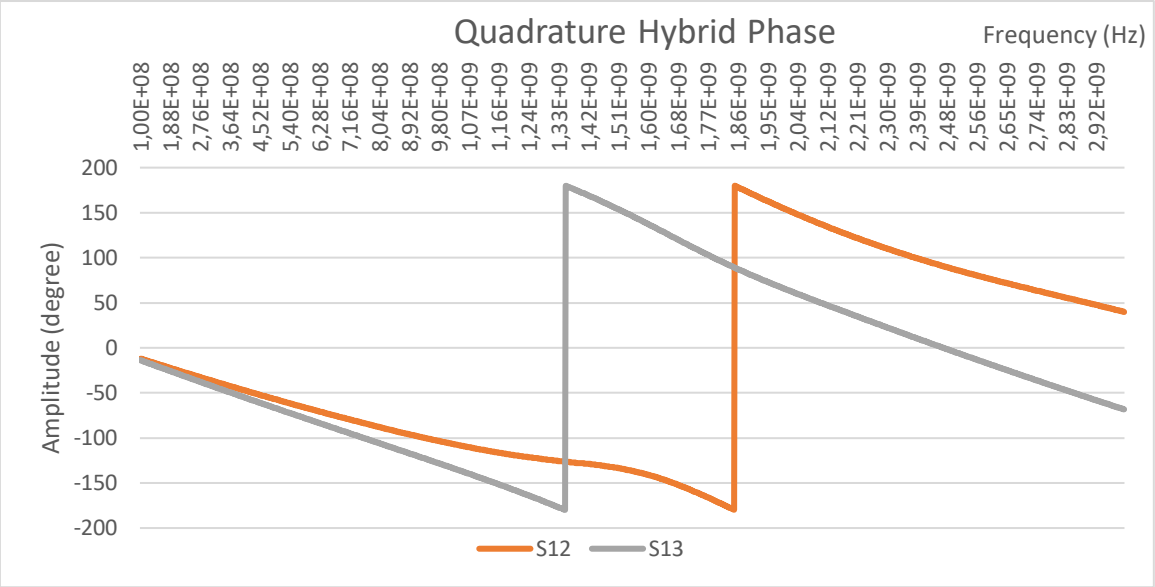

Figure 4.10 RT-DUROID 5880 Quadrature Hybrid Ports 2 and 3 Phase Comparison.

4.2.2 Rat-Race

The Rat-Race, being one of the best simulation results circuit, has been chosen to be produced in both substrates, first in the RT-DUROID 5880 and later on the FR-4. The results are exhibited on this section.

4.2.2.1 RT-DUROID 5880

Figure 4.11 shows the prototype of the Rat-Race circuit impressed on the RT-DUROID 5880 substrate. It was done with the 2,2 dielectric permittivity substrate and then the PCB was finished by welding the circuit connectors, one for each port.

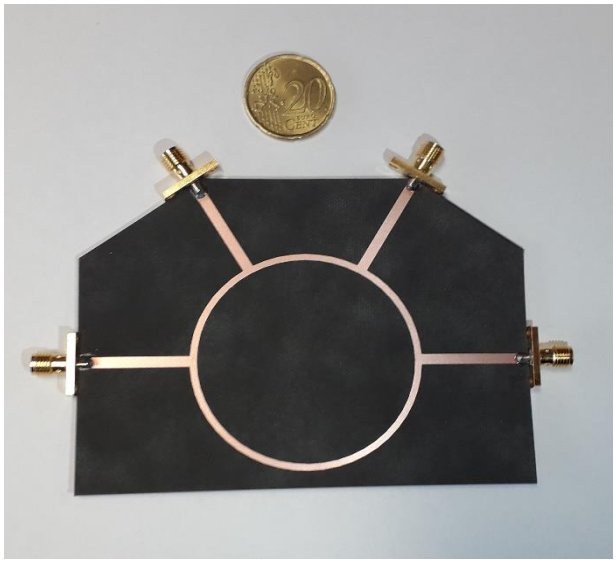

Figure 4.11 RT DUROID 5880 Rat-Race Prototype.

Once again, this circuit was fabricated and measured with a Vector Network Analyzer (VNA), which was calibrated to measure the respective S-parameters (Fig. 4.12). This allowed a valid comparison between the theory, the simulations and the measured results.

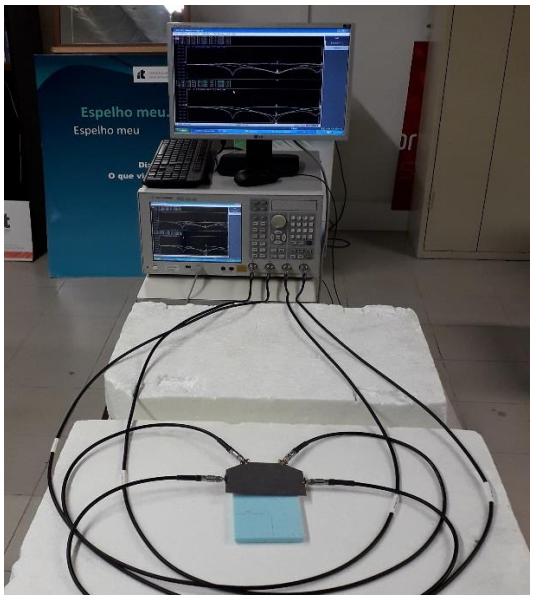

Figure 4.12 RT DUROID 5880 Rat-Race VNA Analysis.

As the previous one, this circuit also suffered a centre frequency shifting, figure 4.13, possibly from manufacturing errors, like inaccuracy when cutting the printed circuit board.

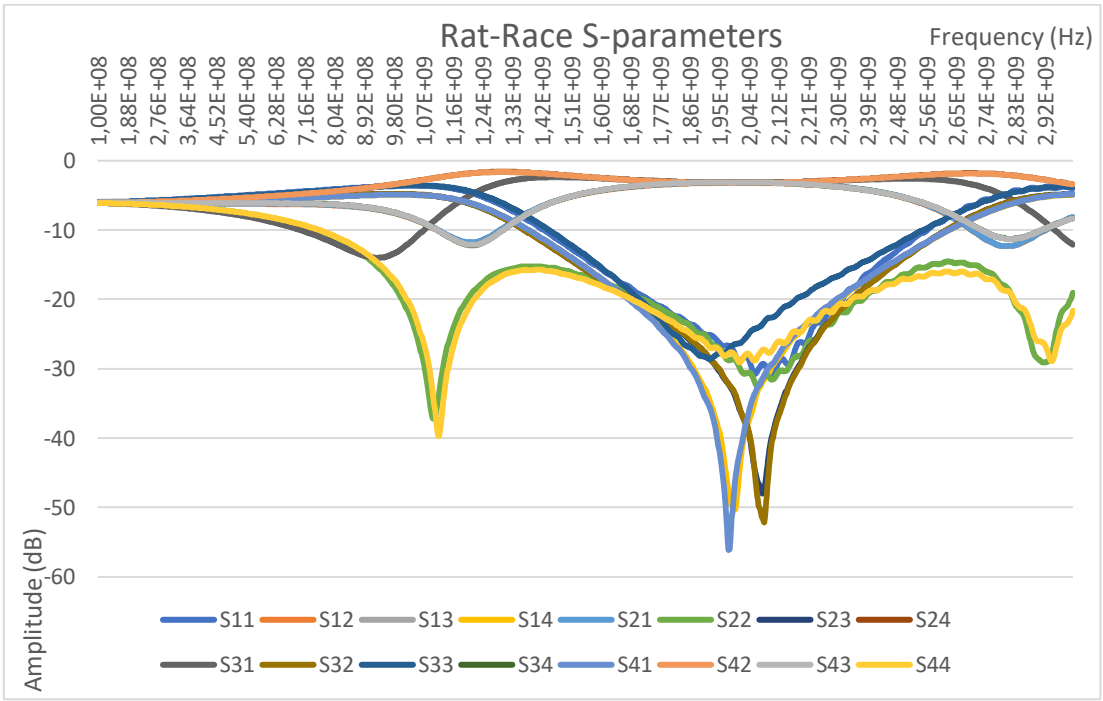

Figure 4.13 RT DUROID 5880 Rat-Race S-parameters.

Data from figure 4.14, shows that besides centre frequency shifting - possibly from circuit making errors, like inaccuracy when cutting the printed circuit board – this circuit also has short

amplitudes variation when at the centre frequency. As all ports achieve a lower than -27dB at around 2 GHz, suggests, even though that the circuit works correctly it should have been projected for a higher centre frequency.

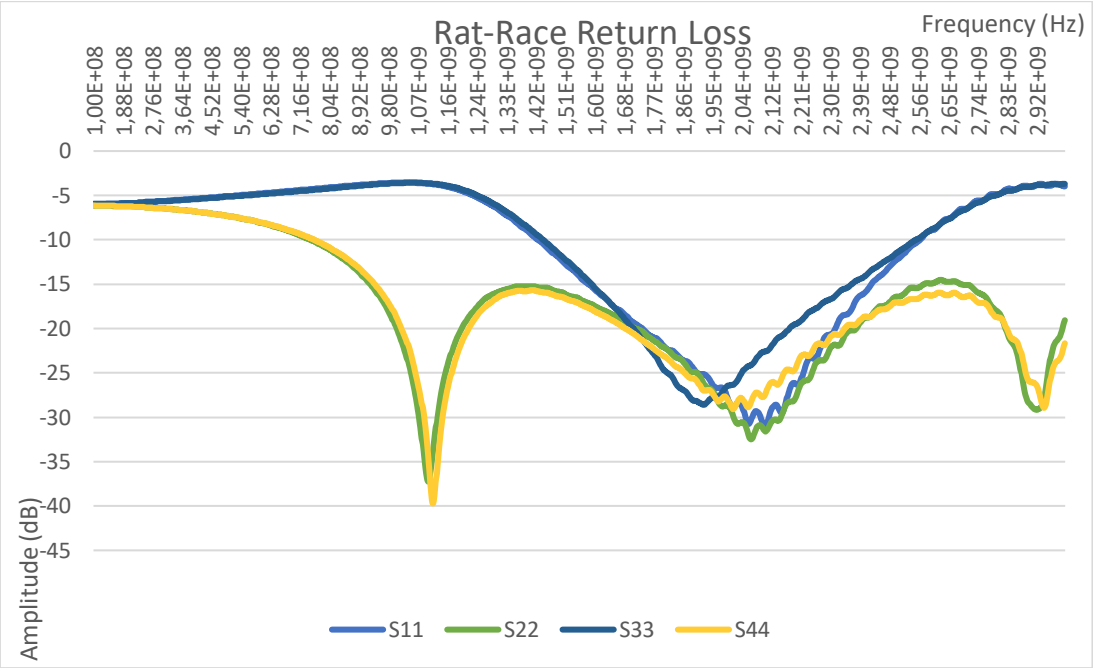

Figure 4.14 RT DUROID 5880 Rat-Race Return Loss.

Table 6 RT DUROID 5880 Rat-Race Return Loss Values.

Parameters	Centre Frequency (GHz)	Max Return Loss (dB)	Band > 16dB (GHz)
S11	2.104	-31.03	1.578 - 2.422
S22	2.064	-32.51	1.374 - 2.578
S33	1.920	-28.60	1.585 – 2.364
S44	2.008	-29,06	1.408 – 2.624

Table 6 shows that the device bandwidth is approximately 1585 – 2364 MHz, providing a very good bandwidth, of around 750 MHz, for an hand-made circuit.

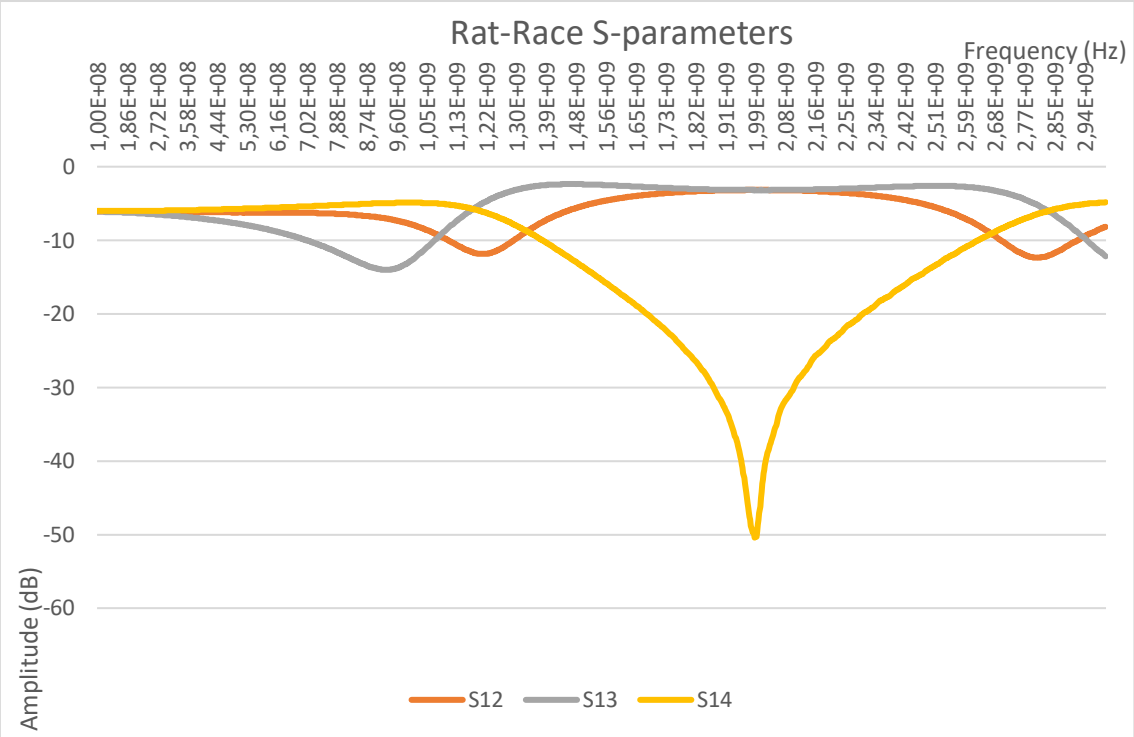

Figure 4.15 RT DUROID 5880 Rat-Race Insertion Loss.

The figure 4.15 show the prototype insertion losses. It is observed that there is a -3 dB equal power split between the second and third output ports, leaving port four isolated.

The S12 and S13 response loss is almost perfect, since their amplitude is around -3dB, and they are almost synchronized in phase, figure 4.16. The S14 response loss parameter, is also very good, obtaining an over -50dB isolation.

The measured results are approximated the same as the theoretical and the simulated ones.

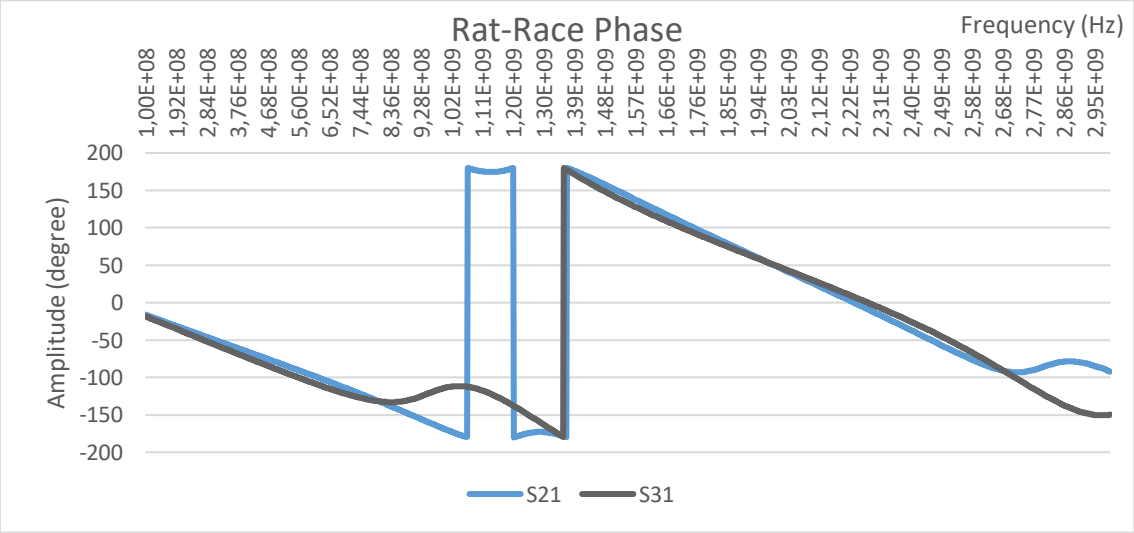

Figure 4.16 RT DUROID 5880 Rat-Race Ports 2 and 3 Phase Comparison.

4.2.2.2 FR-4

Figure 4.17 shows the prototype of the Rat-Race circuit impressed on the FR 4 substrate. Firstly, the circuit was printed on the board and then the four ports were weld to the substrate. This device is smaller than the last one, due to the fact that it was dimensioned for a higher dielectric permittivity substrate.

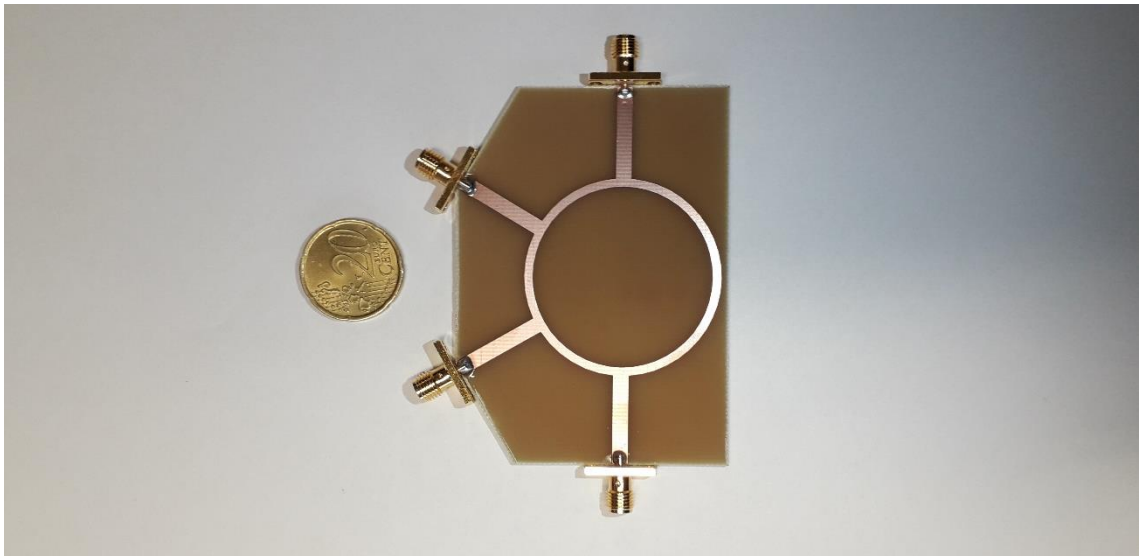

Figure 4.17 FR-4 Rat-Race Prototype.

Once more, this circuit was fabricated and measured with a Vector Network Analyzer (VNA), which was calibrated to measure the respective S-parameters (Fig. 4.18). This enabled to compare the theory with the simulations and the measured results.

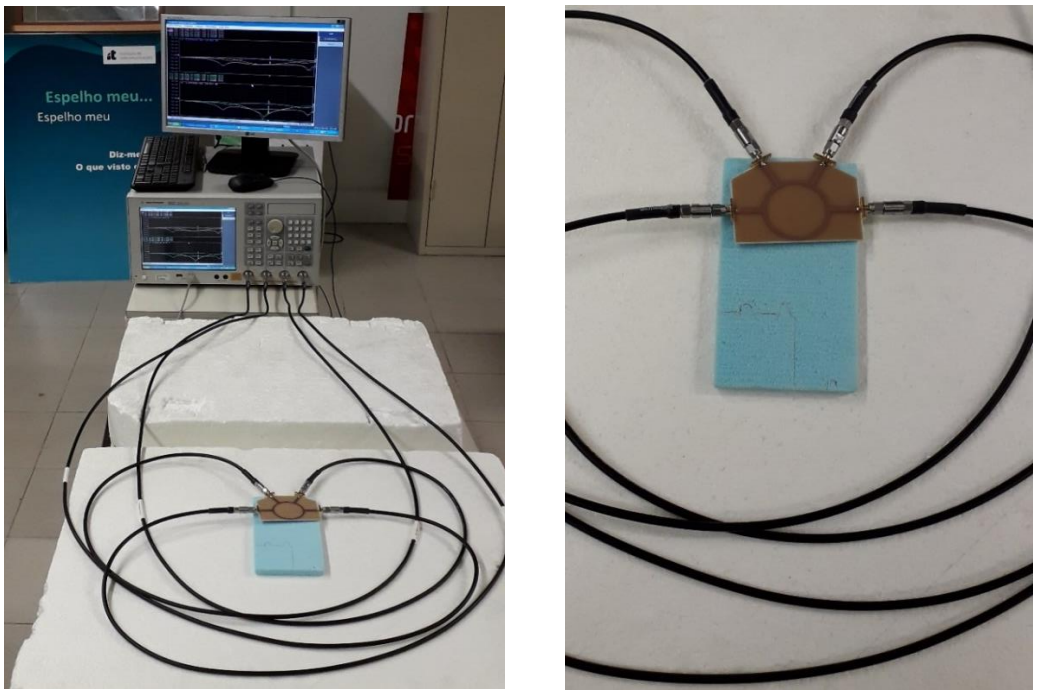

Figure 4.18 FR-4 Rat-Race VNA Connections and Analysis.

Figure 4.19 shows the Rat-Race coupler S parameters with an operating frequency of 2GHz.It could be concluded that the output presented is very similar to the simulated one, being noticeable a slight frequency shift. As stated before, the main reason for this effect is the homogeneity of the substrate, i.e. since being non-homogeneous leads to non-symmetry, the power that is delivered to each port is not equal.

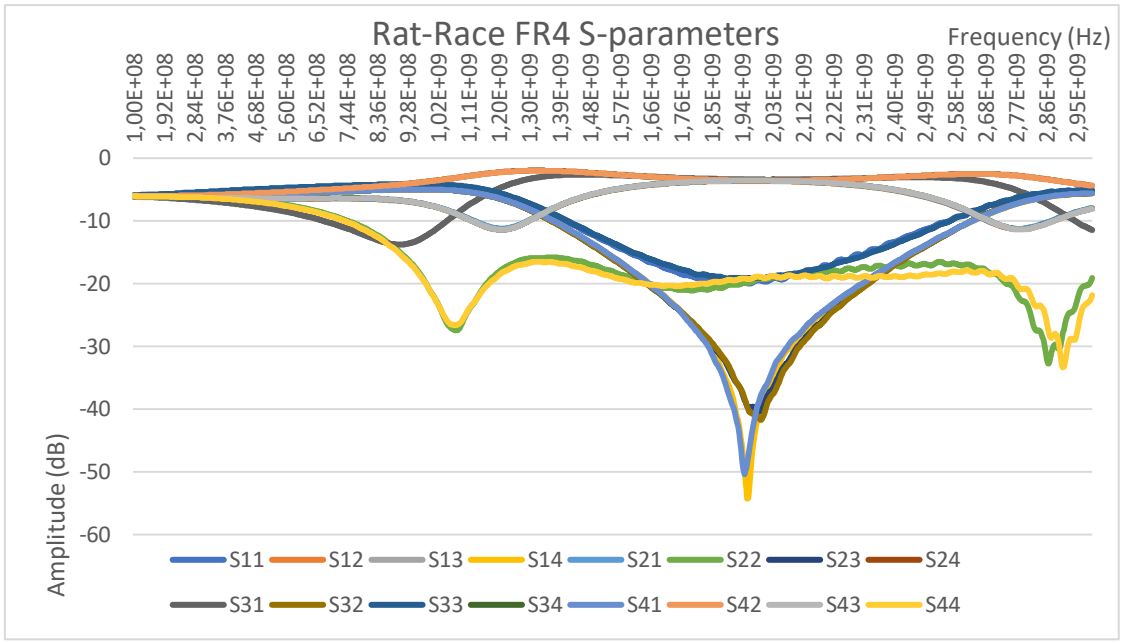

Figure 4.19 FR-4 Rat-Race S-parameters.

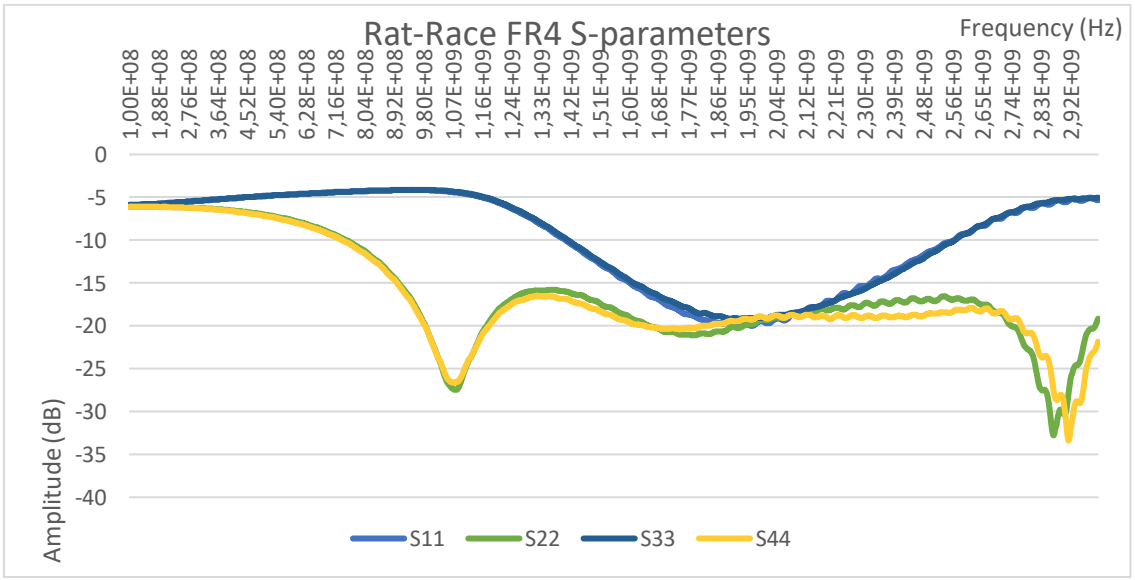

Figure 4.20 FR-4 Rat-Race Return Loss.

Figure 4.20 show the port return losses. As happened in the RT DUROID 5880 substrate, there is a slight frequency variation around centre frequency, but all ports achieve a lower than -19 dB at around 2GHz, revealing even though that the device works correctly it should have been projected for a higher centre frequency.

Table 7 FR-4 Rat-Race Return Loss Values.

Parameters	Centre Frequency (GHz)	Max Return Loss (dB)	Band > 15dB (GHz)
S11	1.962	-20.04	1.598 - 2.320
S22	1.954	-19.84	0.906 – 3.000
S33	1.892	-19.14	1.610 – 2.332
S44	1.872	-19.75	0.900 – 3.000

Table 7 displays the band variation for each port, revealing that this device would work well during approximately 700 Hz, from 1.610 GHz to 2.320 GHz.

The insertion losses presented in figure 4.21 show some good results. It is observed that there is a -3dB equal power split between the second and third output ports, leaving port four isolated. The S12 and S13 parameters are almost flawless, obtaining an -3dB around amplitude (Fig. 4.21), and being again, nearly synchronized in phase (Fig. 4.22). Moreover, the S14 parameter shows a value of closely -55dB, providing a very good ports 1 and 4 isolation relation.

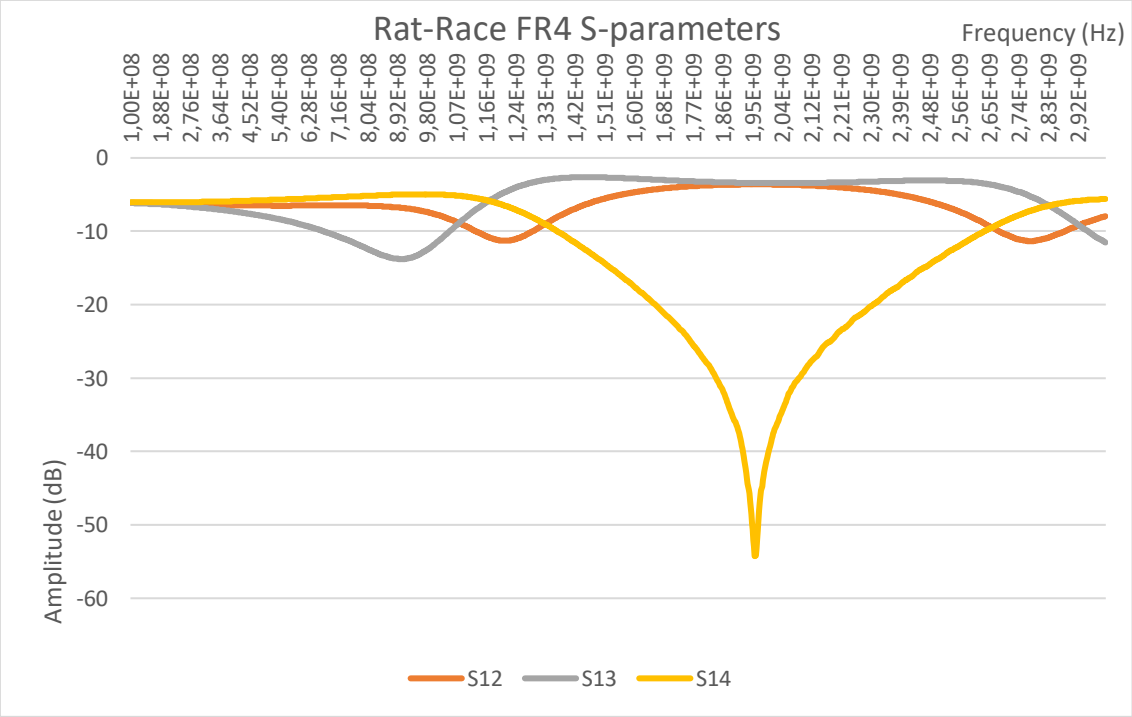

Figure 4.21 FR-4 Rat-Race Insertion Loss.

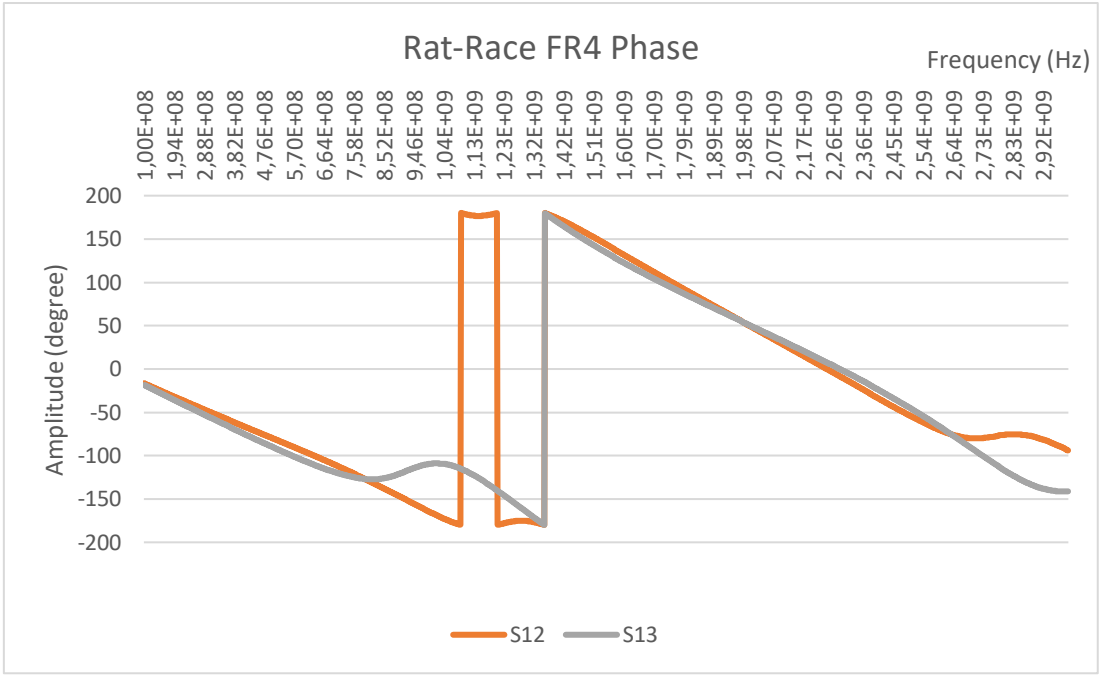

Figure 4.22 FR-4 Rat-Race Ports 2 and 3 Phase Comparison.

4.2.3 Wilkinson Power Divider

Figure 4.23 shows the prototype of the Wilkinson Power Divider circuit impressed on the RT-DUROID 5880 substrate. As on the other devices, the PCB was finished by welding the connectors to the ports, but this time this circuit had a 100-ohm resistor weld that connects both branches.

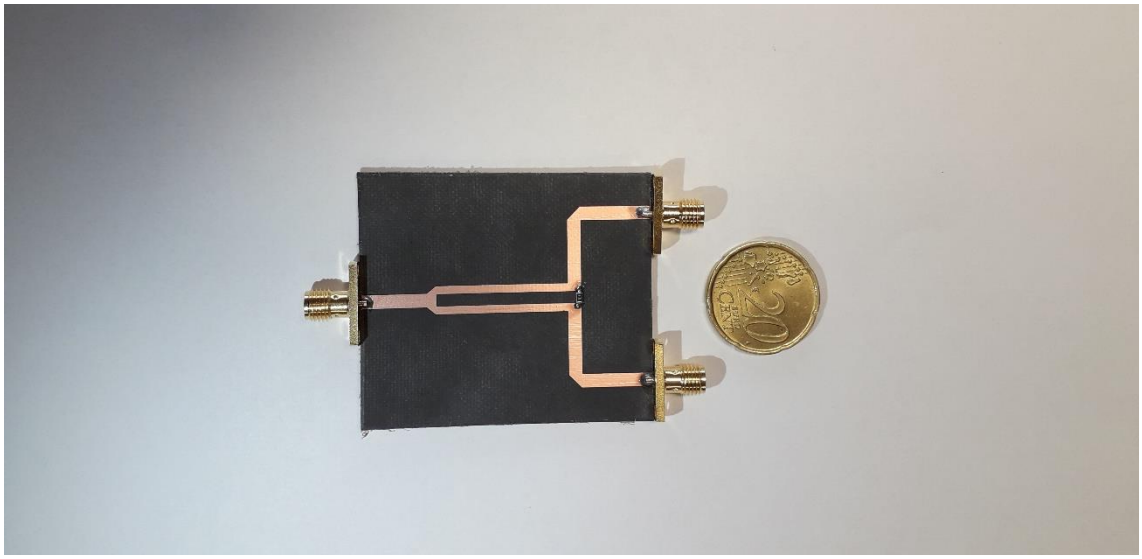

Figure 4.23 RT-DUROID 5880 Wilkinson Power Divider prototype.

Again, this circuit was fabricated and measured with a Vector Network Analyzer (VNA), which was calibrated to measure the respective S-parameters (Fig. 4.24), that enabled the comparison between the theory, the simulations and the measured results.

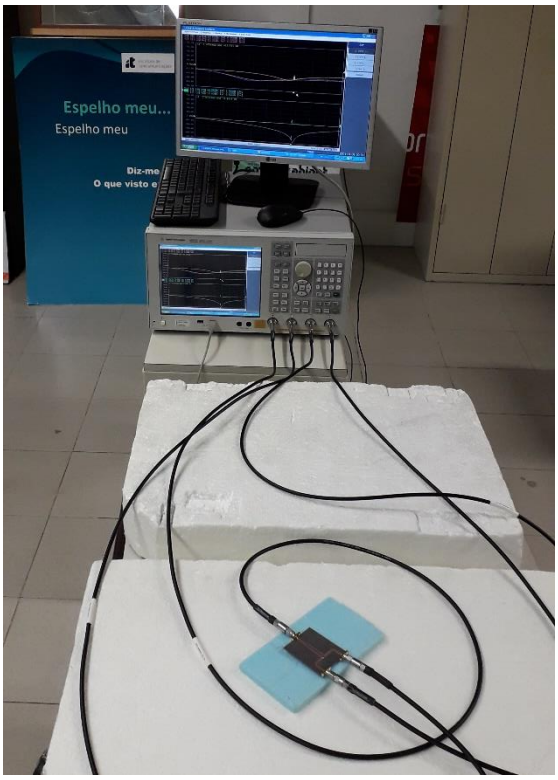

Figure 4.24 RT-DUROID 5880 Wilkinson Power Divider VNA Analysis.

Figure 4.25 shows the wilkinson power divider coupler S-parameters with an operating frequency of 2GHz. It is visible the non-perfect return loss parameters by S22 and S33, possibly because of design problems.

It could be concluded that the output presented is very similar to the simulated one, that presented the same wide bandwidth.

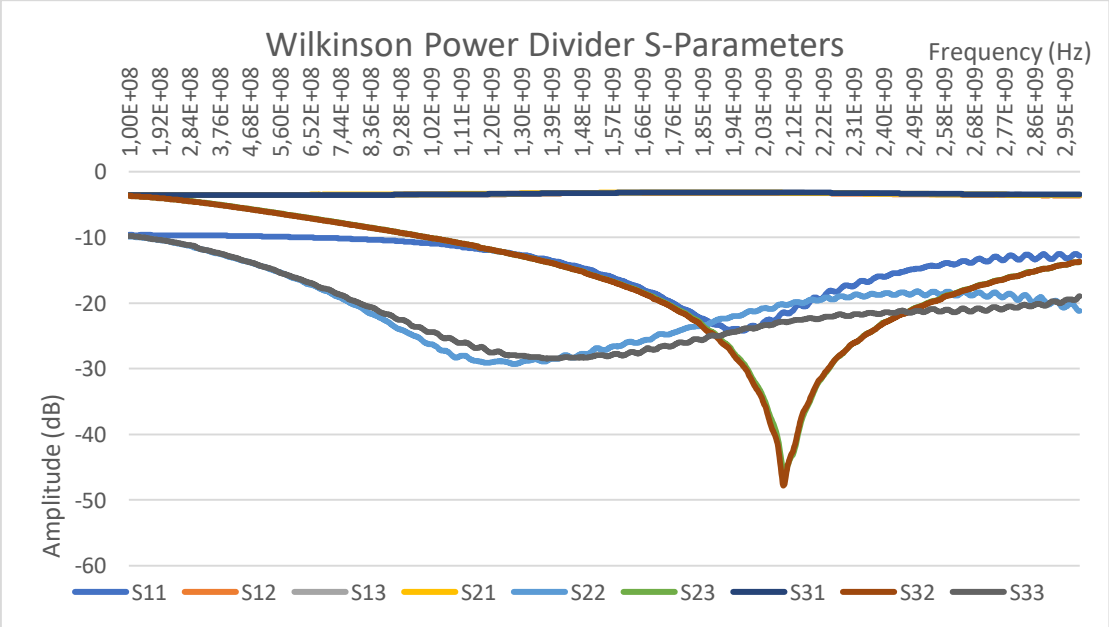

Figure 4.25 RT DUROID 5880 Wilkinson Power Divider S-parameters.

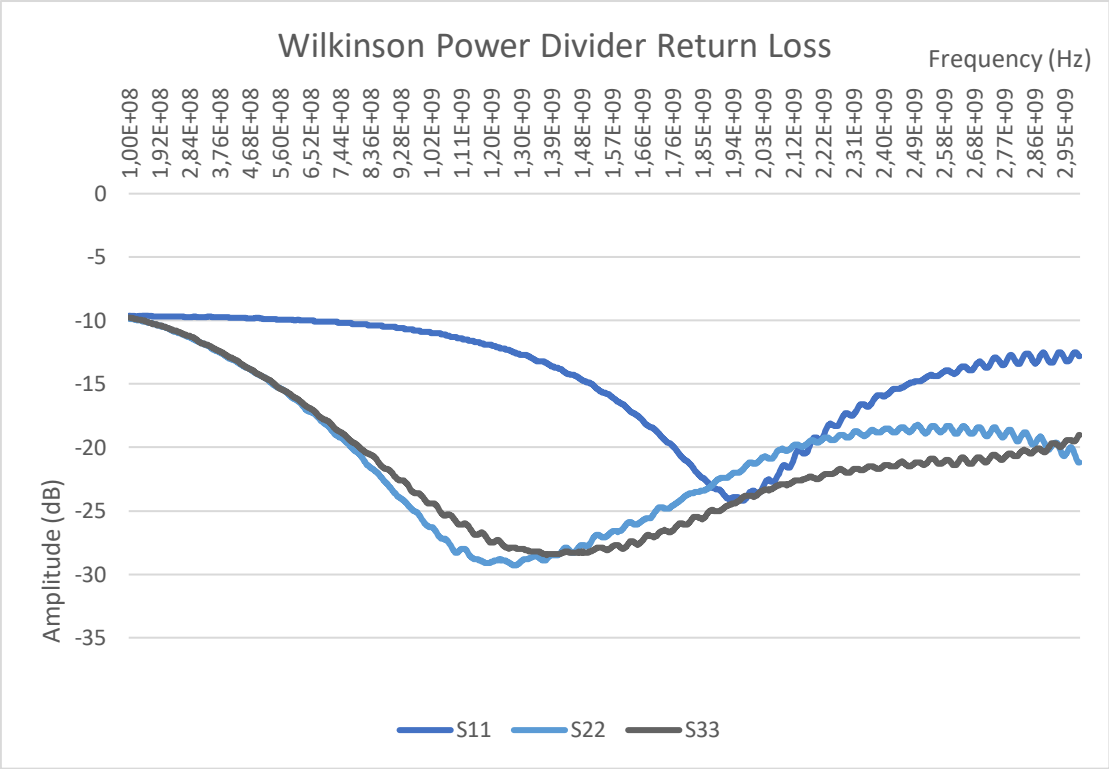

Figure 4.26 RT DUROID 5880 Wilkinson Power Divider Return Loss.

Figure 4.26 show the ports return losses where isolation was measured at around 1968 MHz. As happened before, a slight frequency oscillation near the centre frequency is noticeable, suggesting an amplitude increase to stabilize the circuit, but all ports achieving a lower than -20dB at around 2 GHz.

Table 8 RT DUROID 5880 Wilkinson Power Divider Return Loss Values.

Parameters	Centre Frequency (GHz)	Max Return Loss (dB)	Band > 15dB (GHz)
S11	1.968	-24.2	1.512 - 2.476
S22	1.270	-29.3	0.538 – 3.000
S33	1.374	-28.5	0.542 – 3.000

The factors explained above can be seen on the S22 and S33 very wide bands, around 2.5 GHz, when compared to the circuit working band, around 900 MHz (Table 8).

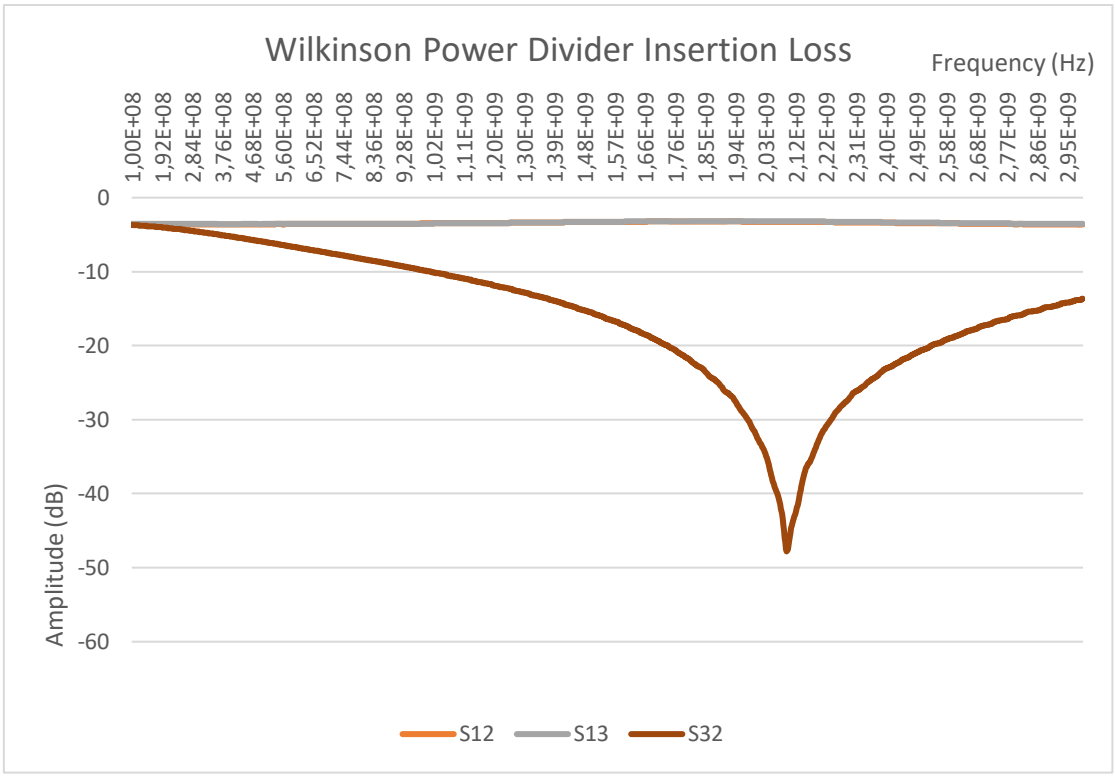

Figure 4.27 RT DUROID 5880 Wilkinson Power Divider Insertion Loss.

The insertion losses presented in figure 4.27 show that the circuit achieved good results. It is observed that the S12 and S13 values are very good, near -3dB, and port 2 and port 3 have also a very good isolation factor of almost -50 dB. This reveals that all the signal entering port 1, gets divided between 2 and 3, with no signal from one to the other, i.e. that there is an equal power split between the 2 and 3 output ports, leaving port 4 isolated. Also, these two ports are perfectly synchronized in phase (Fig. 4.28).

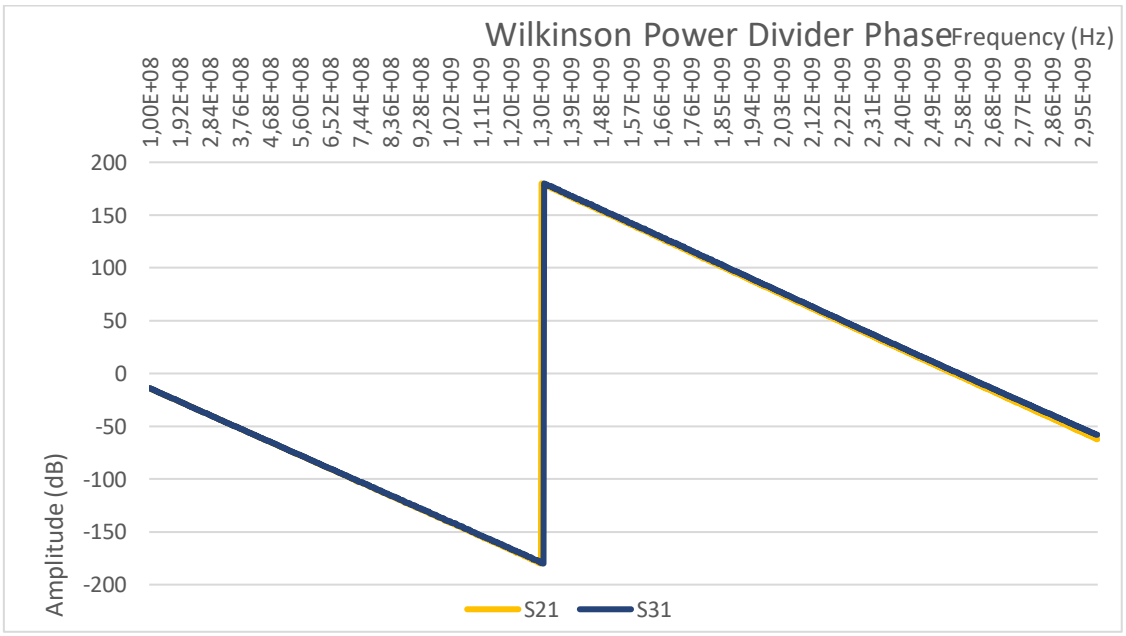

Figure 4.28 RT DUROID 5880 Wilkinson Power Divider Ports 2 and 3 Phase Comparison.

Chapter 5

Conclusion

5.1 Review of the Performed Work and Main Findings

5.1.1 Summary

The main purpose of this research was to design, simulate, print and analyse three different directional couplers - the Quadrature Hybrid, the Rat-Race and the Wilkinson Power Divider, in three very different substrates, RT- DUROID 5880, FR-4 and EPSILAM 10, with the aim of studying the possible differences between the circuits, specifically how the signal is split and what the resultant output signals look like in terms of amplitude and phase.

The fulfilment of this overall objective resulted in the organization of five core chapters. The second chapter provides a literature review of the Microstrip Line technology that was the base to fabricate the printed circuit boards and of the Coupled Lines technique used to print the circuits. It also characterizes the three directional couplers and the even-odd mode circuit analysis of them, in order to understand their performance characteristics and derived scattering matrixes. The following chapter presents the CST Microwave Studio EM as the simulation tool to document and replicate the Theoretical Model. It also details the design and layout of the Quadrature Hybrid, the Rat-Race and the Wilkinson Power Divider directional couplers in the three substrates: RT-DUROID 5880, FR-4 and EPSILAM 10. The fourth chapter covers the circuit fabrication and testing with the result and analysis. Finally, the last chapter provides the main conclusions of this work and suggestions for further research.

5.1.2 Main Findings

The work presented indicates that the Quadrature Hybrid, the Rat-Race and the Wilkinson Power Divider directional couplers can be built using simple microstrip manufacture techniques and coupled lines techniques. Moreover, regarding the 3 substrates that were designed, constructed and simulated, only 2 of them achieved adequate results – the RT- DUROID 5880 and FR-4, so the EPSILAM 10 had to be discharged as it was not suitable to this kind of approach. Furthermore, as the FR-4 is not a homogeneous substrate, it was only tested on the Rat-Race circuit. The RT-DUROID 5880 substrate proved to work adequately on all circuits. The comparison of figure 5.1

with the one in chapter 1 (Fig. 1.1), shows the gap between the initial proposal and the possible one.

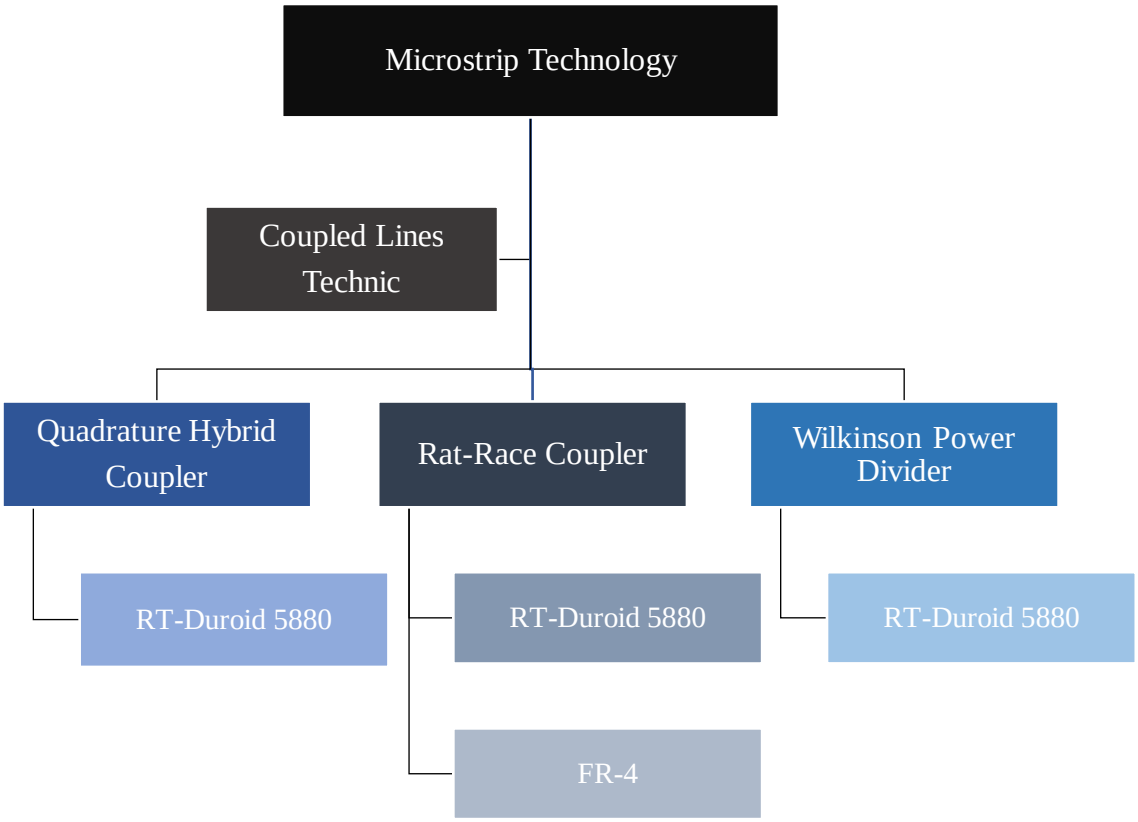

Figure 5.1 Outline of the main work done in this dissertation.

Nevertheless, the results obtained indicate that the proposed couplers design and fabrication work very well over their frequency bands for all the couplers.

Furthermore, the analysis, design and manufacture of the three different directional couplers permitted to recognize the overall impact of the design and of the substrate in which they were applied, in their final performance. The simulation results attained with the CST software sanctioned a deeper analysis of the S-parameters, as well as a better understanding of the electric and power flows of these devices at the dimensioned frequency.

Finally, the results acquired with the physical devices were very similar to the simulation results, demonstrating an excellent agreement between the results, which allows to conclude that the methodology used in this dissertation is appropriated to this type of circuit projection.

5.2 Limitations and Future Work

Although the provided analyses and methodology have constituted a good approach, the weaknesses and limitations of each of the three directional couplers developed in the research study have indicated the following areas as recommendations for further work.

Hand-made couplers can be feasible. During the design and fabrication of this circuits, the most critical aspect to achieve in an equal-split power divider is a perfect symmetry. As stated before, the results from the hand-made couplers show a slight lack of symmetry that resulted in various return loss frequency shifts and in a larger than desired amplitude balance values. Consequently, in the future, the design and fabrication procedures could be simplified by computer-aided design and manufacturing, maybe linked to a design database for different configurations that take in consideration the fabrication limitations and some other criteria intake by user. It could also compare the usage of KeySight Technologies Advance Design System (ADS) versus the usage of CST, when building and simulating the system and later on by printing the circuits.

Another possible important topic to further investigation is the improvement of the design models, i.e., studying them for different frequencies, like they suggest, working on a higher frequency or trying another circuit setup, as for instance a Wilkinson Power Divider with rounded junctions. Moreover, all the circuit could be construct in a different way, using for example a laser to cut the substrates avoiding imperfections and improving accuracy.

Bibliography

[1] S. Shelar e N. Kolhare, "Design And Analysis of Hybrid Coupler," *International Journal of Engineering Research & Technology,* May 2014.

[2] "History of microstrip," microwave101, 20 February 2019. [Online]. Available: https://www.microwaves101.com/encyclopedias/history-of-microstrip.

[3] G. Kalpanadevi, M. K. N. Nishaw, E. Priyamalli, V. Radhika e V. S. Priyanga, "Design and Analysis of Wilkinson Power Divider Using Microstrip Line and Coupled Line Techniques," *IOSR Journal of Electronics and Communication Engineering,* nº 2278-8735, pp. 34-40, 2017.

[4] S. B. Cohn, "Slot Line on a Dielectric Substrate," *IEEE TRANSACTIONS ON MICROWAVE THEORY AND TECHNIQUES,* Vols. 17, nº 10, pp. 768-778, 1969.

[5] T.-L. Wu, "Transmission Lines and Components," em *Microwave Filter Design,* Department of Electrical Engineering of National Taiwan University, 2011.

[6] M. V. Schneider, in *Microstrip lines for microwave integrated circuits,* BSTJ, 1969, pp. 1421-1444.

[7] R. E. Collin, Foundations for Microwave Engineering, McGraw-Hill International Editions, 1992.

[8] M. Kobayshi, "A dispersion formula satisfying recent requirements in microstrip CAD," *IEEE Trans. Microwave Theory Tech,* Vols. 36, pp. 1246-1250, 1988.

[9] D. M. Pozar, in *Microwave Engineering,* New York, Wiley, 1998, pp. 160-167.

[10] E. Tutkur, "Wideband Direction Couplers and Power Splitters," *Thesis for the degree of Master of Science,* 2014.

[11] L. S. Napoli e J. J. Hughes, "Characteristics of coupled microstrip lines," *RCA Rev,* nº Sept, pp. 479-498, 1970.

[12] S. B. Cohn, "History of Microwave Passive Components with Particular Attention to Directional Couplers," *IEEE TRANSACTIONS ON MICROWAVE THEORY AND TECHNIQUES,* vol. 9, nº MTT-32, pp. 1046-1053, 1984.

[13] K. C. Gupta, R. Garg e I. J. Bahl, Microstrip Lines and Slotlines, Dedham: Artech House, 1979.

[14] T. J. Rouphael, "Microwave Network Design and Analysis," 2014. [Online]. Available: https://www.sciencedirect.com/topics/engineering/directional-couplers. [Accessed 21 February 2019].

[15] H.-X. Xu, G.-M. Wang e K. Lu, "Microstrip Rat-Race Couplers," pp. 117-129, June 2011.

[16] M. Moubadir, H. Aziz, A. Mohameda e I. B. Naima Amar Touhami, "Miniaturized Design of Rat-race Coupler by Utilizing T-Shape Stubs," *International Conference Interdisciplinarity in Engineering,* Vols. %1 de %2INTER-ENG, nº 11, January 2017.

[17] J. Stiles, "The 180º Hybrid," *The 180 Degree Hybrid,* 09 04 2007.

[18] "Advantages of Rat Race Coupler | disadvantages of Rat Race Coupler," RF Wireless World, [Online]. Available: http://www.rfwireless-world.com/Terminology/Advantages-and-Disadvantages-of-Rat-Race-Coupler.html. [Acedido em 15 02 2019].

[19] J. Reed e G. J. Wheeler, "A Method of Analysis of Symmetrical Four-Port Networks," em *IRE Transactions on Microwave Theory and Techniques,* 1956, pp. 246-252.

[20] "Quadrature Couplers," microwave101, 2019. [Online]. Available: https://www.microwaves101.com/encyclopedias/quadrature-couplers. [Acedido em 08 March 2019].

[21] J. Stiles, "The 90º Hybrid Coupler," *The Quadrature Hybrid Coupler,* 17 04 2009.

[22] J. Corsini, J. Malaver e S. Lushllari, "90 Degree Hybrid Coupler," pp. 23-24, 25 April 2013.

[23] "Wilkinson Power Splitters," microwave101, 2019. [Online]. Available: https://www.microwaves101.com/encyclopedias/wilkinson-power-splitters. [Acedido em 09 March 2019].

[24] "Wilkinson Power Divider," Wikipedia, 2019. [Online]. Available: https://en.wikipedia.org/wiki/Wilkinson_power_divider. [Acedido em 20 March 2019].

[25] "Power dividers and directional couplers," Wikipedia, 2019. [Online]. Available: https://en.wikipedia.org/wiki/Power_dividers_and_directional_couplers. [Acedido em 18 March 2019].

[26] "Advantages of Wilkinson power divider or combiner | disadvantages of Wilkinson power divider or combiner," RF Wireless World, [Online]. Available: http://www.rfwireless-world.com/Terminology/Advantages-and-Disadvantages-of-Wilkinson-Power-Divider-Combiner.html. [Acedido em 11 02 2019].

[27] J. Stiles, "The Wilkinson Power Divider," *The Wilkinson Power Divider,* 14 04 2009.

[28] "RT/duroid® 5880 Laminates," Rogers Corp., 2019. [Online]. Available: https://www.rogerscorp.com/acs/products/32/RT-duroid-5880-Laminates.aspx. [Acedido em 20 March 2019].

[29] "FR-4," Wikipedia, 2019. [Online]. Available: https://en.wikipedia.org/wiki/FR-4. [Accessed 29 March 2019].

[30] W. J. Getsinger, "Microstrip dispersion model," *IEEE Trans. Microwave Theory Tech.,* Vols. 21, pp. 34-39, 1973.